NASA CR-132562

DEVELOPMENT AND MODIFICATION OF A DIGITAL PROGRAM FOR FINAL APPROACH TO LANDING

By William G. Duff
and
Charles R. Guarino

Prepared under Contract No. NAS 1-11992 by
ATLANTIC RESEARCH CORPORATION
EMM Department
Alexandria, Virginia 22314
for
NATIONAL AERONAUTICS AND SPACE ADMINISTRATION

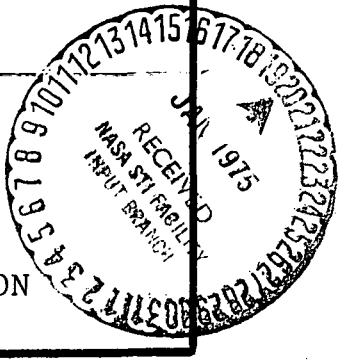

FOREWORD

This report was prepared for the National Aeronautics and Space Administration, Langley Research Center, by Atlantic Research Corporation under Contract Number NAS 1-11992.

The project was performed under the technical direction of William G. Duff at Atlantic Research, and Richard M. Hueschen of NASA Langley. Other contractor personnel who contributed directly to this project include:

Charles R. Guarino
Mabel E. Harman
— Atlantic Research Corporation

Other personnel who participated in this project include:

Thomas M. Walsh	NASA Langley
Nesim Halyo	University of Virginia

Abstract

This report describes the development and implementation of a dynamic digital computer simulator which may be used to evaluate aircraft performance when operating under the control and guidance of various navigation, landing, and flight control systems. The resulting digital computer program may be used to simulate and evaluate the relationships and interactions between various factors such as the microwave landing system, avionics receivers and onboard processors, aircraft aerodynamics, aircraft automatic control systems, control surfaces, and wind and other external effects. The models used to represent aircraft aerodynamics, control system and control surfaces; weather and wind effects; and the microwave landing system are described.

Example results are presented for a simulation of a Boeing 737 using two sample control systems while subjected to various atomospheric conditions and microwave landing system errors. The limitations and performance capabilities of these control systems are discussed in terms of their ability to utilize the microwave landing system signal.

Table of Contents

1.0 INTRODUCTION

A Microwave Landing System (MLS) has been proposed by the Radio Technical Commission for Aeronautics (RTCA), Special Committee 117 (SC-117), to upgrade instrument landing systems and to eventually replace present VHF-ILS (Reference 1). The new system will alleviate those problems that limited the utility of the UHF-ILS and will permit safe instrument landings under FAA Category III conditions. In addition, the MLS will also serve to lessen the traffic problem around the terminal area by allowing curved approaches, precise interleaving of arriving flights, and multiple final approach paths.

The committee emphasis has been placed on a purely automatic approach with little, if any, pilot intervention. This places an added challenge on autopilots used during the final approach because not only will they have to perform more complicated control functions (i.e., curved approaches) but they will also be relied upon in a more severe environment (CAT III).

The objective of the study described in this report was to develop and implement a digital computer program which may be used to simulate and evaluate the relationships and interactions between

- the proposed microwave landing system
- avionics receivers and on-board processors
- aircraft aerodynamics
- aircraft autopilot systems
- control servo systems
- control surfaces
- wind and other external atmospheric effects.

The result is a dynamic simulator which evaluates aircraft performance when operating under the control and guidance of various navigation, landing, and flight control systems on the ground and in the air.

The simulator incorporates lateral and longitudinal equations of motion, a wind model, an MLS error model, and differential equations representing aircraft control system and control surface operation. At regular time intervals, aircraft position is calculated and the performance of the electronic navigation or landing systems is simulated to generate indicated aircraft position to either the pilot or autopilot. Control commands are then applied to the control surfaces and the aircraft is allowed to fly an increment of time with the new control settings. The new aircraft position is calculated and the above procedure repeated until the simulation is terminated. Statistical parameters relative to aircraft position, deviation from desired flight path and attitude may be derived from the output to evaluate aircraft performance when using a particular navigation or landing system.

Conceptually, the simulator provides a test bed for the evaluation of airborne systems that utilize MLS information with the MLS system being represented in terms of the accuracy and characteristics of information to the aircraft control functions. This study considered two control systems that could conceivably be used with a Microwave Landing System. The two control systems modeled differ greatly in complexity and cost. By adequately modeling the conditions under which each control system is to perform, it will be possible to determine how compatible each control system is with the MLS. In addition, insight can be obtained in designing future autopilots by identifying crucial input parameters.

The types of errors that an MLS generates and their effects upon the control systems were also studied. An attempt was made to identify the maximum allowable noise level and its permissible characteristics under various atmospheric conditions for satisfactory final approach performance.

The control systems studied are the System "A" and System "C" control laws as described in Reference 2. System "A", the simpler control system is, according to Boeing, representative of conventional autoland control systems. The configurations and gains of System "A" are typical of systems designed before Inertial Navigation Systems were available. It is not, however, an exact duplication of classical autoland systems in service.

The second control system studied is referred to as System "C". This system relies extensively on inertial information to provide a high-quality damping signal. The estimate of deviation from the localizer or glideslope is smoothed with position information obtained from the Inertial Navigation System (INS).

Both Systems "A" and "C" were originally designed by Boeing for use with the Boeing 727-100 aircraft. This study, however, is concerned with control systems that could be used with the Boeing 737 aircraft. In order to proceed with this study it was first necessary to modify the gains of both control systems to obtain satisfactory performance. For a complete description of the changes that were made to both control systems refer to Section 6.

The specially modified autopilots were subjected to various atmospheric conditions and MLS anomalies to determine their limitations and performance capabilities when used with an MLS. A description of the atmospheric environment model is presented in Section 5, and the models of MLS anomalies are presented in Section 7. The types of

MLS errors that could be present are discussed and results are shown for their influence on both control systems. In addition, a detailed analysis model is presented for the errors that a scanning-beam or Doppler microwave landing system could produce.

References

(1) RTCA SC-117, "A New Guidance System for Approach and Landing", DO-148, December 18, 1970.

(2) "Inertially Augmented Automatic Landing System, Autopilot Performance with Imperfect ILS Beams," FAA-RD-72-22, April 1972.

2.0 GENERAL DESCRIPTION OF SIMULATION

A computer program was developed which models the final approach phase of flight of an aircraft. The aircraft is subjected to various atmospheric conditions and is controlled by an autoland system which can correct for errors in position and altitude. Figure 2-1 shows a general block diagram of the simulator while Figure 2-2 illustrates an aircraft preceeding along a desired flight path. The simulator begins by considering an aircraft at point P_1 together with its orientation, velocity, initial conditions and control settings. The aircraft then flies a distance corresponding to a time increment Δt and its performance at point P_2 is computed through the general equations of motion for the aircraft.

The pilot or autopilot depends on certain navigational aids to determine position and performance relative to a desired flight path. Errors in the navigation or landing system create errors in knowledge of the true status of the aircraft. As indicated in Figure 2-2, point $\hat{P}_2$ indicates the estimated position. This estimate is based on the use of various navigation and landing systems, and because of electronic system errors, the estimated position will not correspond to the exact position. In the simulation, electronic system errors are modeled for the particular navigation or landing system being considered. Control surface commands are generated based on the estimated status. The generation of erroneous commands results in the aircraft

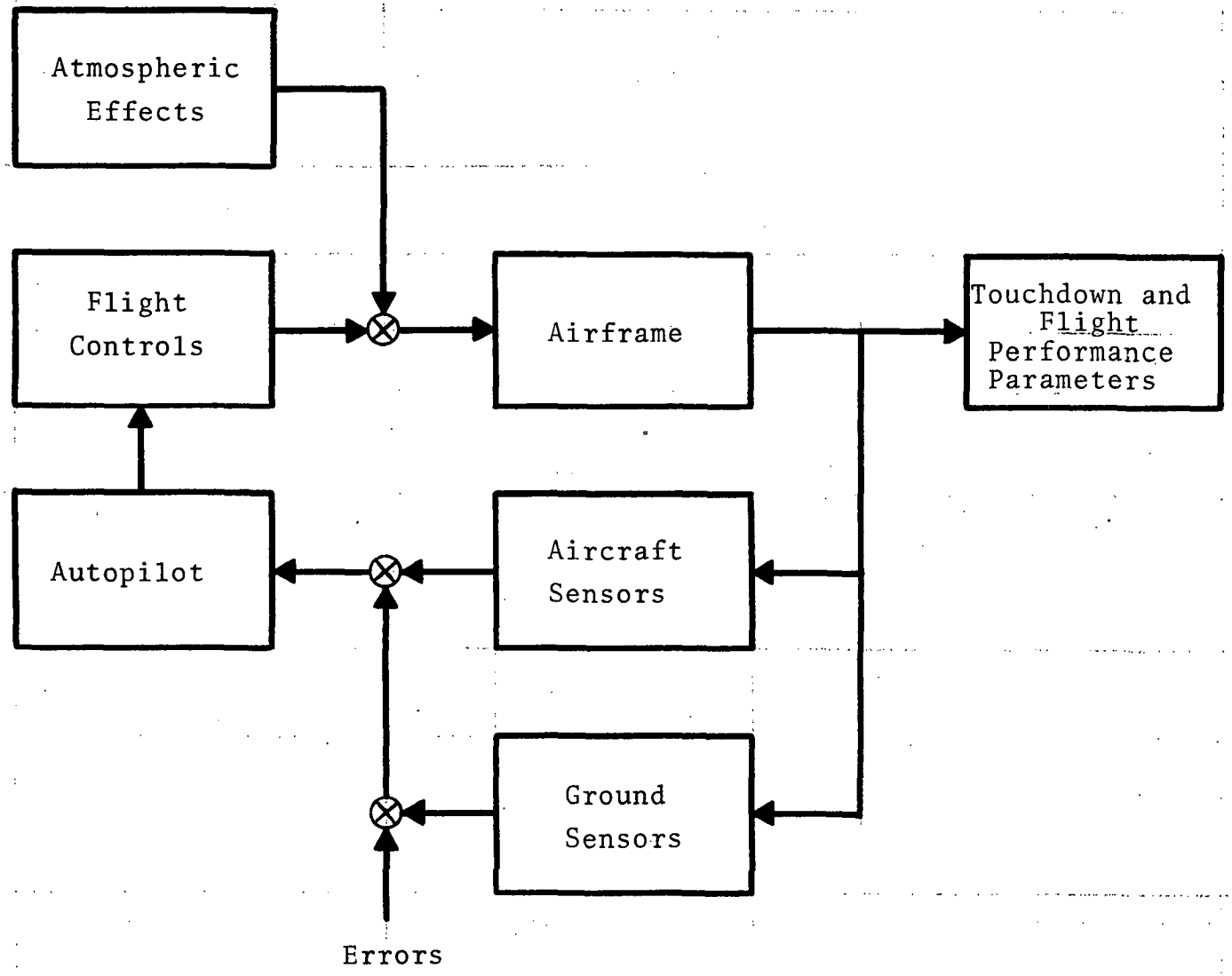

Figure 2-1. General Block Diagram of Simulator.

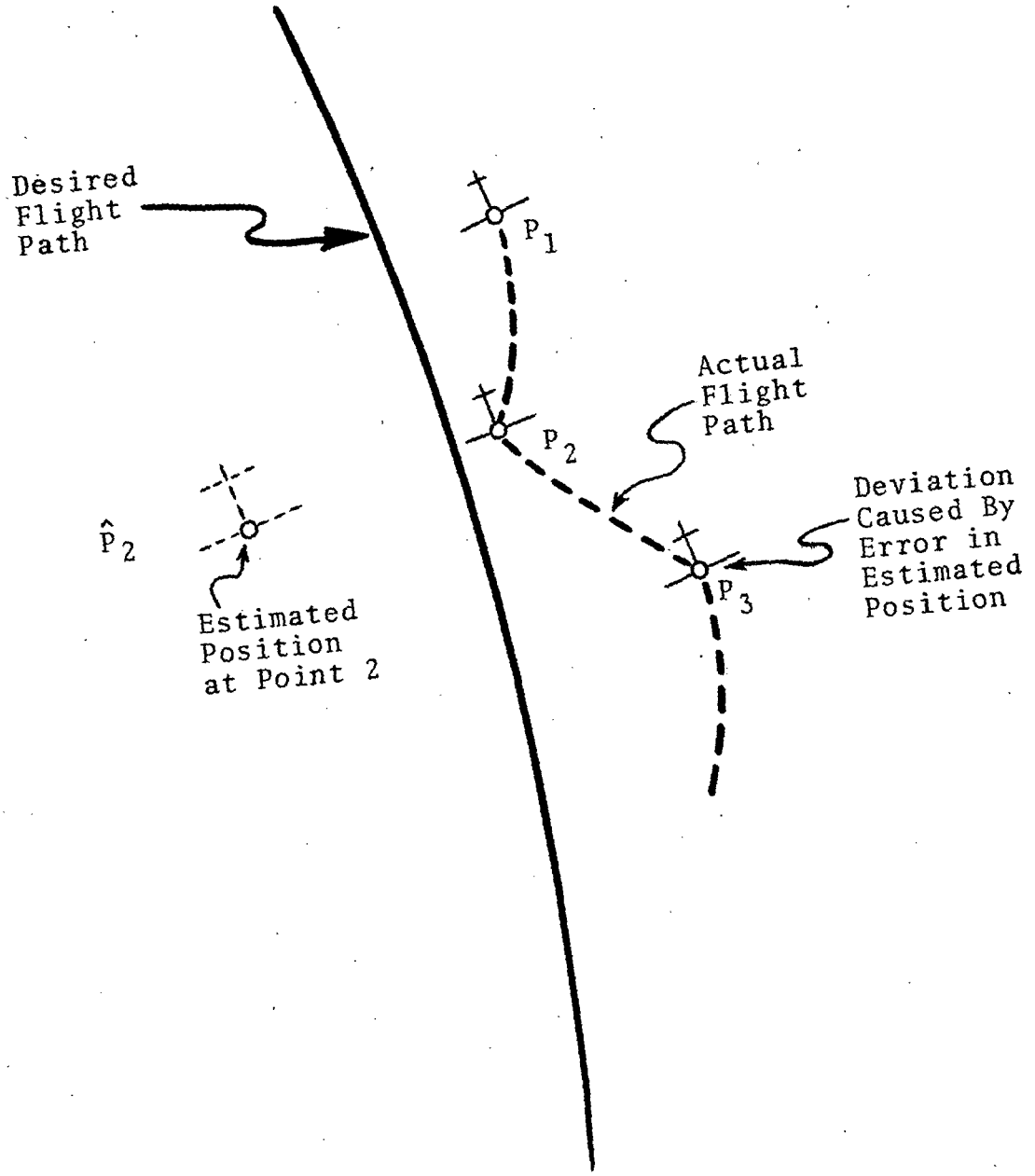

Figure 2-2. Flight Path Errors Caused by Errors in Estimated Position.

deviating from the desired flight path as illustrated in Figure 2-2. Based on commands given at point P_2 the aircraft position at point P_3 is determined and the process is repeated until the simulation is terminated. Through the use of this general simulation procedure, error characteristics of navigation and landing equipments can be related to aircraft performance while under the influence of these equipments.

Those blocks in Figure 2-1 that can be characterized by differential equations are put into the following state space format.

$$\dot{X} = AX + BU \qquad (2\text{-}1)$$

where

- X is the n-dimensional vector describing the particular block
- A is an nxn system matrix
- B is an nxΓ control matrix
- U is an Γ - dimensional control vector

Runge-Kutte third-order numerical integration techniques are used to integrate Equation 2-1 from initial conditions through touchdown. There are no restrictions on the matrices A and B; they may be time-varying or nonlinear. In dealing with the airframe block the nonlinear A and B matrices were linearized about an equilibrium point. This is not due to a limitation in the program but rather to the fact that the nonlinear parameters were not available.

The autopilots used in this simulation, however, do contain nonlinear terms and they were entered into the simulation without linearization.

The desired flight path is a straight line segment in three dimensional space. The line segment is the intersection of a plane elevated 2.5 degrees above the ground plane and a plane perpendicular to the ground plane passing through the centerline of the runway. The program could accept any line segment or combination of line segments to describe the flight path. However, it is important to realize that the C Control System was designed to fly an aircraft down a 2.5-degree glideslope. The selection of any other glideslope angle will necessitate changing the appropriate gains in the control system.

In addition, the runway was assumed to be 10,000 feet long. This length was chosen because several constants in the control system were given in terms of microamperes which had to be converted to degrees. Localizers are commonly adjusted to produce one microampere of deviation current for every 2.34 feet of lateral displacement from the course center, at the threshold of the runway. This sensitivity is required by FAA regulation for CAT II runways. For a typical 10,000-foot runway this yields an angular sensitivity of 75 microamperes per degree. This conversion factor was used to convert all microamp constants to degree constants.

3.0 Results and Conclusions

The performance of the 737 is illustrated with the "A" control system in Figure 3-1 and with the "C" control system in Figure 3-2. In both cases, multipath errors and wind were absent. From these figures it can be seen that the "A" lateral control system is critically damped, whereas, the "C" system is not. Also for the problems illustrated, the "A" system aircraft does not overshoot the glideslope beam as drastically as the "C" system does. The improved performance of the "A" aircraft is the result of changing the control system constants, as explained in Section 6.

In Figure 3-3 and 3-4 the results of subjecting the "A' aircraft to 50% and 100% of worst-case wind is shown (multipath errors are absent). The aircrafts performance is quite adequate until it reaches shear height at about 170 seconds into flight. The wind shear causes the aircraft to deviate substantially from the localizer. From Figure 3-4 this deviation amounts to approximately 60 feet.

The "A" system can be compared to the "C" system, by studying Figures 3-5 and 3-6. The "C" system does not deviate greatly from the glideslope or the localizer as it experiences a wind gradient. This difference in performance can be attributed entirely to the Inertial Navigation System that the "C" system utilizes. However, this is a result of the initial conditions assumed.

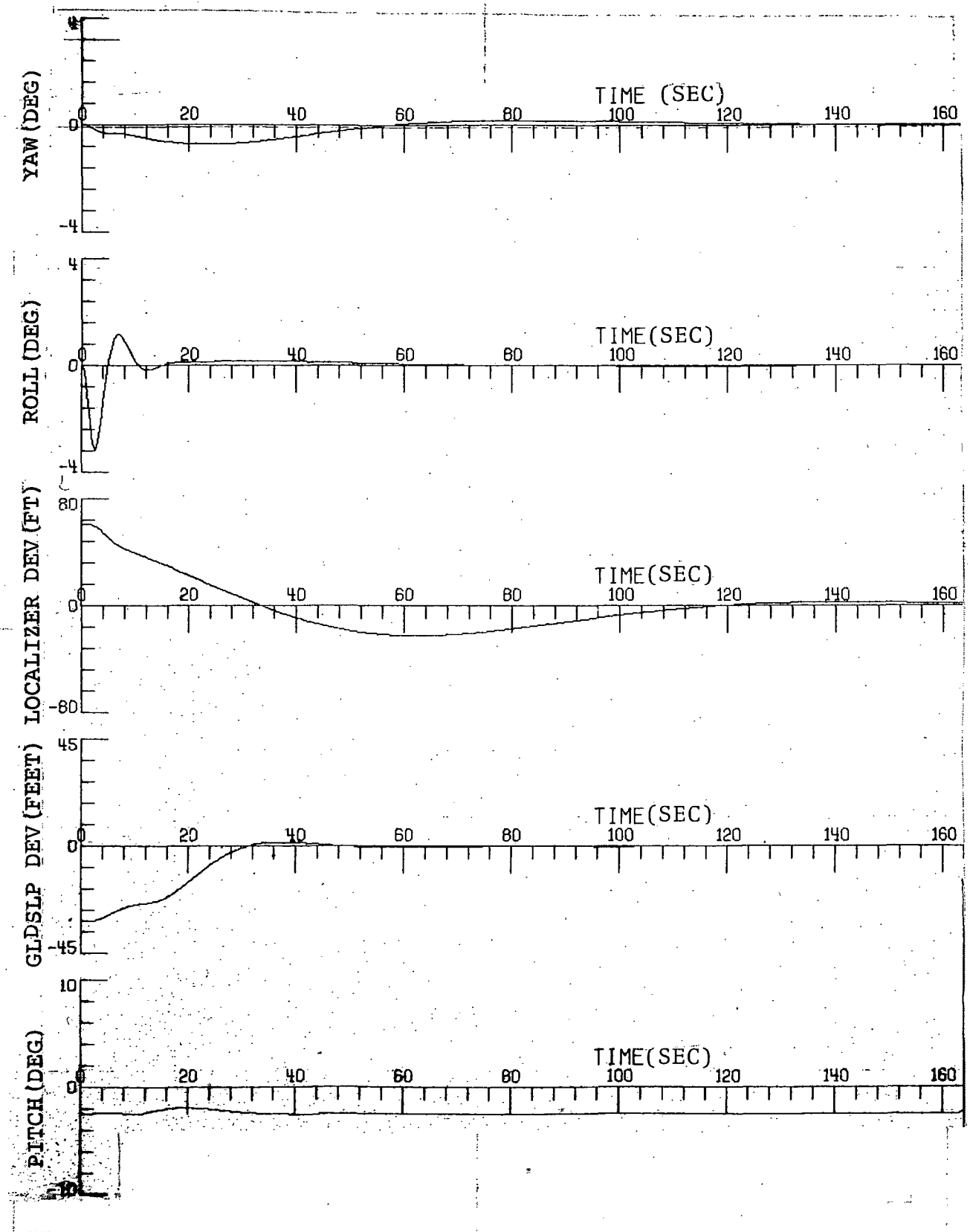

Figure 3-1. "A" Control System, Wind = 0, MLS Error = 0.

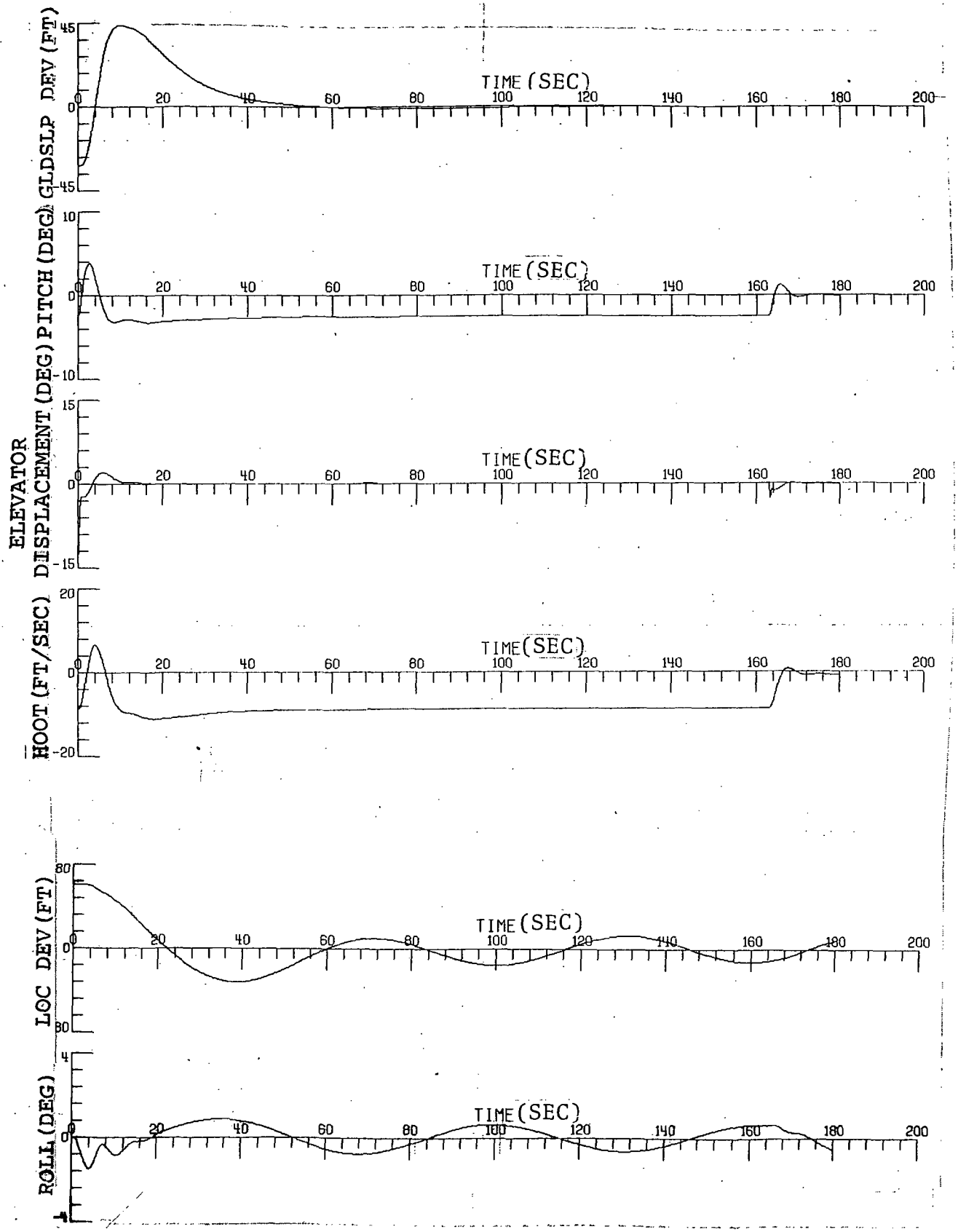

Figure 3-2. "C" Control System, Wind = 0, MLS Error = 0.

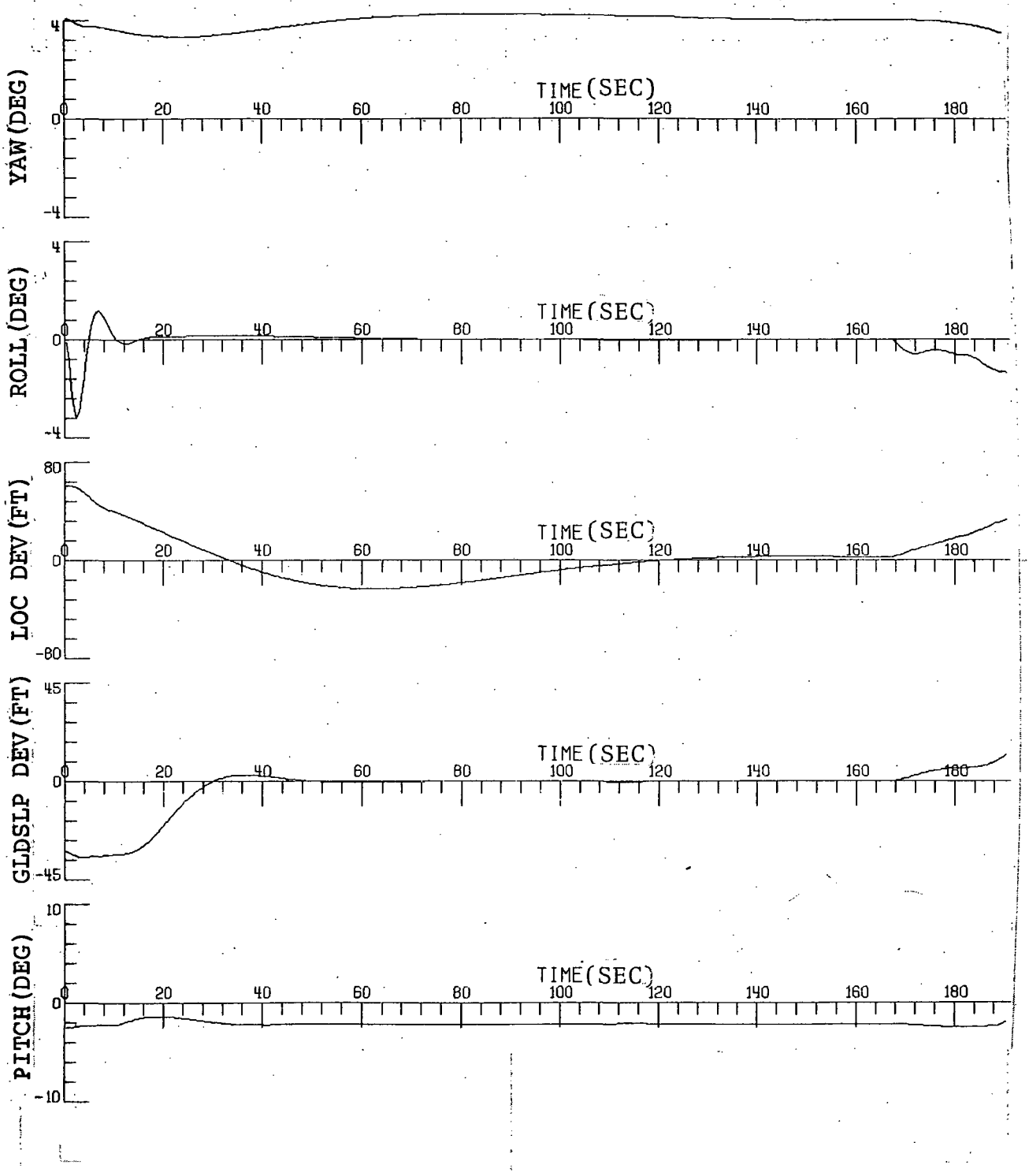

Figure 3-3. "A" Control System, Wind = 17.5 kts., MLS Error = 0.

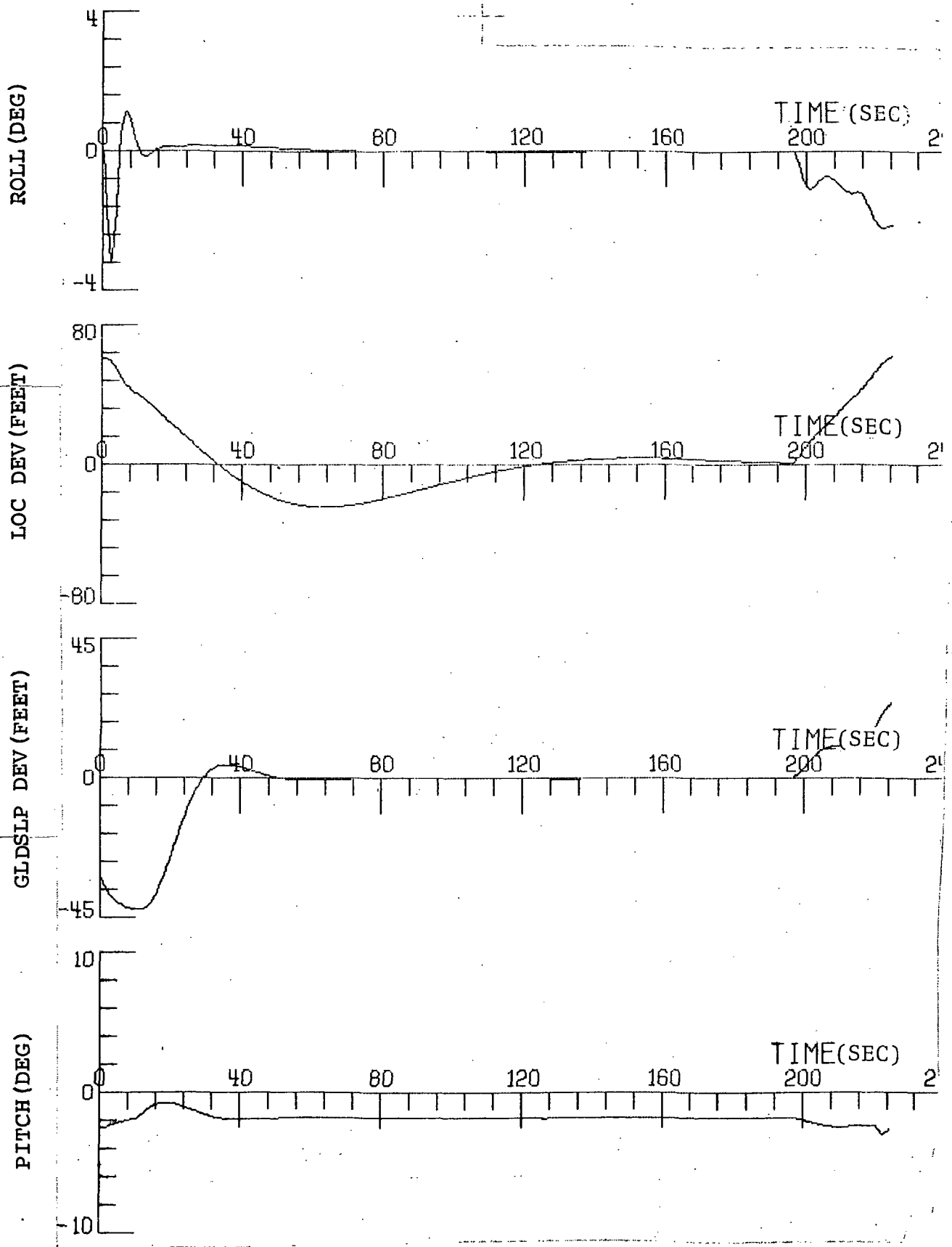

Figure 3-4. "A" Control System, Wind = 35 kts., MLS Error = 0.

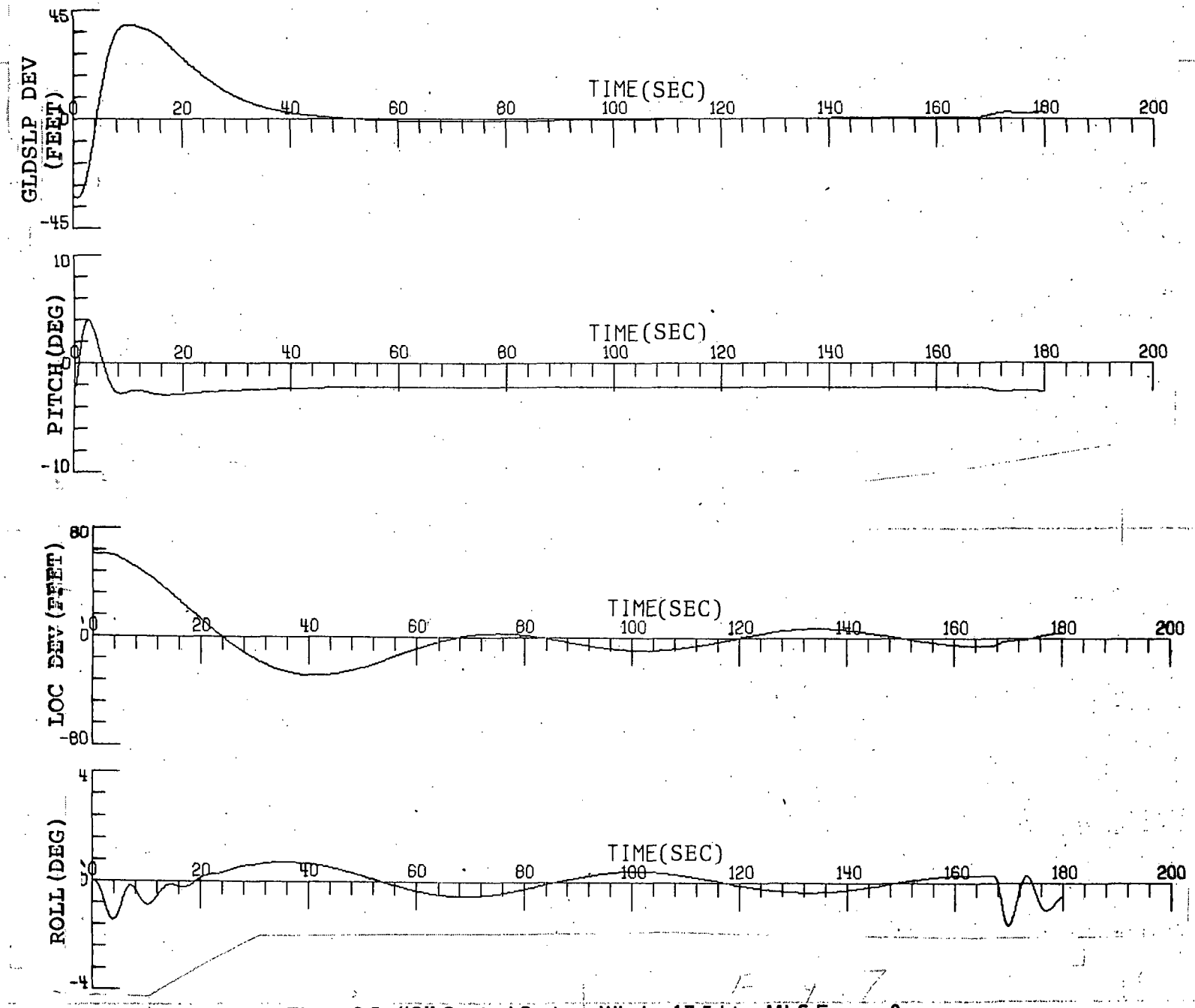

Figure 3-5. "C" Control System, Wind = 17.5 kts., MLS Error = 0.

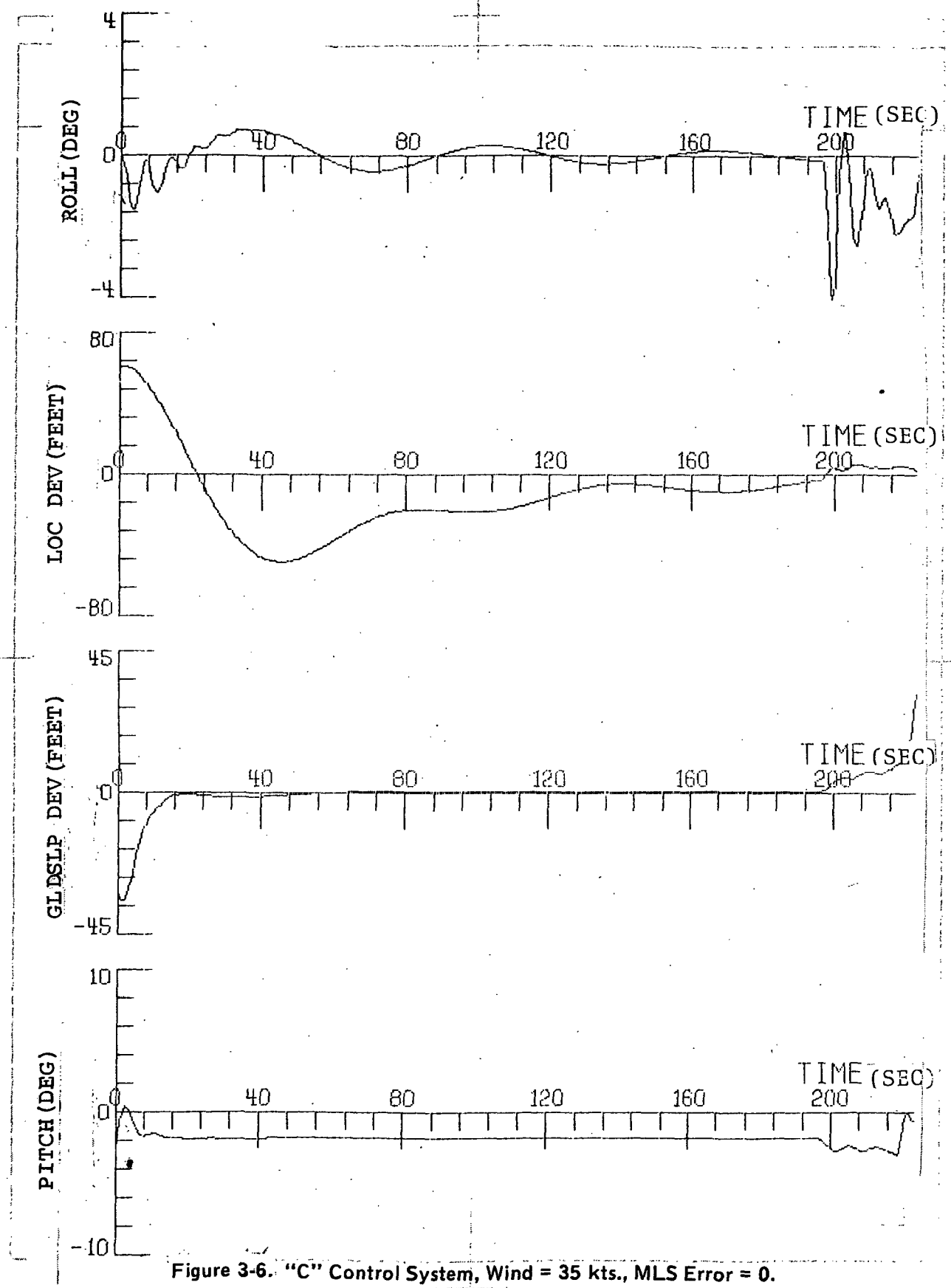

Figure 3-6. "C" Control System, Wind = 35 kts., MLS Error = 0.

Results obtained from the MLS models are shown in Figures 3-7 and 3-8. A parametric study was made on the effects of building location on the aircrafts ability to follow the glide-slope and localizer. The geometry of the situation is shown in Figure 3-9. Specular reflections occur approximately at the point of maximum angular error. The aircraft flies through this point in several seconds. However, there is still considerable variation about the specular point. As is expected, the specular point changes as the building geometry changes.

In addition to discrete multipath error, an analysis was made on the random error components. It was assumed that these error components were Gaussian distributed with variances equal to RTCA requirements for CAT. III K configuration. In the program the correlation time for both localizer and glideslope were vaired. The results are shown in Figures 3-10 to 3-15. As was expected the "C" control system was far less susceptible to MLS errors than the "A" system. The "A" system, however, which might be more typical of the type of control system employed with MLS, is more sensitive to certain correlation times. This clearly demonstrates the need to investigate the statistical nature of the MLS errors.

An important observation that should be noted is that the errors resulting from discrete multipath are non-stationary. Qualitatively, a stationary time series is one which is in statistical equilbrium, whereas, a non-stationary series is such that its properties change with time. Series occurring in nature are usually one of three kinds. First are those which exhibit stationary properties over long periods, for example outputs from noise generators. Second are those which are reasonably stationary over short periods, for example, measurements of atmospheric turbulence. Finally, there are series which are obviously non-stationary in the sense that their visual properties are continuously changing with time. An example of such is the discrete multipath case. Section 7.2 discusses this in more detail.

Most methods of dealing with non-stationary time series are based on techniques for removing or filtering out the non-stationary part, leaving behind a series which can be treated as stationary. It is this fact which clearly demonstrates the utility of the present program. The non-stationary errors can be conveniently generated for many different airport environments. Different filtering schemes can be digitally tested before they are breadboarded and used upon an actual aircraft.

Presently the program considers only straight-in approaches with a single building causing the interference. However, it is easily imagined that several buildings coupled with a curved approach will lead to considerably different error characteristics than those presented here. The program can be changed without great difficulty to account for these cases. It is only by knowing and appreciating the statistical properties of the MLS errors that an adequate design can be made to minimize their effects. The ground work has been layed in this program so that it may be efficiently used as a test bed for all future design efforts.

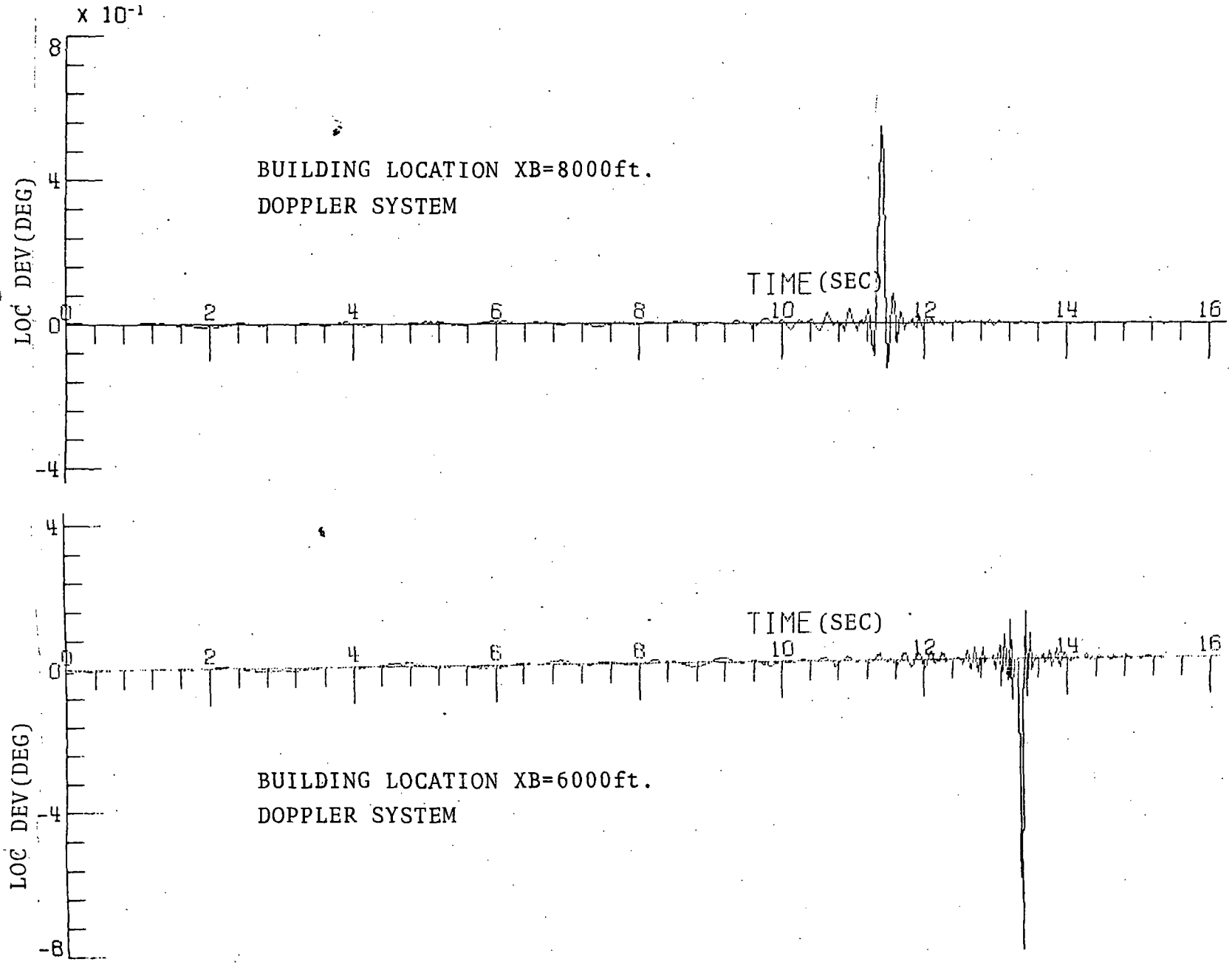

Figure 3-7. Angular Error as a Function of Building Location.

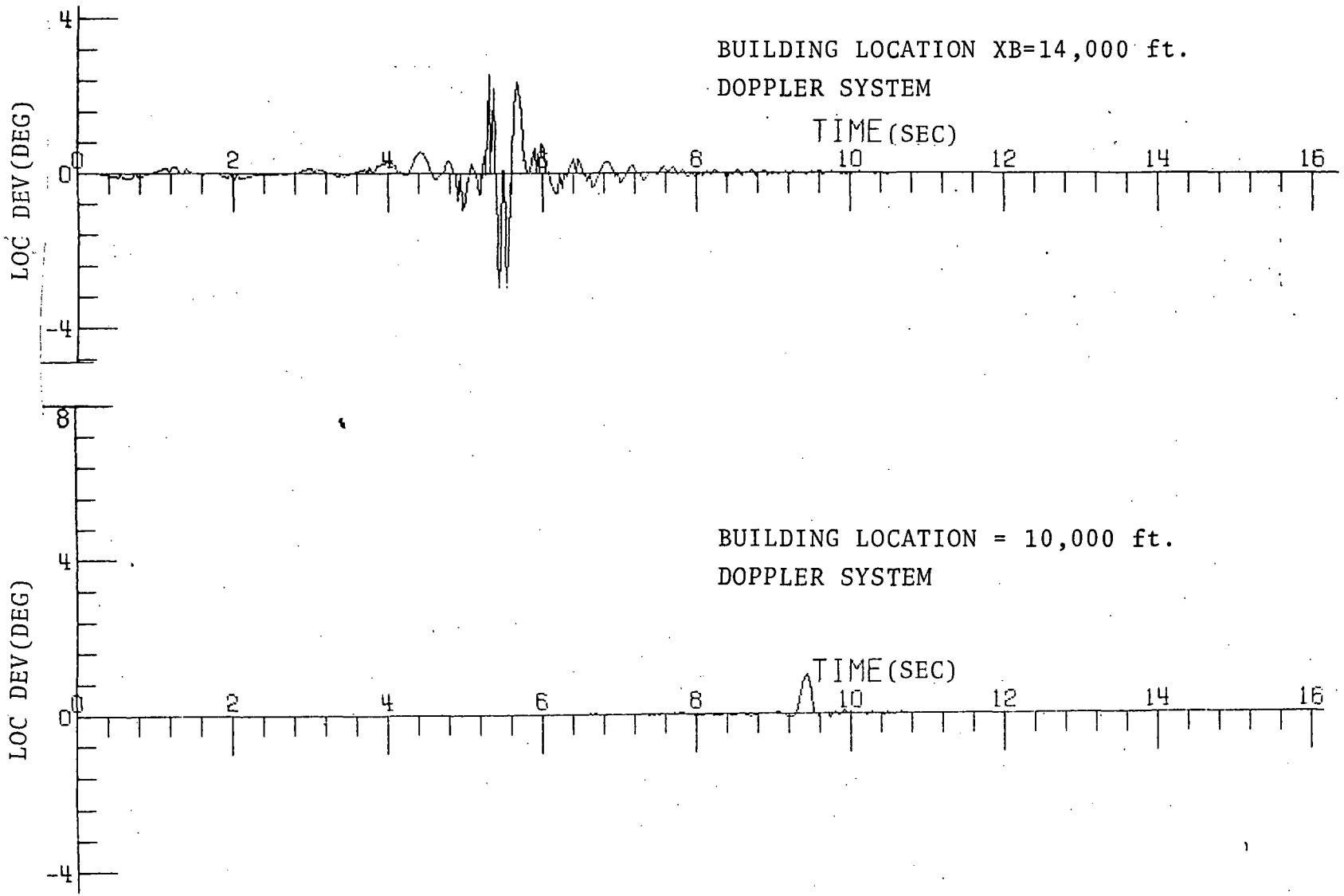

Figure 3-8. Angular Error as a Function of Building Location.

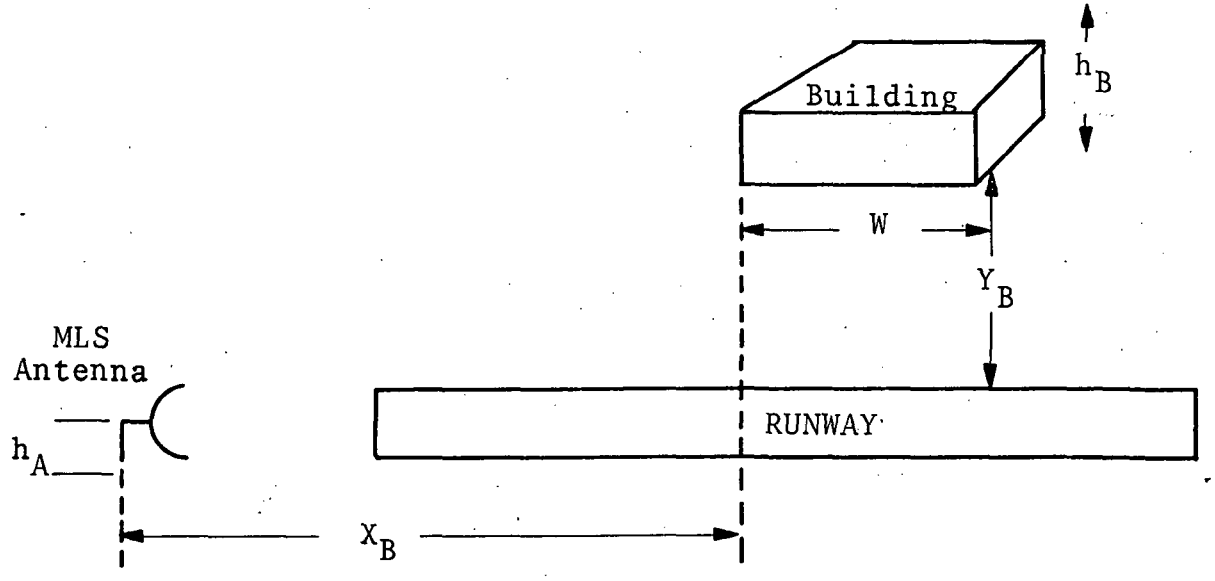

Figure 3-9. Airport Geometry.

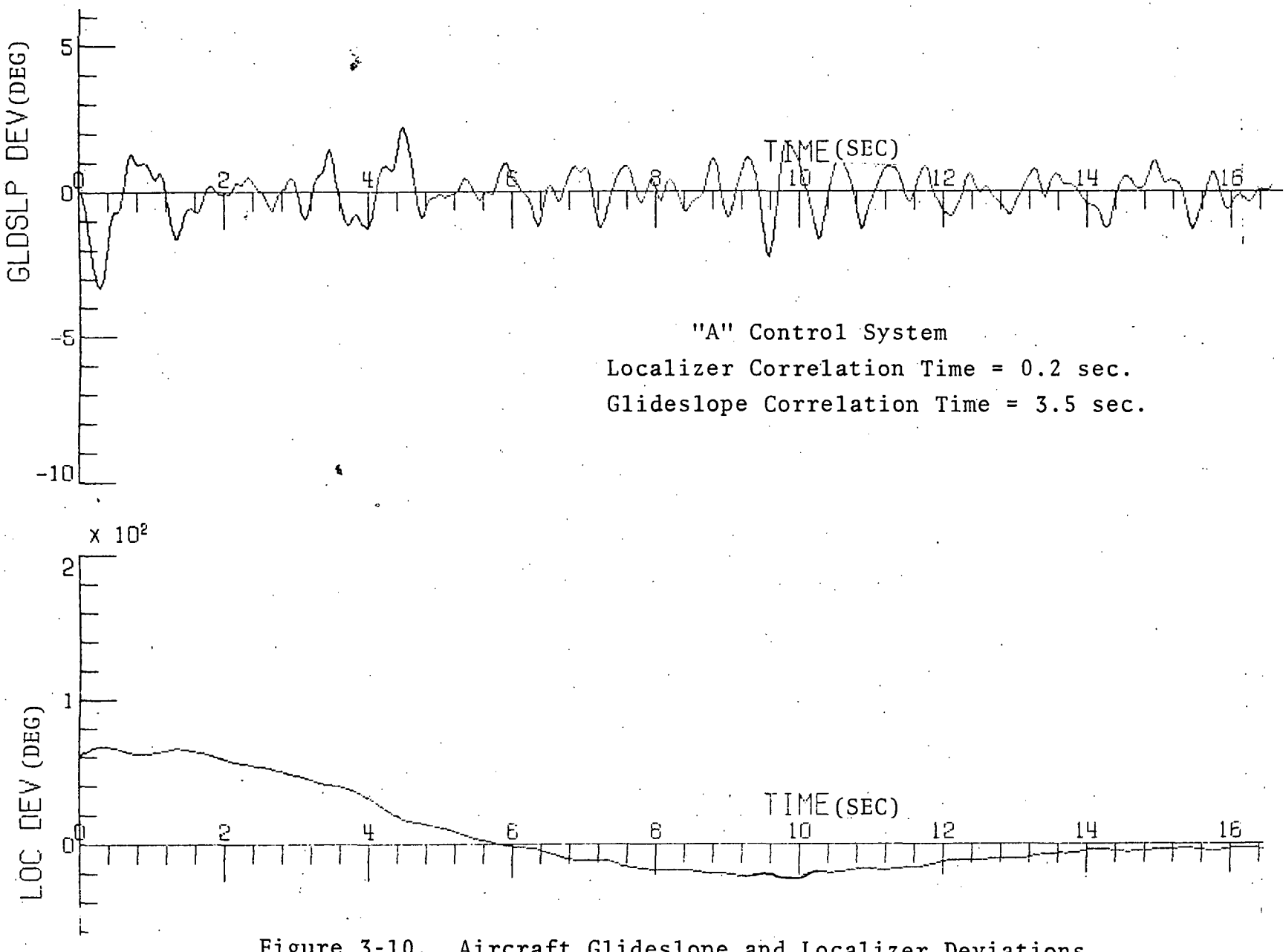

Figure 3-10. Aircraft Glideslope and Localizer Deviations as a Function of Correlation Time.

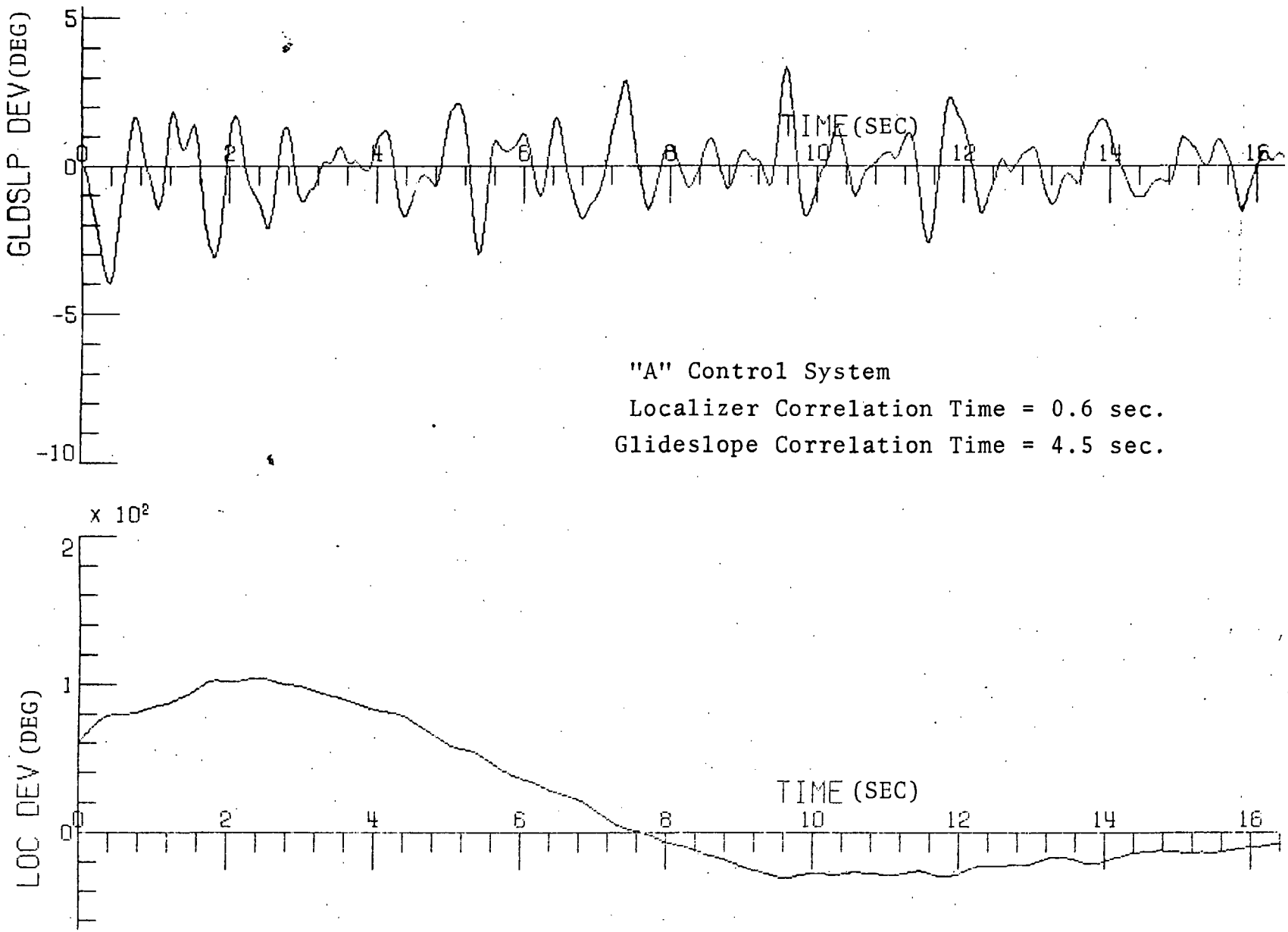

Figure 3-11. Aircraft Glideslope and Localizer Deviation as a Function of Correlation Time.

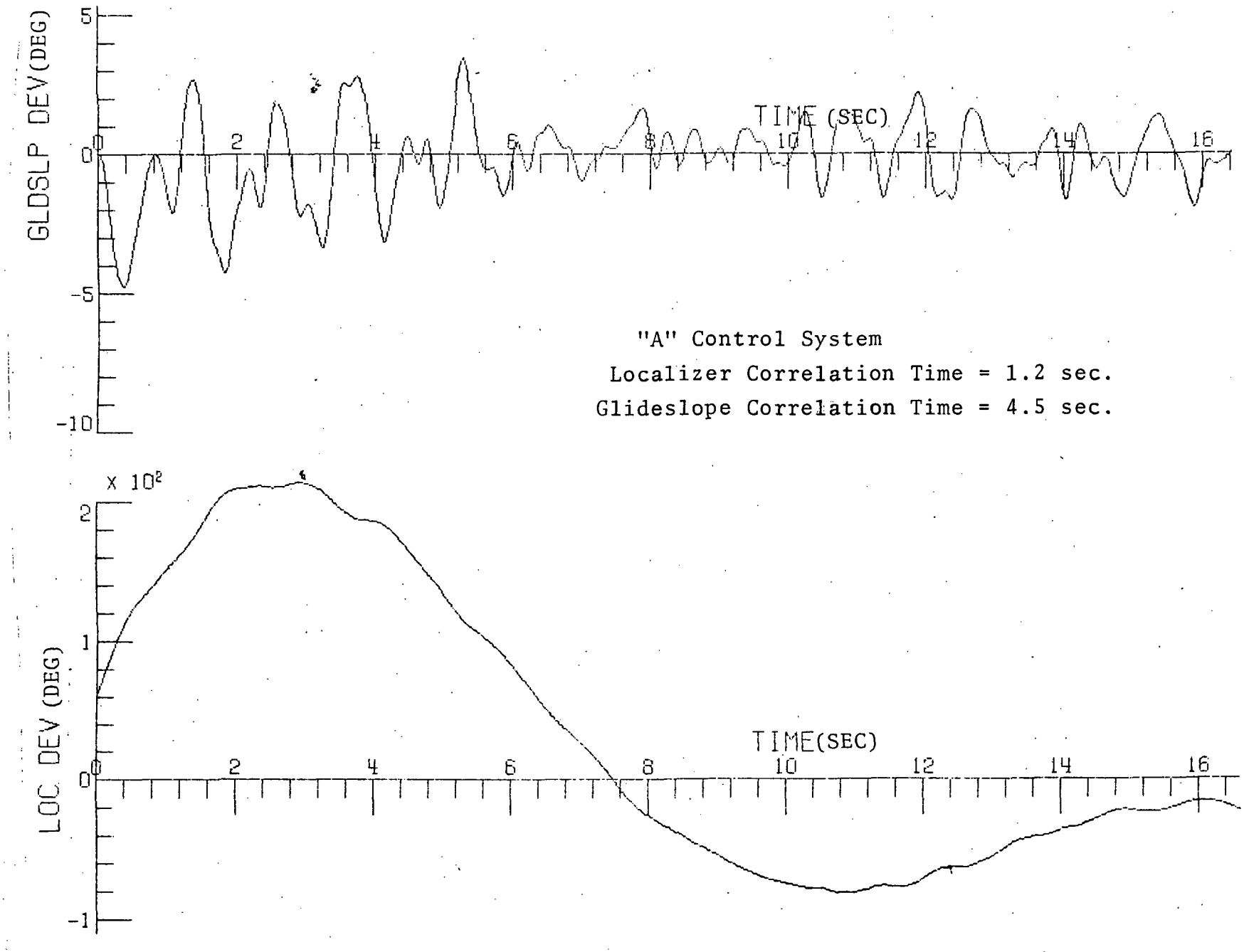

Figure 3-12. Aircraft Glideslope and Localizer Deviation as a Function of Correlation Time.

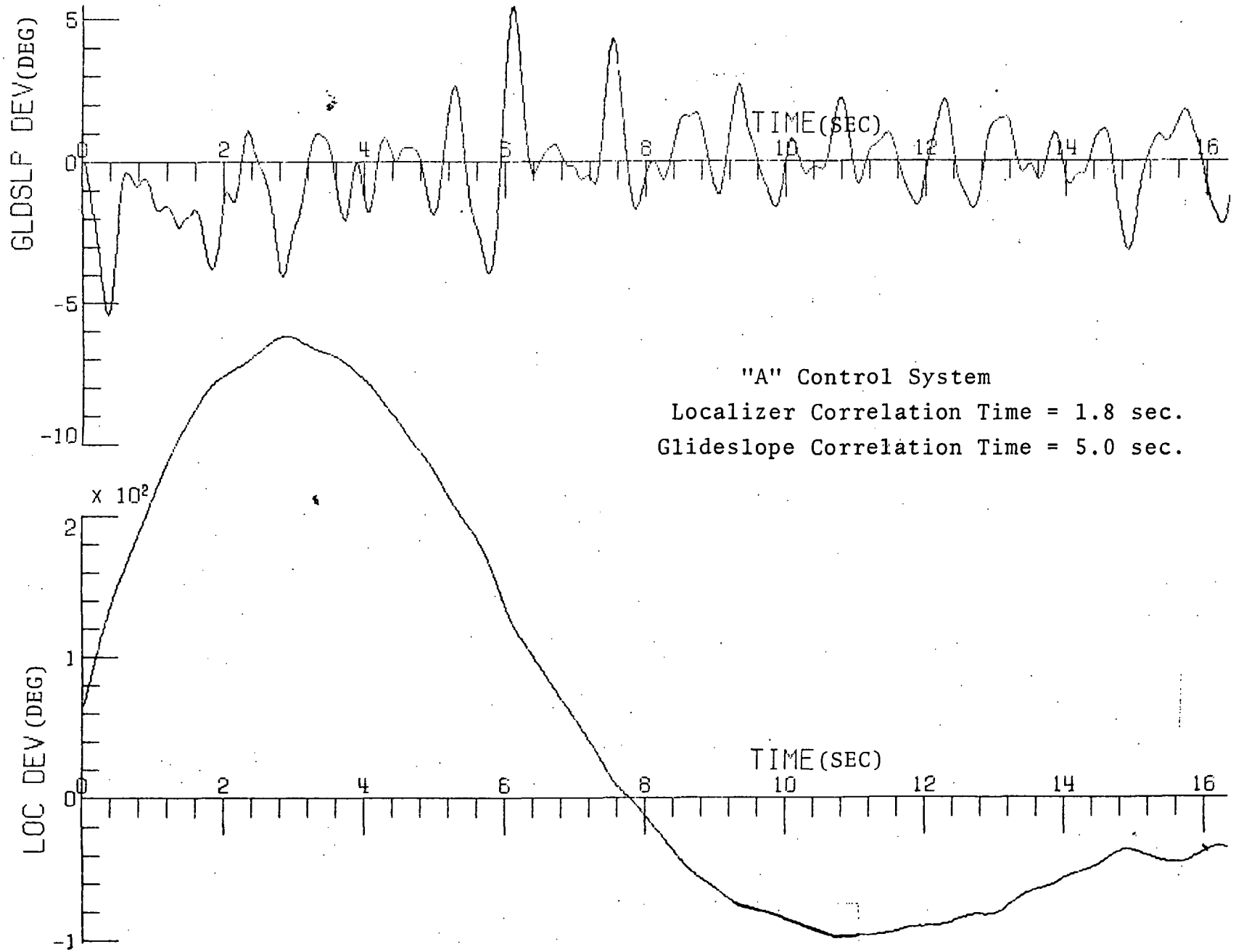

Figure 3-13. Aircraft Glideslope and Localizer Deviation as a Function of Correlation Time.

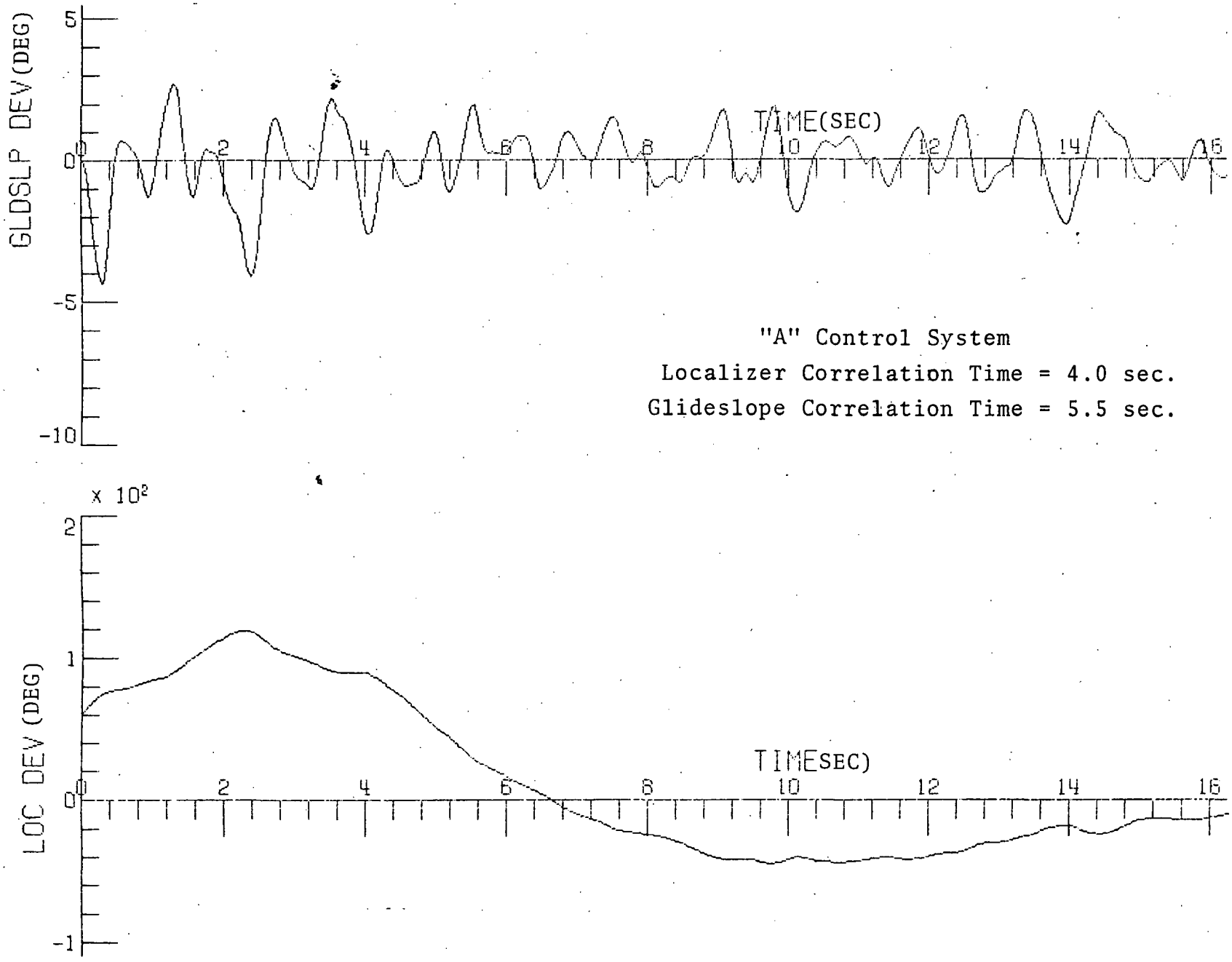

Figure 3-14. Aircraft Glideslope and Localizer Deviation as a Function of Correlation Time.

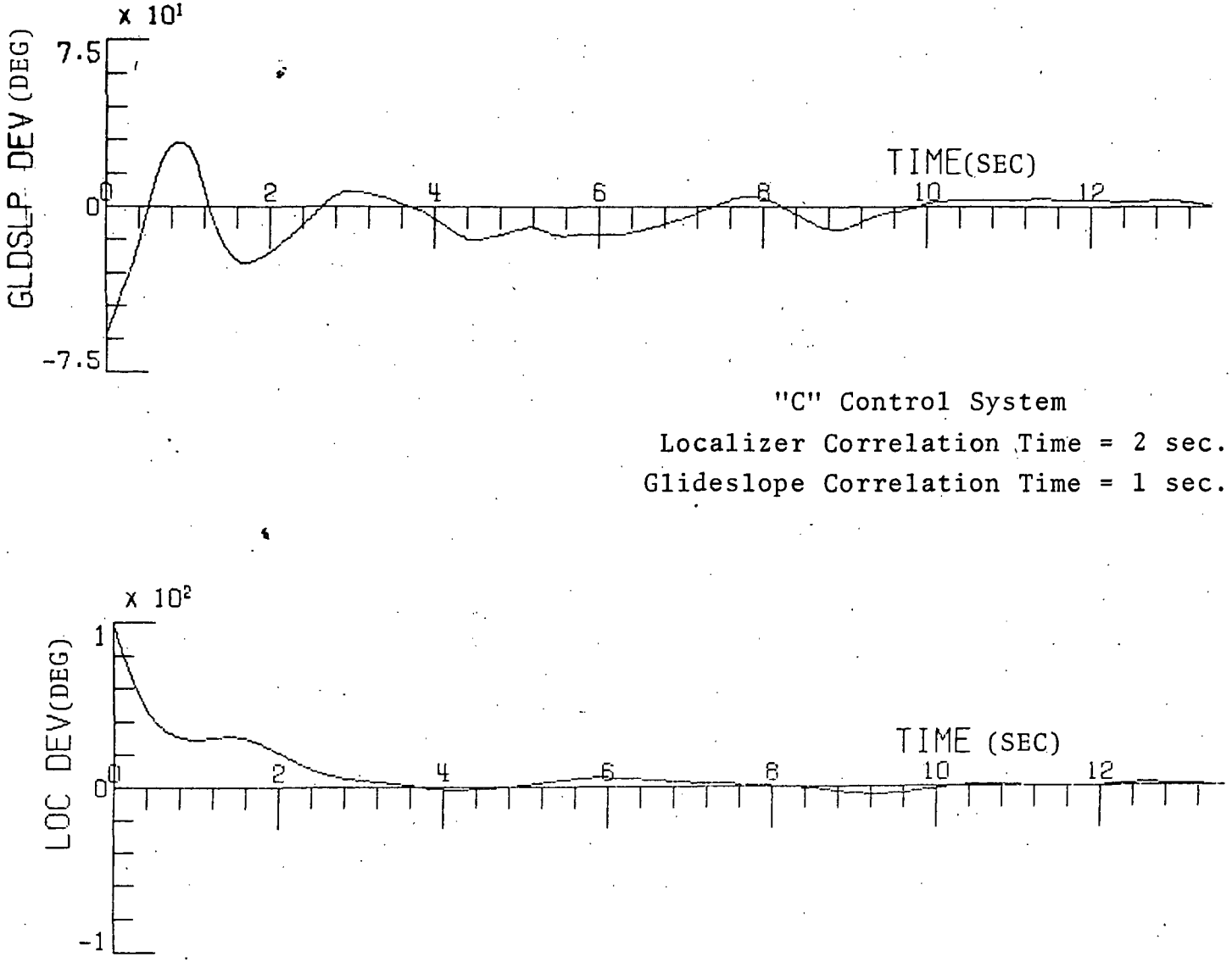

Figure 3-15. Aircraft Glideslope and Localizer Deviation as a Function of Correlation Time.

4.0 AIRCRAFT EQUATIONS OF MOTION

The general rigid-body equations of motion have been derived often in the literature (see Reference 1 and 2). The equations are valid with respect to an orthogonal set of axes fixed to the aircraft. For the purposes of the simulation, the convention adopted for the axes, Euler angles, and rates is shown in Figure 4-1.

The nonlinear equations are linearized by assuming that the aircraft is initially in equilibrium and any resulting changes are small. Therefore, the linear velocities U, V, and W can be expressed as:

$$U = U_o + u \qquad (4-1)$$

$$V = V_o + v \qquad (4-2)$$

$$W = W_o + w \qquad (4-3)$$

The angular velocities can be expressed as:

$$P = P_o + p \qquad (4-4)$$

$$Q = Q_o + q \qquad (4-5)$$

$$R = R_o + r \qquad (4-6)$$

where U_o, V_o, P_o, etc. are the equilibrium values and u,v,p, etc. are the changes in these values resulting from some disturbance.

The body axes used in the simulation are the stability axes which results in V_o and W_o being set equal to zero. In addition, the equilibrium values of aircraft roll, and yaw rates and aircraft roll attitude are considered zero. These assumptions, although not essential, simplify the equations of motion and do not introduce any loss of generality.

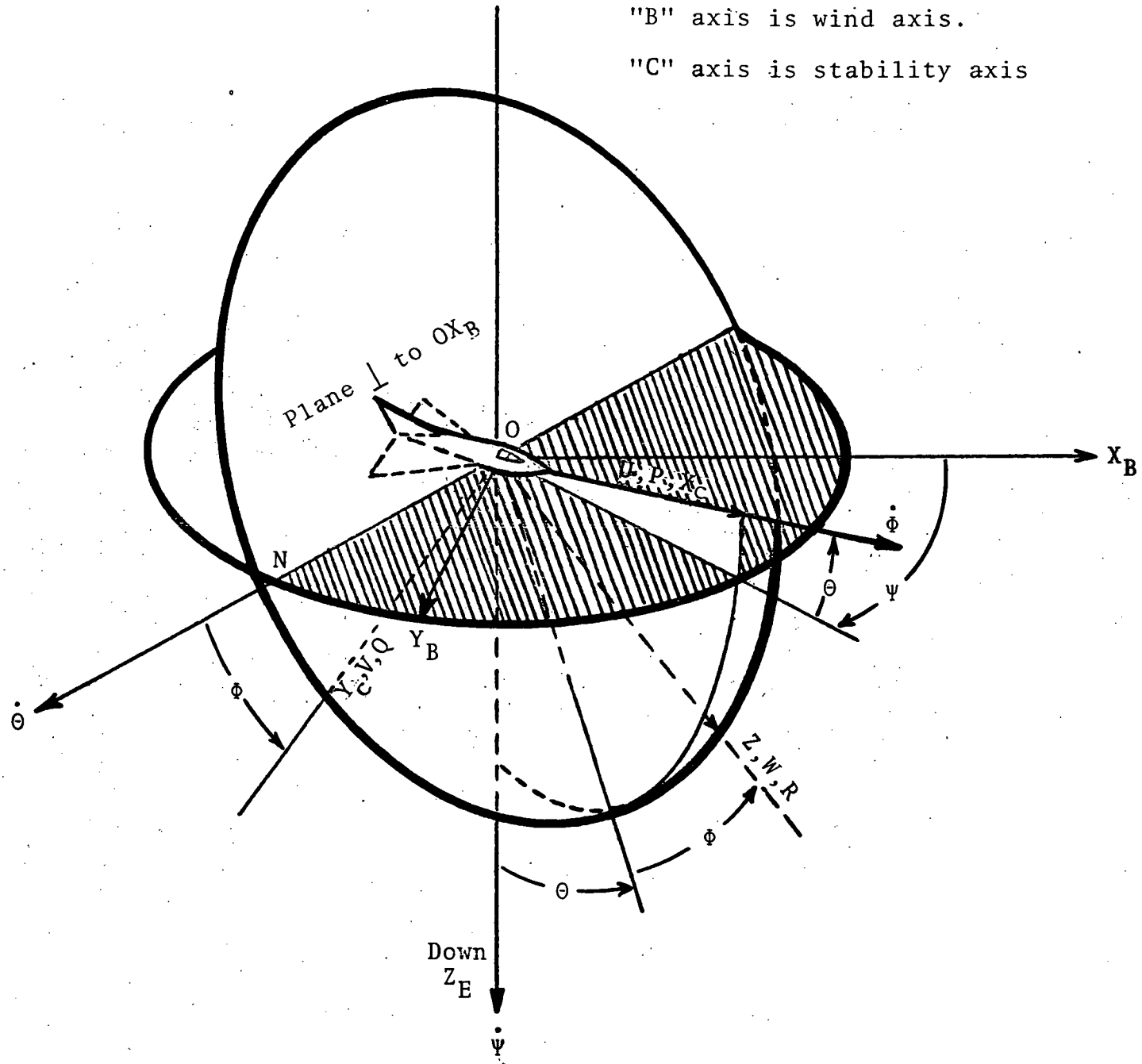

Figure 4-1. Aircraft and "B" and "C" Coordinate Systems.

The aircraft perturbed stability axis equations are as follows:[1]

LONGITUDINAL

TANGENTIAL-FORCE

$$\Sigma F_x = m\dot{V} \tag{4-7}$$

$$\frac{2m}{\rho SV}\dot{u} + \left[2C_D + M\frac{\partial C_D}{\partial M} - \frac{2}{\rho SV}\left(\frac{\partial T}{\partial V}\right)\right] u + \left[C_{D\alpha} - C_L\right]\alpha + \left[C_L\right]\theta = 0 \tag{4-8}$$

NORMAL-FORCE

$$\Sigma F_z = mV \tag{4-9}$$

$$\left[2C_L + M\frac{\partial C_L}{\partial M}\right] u + \left[C_{L\dot{\alpha}} + \frac{2M}{\rho SV}\right]\dot{\alpha} + \left[C_{L\alpha}\right]\alpha + \left[C_{L\dot{\theta}} - \frac{2M}{\rho SV}\right]\dot{\theta} + \left[C_{LS}\right]\delta_s = 0 \tag{4-10}$$

PITCHING-MOMENT

$$\Sigma M = I_{yy}\ddot{\theta} \tag{4-11}$$

$$\left[M\frac{\partial C_M}{\partial M}\right] u + \left[C_{M\dot{\alpha}}\right]\dot{\alpha} + \left[C_{M\alpha}\right]\alpha - \left[\frac{I_{yy}}{q S\bar{c}}\right]\ddot{\theta} + \left[C_{M\dot{\theta}}\right]\dot{\theta} + \left[C_{M\delta_e}\right]\delta_e + \left[C_{MS}\right]\delta_s = 0 \tag{4-12}$$

LATERAL

SIDE-FORCE

$$\Sigma F_r = mV(\dot{\beta} + \dot{\psi}) \tag{4-13}$$

$$\left[-\frac{2M}{\rho SV}\right]\dot{\beta} + \left[C_{y\beta}\right]\beta + \left[C_{yp}\dot{\phi}\right] + \left[C_L\right]\phi + \left[C_{yr} - \frac{2M}{\rho SV}\right]\dot{\psi} + \left[C_{y\delta_r}\right]\delta_r + \left[C_{y\delta_\alpha}\right]\delta_\alpha + \left[C_{y\delta_s}\right]\delta_s = 0 \tag{4-14}$$

1. For a detailed discussion of the terms and conditions associated with these equations, the reader is referred to References 1, and 2.

YAWING-MOMENT

$$\Sigma N = I_{zz}\ddot{\psi} \tag{4-15}$$

$$[C_{N\beta}]\beta + [\frac{I_{xz}}{qSb}]\ddot{\phi} + [C_{np}]\dot{\phi} + [-\frac{I_{zz}}{qSb}]\ddot{\psi} + [C_{Nr}]\dot{\psi} + [C_{N\delta_r}]\delta_r$$

$$+ [C_{N\delta_a}]\delta_a + [C_{N\delta_s}]\delta_s = 0 \tag{4-16}$$

ROLLING-MOMENT

$$\Sigma L = I_{xx}\ddot{\phi} \tag{4-17}$$

$$[C_{\ell\beta}]\beta + [-\frac{I_{xx}}{qSb}]\ddot{\phi} + [C_{\ell p}]\dot{\phi} + [\frac{I_{xz}}{qSb}]\ddot{\psi} + [C_{\ell r}]\dot{\psi} + [C_{\ell\delta r}]\delta_r$$

$$+ [C_{\ell\delta_a}]\delta_a + [C_{\ell\delta_s}]\delta_s = 0 \tag{4-18}$$

The Stability Derivatives are given in Table 4-1.
The units of physical quantities are as follows.

Mass	→	slugs	Force	→	pounds
Distance	→	feet	Angles	→	radians
Time	→	seconds			

Table 4-1

C_L	
$2M/\rho SV$	1.8350
$2C_L + M\frac{\partial C_L}{\partial M}$	12.3500
$C_{L\dot{\alpha}}$	3.6700
C_{Lq}	5.9600
$C_{L\dot{\theta}}$	- .1890
C_{LS}	.2720
$2C_D + M\frac{\partial C_D}{\partial M} - \frac{2}{\rho SV}\frac{\partial T}{\partial V}$	.8900
$C_{D\alpha}$	.6200
Mu	.5620
$C_{M\alpha}$	0.0
$C_{M\dot{\alpha}}$	- 2.0600
C_{Mq}	- .1150
$C_{M\dot{\theta}}$	- .7050
C_{MS}	- 3.2600
$C_{M\delta_e}$	- 2.1400
$I_{yy}/qS\bar{c}$	1.6950

C_L	
$2M/\rho SV$	1.83500
$C_{y\beta}$	12.35000
C_{yp}	- 1.41000
C_{yr}	.05200
$C_{y\delta_r}$	.09300
$C_{y\delta_a}$	.40100
$C_{y\delta_{sp}}$	.02000
$C_{n\beta}$	- .13400
C_{np}	.26900
C_{nr}	- .01150
$C_{n\delta_r}$	- .08050
$C_{n\delta_a}$	- .20100
$C_{n\delta_{sp}}$	- .01720
I_{xz}/qSb	.02750
I_{zz}/qSb	- .00232
$C_{l\beta}$	.28100
C_{lp}	- .37800
C_{lr}	- .10500
$C_{l\delta_r}$	.11900
$C_{l\delta_a}$	.05700
$C_{l\delta_{sp}}$	.08000
I_{xx}/qSb	.20000
	.07920

The aircraft perturbed variables are calculated and added to the equilibrium values defined in the stability axes. To obtain the aircraft trajectory with respect to the runway, it is necessary to relate the stability axes to the earth-fixed coordinates. This is done using the following T matrix which rotates a vector from the earth-fixed axes to the stability axes.

$$T = \begin{vmatrix} \cos\theta\cos\Psi & \cos\theta\sin\Psi & -\sin\theta \\ \cos\Psi\sin\phi\sin\theta-\sin\Psi\cos\phi & \cos\Psi\cos\phi+\sin\Psi\sin\phi\sin\theta & \cos\theta\sin\phi \\ \sin\Psi\sin\phi+\cos\Psi\cos\phi\sin\theta & \sin\Psi\cos\phi\sin\theta-\cos\Psi\sin\phi & \cos\theta\cos\phi \end{vmatrix}$$

For the purposes of analysis it was necessary to calculate the characteristic roots for the 737 (stick fixed). For the longitudinal equations the following equation results.

$$S^4+1.204S^3+1.49S^2+.0867S+.0545=0 \qquad (4\text{-}19)$$

Which reduces to

$$(S^2+.0286S+.0385)(S^2+1.17S+1.41)=0 \qquad (4\text{-}20)$$

From this the following characteristic modes can be identified.

ζ_S	= .493		Short-period oscillation
ω_S	= 1.190	rad/sec	
ζ_p	= .073		Phugoid oscillation
ω_p	= .196	rad/sec	

The lateral equations of motion result in the following characteristic equation:

$$S^5+1.8S^4+2.17S^3+2.2S^2-.018S=0 \qquad (4\text{-}21)$$

which reduces to

$$S(S+1.32)(S-.008)(S^2+.48S+1.696)=0 \qquad (4\text{-}22)$$

The characteristic modes are identified as follows:

$S^2+.48S+1.696$

$\zeta_D = .188$

$\omega_D = 1.280$ rad/sec DUTCH ROLL

$S+1.32$ ROLL SUBSIDENCE

$S-.008$ SPIRAL DIVERGENCE

References

(1) Blakelock, J.H.; "Automatic Control of Aircraft and Missiles", John Wiley & Sons, 1965.

(2) Etkin, Bernard; "Dynamics of Atmospheric Flight", John Wiley & Sons, 1972.

5.0 ATMOSPHERIC MODELS

Two of the most critical obstacles affecting an aircrafts ability to land successfully are poor visibility and atmospheric conditions or wind. The wind can be considered as being composed of a deterministic component and a random component (wind gusts). Both of these components are considered in the simulation. The models used are described in the following sections.

5.1 Deterministic Wind Model

The deterministic components of wind are comprised of steady winds and wind shear. It has been shown that the shear wind has a mean structure which is not uniform in space; thus, there can be spatial gradients in the time-averaged velocity. The vertical extent of the boundary layer in strong winds depends in great part on the roughness of the underlying terrain. Typically it is several hundred feet.

A model for shear wind takes the following form;

$$W = kh^n \tag{5-1}$$

where W is the wind velocity, k is a constant, h is the height above the ground and n is a constant which depends upon the terrain. Normally, a reference altitude of 50 feet is used to define steady wind. The mean wind at any other altitude is a function of the wind shear profile. When this representation is used the above equation is modified as follows:

$$W_i = W_o \left(1+n \log \frac{hi}{ho}\right) \tag{5-2}$$

Where W_o is the mean reference wind and h_o is the reference altitude. Over a smooth ocean n is approximately 0.16 whereas over a city with many tall buildings n is approximately 0.4.

For the simulation a "worst-case" wind profile was defined by setting n = 0.5 and W_o = 25 knots. In addition, a straight-line approximation was used for the power law variation in wind. It is felt that this approximation preserves the major characteristics of the empirically derived shear profile. A plot of wind shear is shown in Figure 5-1. The piecewise linear approximation used for wind shear is

$W = 34$ knots for $h > 200$ feet

$W = .04\ h + 24.5$ for 100 feet $< h < 200$ feet

$W = .08\ h + 21.0$ for $h < 100$ feet.

The headwinds and crosswinds are chosen as the worst-case mean reference winds, i.e., headwind = 25 knots. The angle that the wind makes with reference to the runway is an option that can be specified.

In addition, the program has been designed so that the user may specify a percentage of worst-case wind. That is, it is possible to vary the effects of wind from no wind to worst case.

The effect of the wind is to change the aircraft forward velocity and to perturb the slideslipe and angle of attack. That is, variables $'u_W$ β_W, and $'\alpha_W$ can be defined as follows:

$$'u_W = \frac{u_W}{U_o} = \text{normalized wind in the X direction}$$

$$\beta_W = \frac{v_W}{U_o} = \text{sideslipe produced by wind in the Y direction}$$

$$'\alpha_W = \frac{w_W}{U_o} = \text{angle of attack resulting from wind in the Z direction.}$$

where u_W, v_W, and w_W are the perturbed wind components in the X, Y, and Z directions respectively, and U_o is the equilibrium velocity in the X direction.

The perturbed quantities due to the wind are then added into the equations of motion for the aircraft. The airspeed input into the aircraft velocity control system is also modified. Without wind, it was attempting to drive 'u to zero. With wind, it attempts to drive $'u + 'u_W$ to zero.

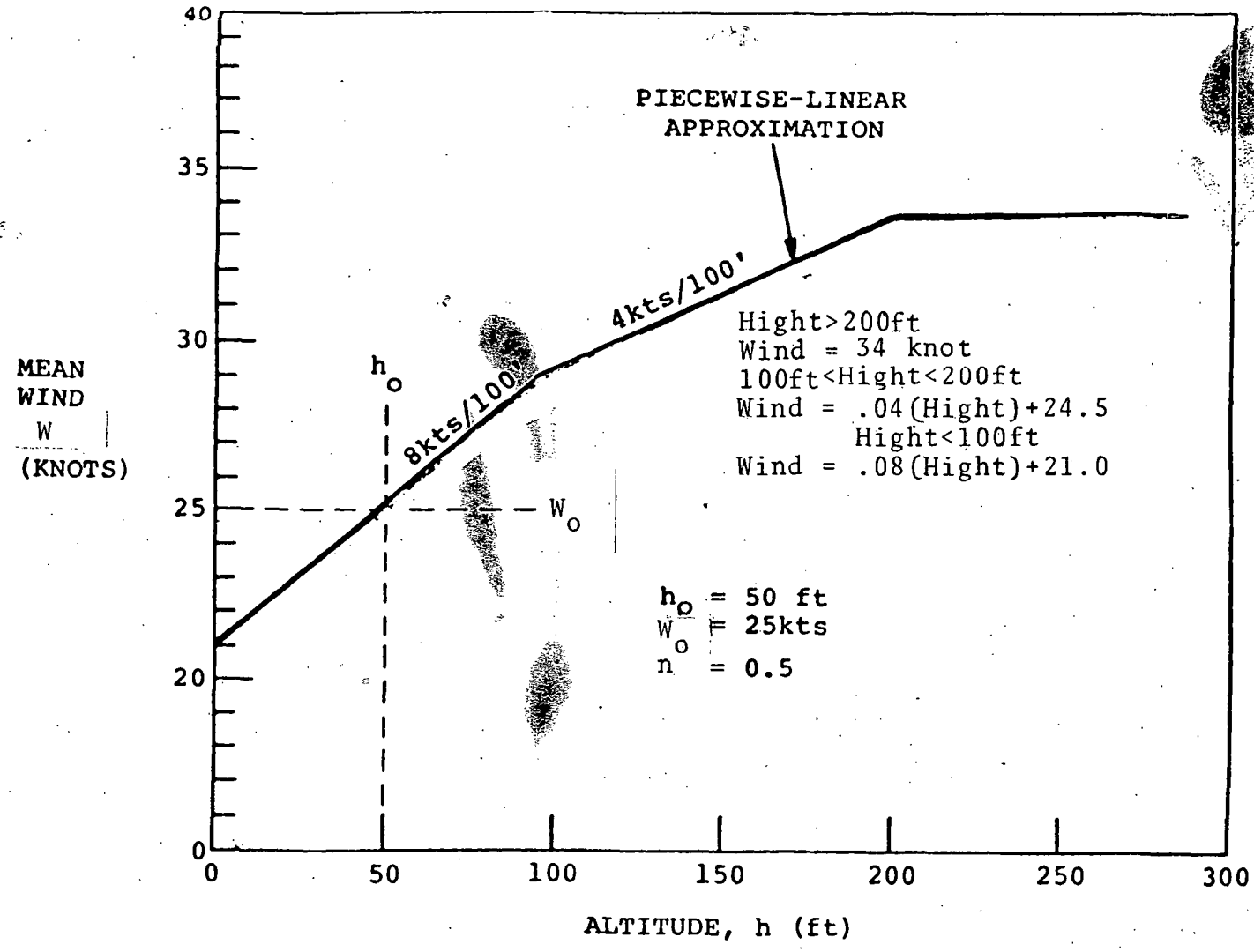

Figure 5-1. Wind Shear Profile

5.2 Gust Wind Model

Wind gusts are random and must be modeled in terms of their appropriate statistical characteristics. The gust wind models used in the final approach to landing digital simulation are discussed in the following paragraphs.

Several investigators have conducted extensive measurementsprograms and have determined the statistical properties (in particular the autocorrelation function and the power spectral density) associated with gust wind components. The specific gust wind model described herein is based on the work performed by Dryden.[1]

For the landing simulation, the basic approach used in simulating wind gusts is to generate numerically a finite sequence of random variables having the statistical properties of a set of uniformly spaced samples of a stationary Gaussian process with an autocorrelation function or a power spectral density which corresponds to that which is associated with wind gusts. It is assumed that the process which is sampled has zero mean and a power spectrum $P(\omega^2)$ which is rational and of order K in ω^2. The method described here requires either the correlation function or the power spectrum of the sampled time series.

5.2.1 Theoretical Background

The basic idea of the procedure described here is to calculate the transfer function H(Z) of a linear filter which would convert white noise into noise with a specified correlation function $\phi(m)$, and then to use H(Z) expressed as a recursion relationship to compute y(n) from u(n) where u(n) is a sequence

of independent Gaussian variables with mean zero and variance one. For the filter $H(Z)$ to generate a stationary random output it must be operating in the "steady state." That is, it must have had an input of white noise for all $n \geq -\infty$. For computational purposes, however, the input sequence must begin at $n = 0$. It is necessary therefore to provide the correct "initial conditions" by generating K values of $y(n)$ for $0 \leq n \leq k - 1$, by a special method so that these K values together with the corresponding values of $u(n)$ have the same covariance matrix as if the filter were operating in the steady state. This is done by replacing the effect of the input sequence for $n < 0$ by K auxiliary random variables, ξ, which are generated from the auxiliary independent variables $v(i)$.

It is necessary to have $\Phi(Z)$, the sampled power spectrum corresponding to $\phi(m)$.

$$\Phi(Z) = \sum_{m=-\infty}^{\infty} \phi(m)\, Z^{-m} \tag{5-3}$$

$H(Z)$ is determined by:

$$\Phi(Z) = H(Z)\, H(Z^{-1}) \tag{5-4}$$

By breaking up $H(Z)$ in the above manner it is possible to identify the stable and unstable portions. $H(Z)$ has all its poles with the unit circle Γ and $H(Z^{-1})$ has all its poles outside. There are alternate forms for $H(Z)$ depending upon how the poles of $\Phi(Z)$ are associated with $H(Z)$ and $H(Z^{-1})$.

Once $H(Z)$is determined then:

$$H(Z) = \sum_{n=0}^{\infty} h(n)\, Z^{-n} \tag{5-5}$$

where h(n) is obtained by expanding H(Z) in long division. Only the first K values of h(n) are required. It is still necessary however to calculate the initial conditions for y(n). The recursive equation for y(n) is:

$$y(n) = \sum_{m=0}^{\infty} h(m)\, x\,(n-m) \qquad (5\text{-}6)$$

where x(n) represents the input to the filter, then

$$y(0) = \sum_{m=0}^{\infty} h(m)\, x(-m) = h(0)\, x(0) + \xi_0$$

$$\xi_0 = \sum_{m=1}^{\infty} h(m)\, x(-m)$$

$$y(n) = \sum_{m=0}^{n} h(m)\, x(n-m) + \xi_n \quad n \leq K-1$$

$$\xi_n = \sum_{m=1}^{\infty} h(n+m)\, x(-m), \qquad 0 \leq n \leq K-1$$

ξ_n represents the influence of all x(n) for n < 0. If the correlation function of x(n) is known then the covariance matrix of the ξ_i can be obtained, and once the covariance matrix is known we can then simulate the effect of x(n) for n < 0.

The covariance matrix can be obtained as follows:

$$R_{00} = E[\xi_0 \xi_0] = E\left[\sum_{m=1}^{\infty} h(m)x(-m) \sum_{m=1}^{\infty} h(m)x(-m)\right]$$

$$= \sum_{m=0}^{\infty} h^2(m) - h^2(0)$$

$$= \phi(0) - h^2(0)$$

$$R_{11} = \phi(0) - [h(0)]^2 - [h(1)]^2$$

$$R_{10} = \phi(1) - h(1)h(0)$$

After calculating the covariance matrix of the K random variables ξ_i, appropriate sample values of the variables can be obtained by linearly transforming K auxiliary independent Gaussian variables v(i) as follows

$$\xi_i = \sum_{j=0}^{i} C_{ij} V(j)$$

The C_{ij} are calculated as follows

$$\xi_0 = C_{00} V(0)$$

$$E[\xi_0 \xi_0] = E[C_{00} V(0) C_{00} V(0)]$$

$$= E[C_{00}^2 V(0)] = R_{00}$$

$$C_{00} = \sqrt{R_{00}}$$

$$\xi_1 = C_{10} V(0) + C_{11} V(1)$$

$$R_{11} = E[\xi_1 \xi_1] = E\left\{[C_{10} V(0) + C_{11} V(1)]\ [C_{10} V(0) + C_{11} V(1)]\right\}$$

$$R_{11} = C_{10}^2 + C_{11}^2 \qquad C_{11} = \sqrt{R_{11} - C_{10}^2}$$

C_{10} is given by $C_{10} = \dfrac{R_{10}}{C_{00}}$

And Finally

$$H(Z) = \frac{Y(Z)}{U(Z)} = \frac{a_0 + a_1 Z^{-1} + \ldots + a_k Z^{-k}}{1 + b_1 Z^{-1} \quad \ldots + b_k Z^{-k}}$$

results in

$$y(n) = -b_1 y(n-1) \ldots - b_k y(n-K) + a_0 u(n)$$
$$+ a_1 u(n-1) \ldots + a_k u(n-K)$$

5.2.2 Recursive Formulation for the Dryden Spectrum

Given the following power spectrum density for Gust in the u, v, w direction:

$$(1)\quad \Phi_u(\omega) = \sigma_u^2 \frac{2VL_u}{\Pi} \frac{1}{V^2+(L_u\omega)^2} \tag{5-7}$$

$$(2)\quad \Phi_v(\omega) = \sigma_v^2 \frac{VL_v}{\Pi} \frac{V^2+3(L_v\omega)^2}{[V^2+(L_v\omega)^2]^2} \tag{5-8}$$

$$(3)\quad \Phi_w(\omega) = \sigma_w^2 \frac{VL_w}{\Pi} \frac{V^2+3(L_w\omega)^2}{[V^2+(L_w\omega)^2]^2} \tag{5-9}$$

The $\Phi(\omega)$ were defined such that the standard deviation was given as:

$$\Psi(o) = \sigma^2 = \int_0^\infty \Phi(\omega)\, d\omega.$$

However the $\Psi(\tau)$ were defined by the following formula:

$$\Psi(\tau) = \frac{1}{2\Pi} \int_{-\infty}^{\infty} \Phi(\omega) e^{j\omega\tau} d\omega.$$

Thus, it is necessary to multiply the resulting power spectral density by Π.

Lets consider Equation (5-7) first and make the following changes in variables:

$$a = \frac{V}{L_u};$$

$$\Phi(\omega) = \sigma^2 \frac{2V/L_u}{V^2/L_u{}^2+\omega^2}; \quad K_u = \sigma_u^2$$

This then leads to the following $\Psi(\tau)$ where $\Psi(\tau)$ is the auto correlation function:

$$\Psi(\tau) = K_u e^{-a|\tau|}$$

The correlation function of the sampled time series $\phi(m)$ to be simulated:

$$\phi(m) = K_u \, e^{aT|m|}$$

$$\phi(Z) = \sum_{m=-\infty}^{\infty} K_u \, e^{-aT|m|} Z^{-m}$$

$$= K_u \left\{ \sum_{m=-\infty}^{0} e^{aTm} Z^{-m} + \sum_{m=0}^{\infty} e^{-aTm} Z^{-m-1} \right\}$$

$$\Phi(Z) = [K_u] \left[\sum_{m=0}^{\infty} (AZ)^m + \sum_{m=0}^{\infty} \left(\frac{A}{Z}\right)^m - 1 \right]$$

$$\Phi(Z) = [K_u] \frac{(1-A^2)}{(1-AZ^{-1})(1-AZ)}$$

where

$$A = e^{-aT}$$

$$\Phi(Z) = \sqrt{K_u} \frac{\sqrt{1-A^2}}{(1-AZ^{-1})} \cdot \sqrt{K_u} \frac{\sqrt{1-A^2}}{(1-AZ)}$$

Let

$$H(Z) = \sqrt{K_u} \frac{\sqrt{(1-A^2)}}{1-AZ^{-1}}$$

$$h(0) = \sqrt{K_u(1-A^2)}$$

$$C_{00} = \sqrt{\phi(0) - h^2(0)}$$

$$C_{00} = \sqrt{K_u - K_u(1-A^2)} = A\sqrt{K_u}$$

$$\xi_0 = A\sqrt{K_u} \; V(0)$$

$$y(0) = h(0) \; X(0) + \xi_0$$

$$y(0) = \sqrt{K_u(1-A^2)}u(0) + A\sqrt{K_u} \; V(0)$$

$$y(n) = \sqrt{K_u(1-A^2)}u(n) + Ay(n-1)$$

Next consider Equation (5-8)

$$\Phi_V(\omega) = \sigma_V^2 L_V \frac{1+3(L_V\omega)^2}{[1+(L_V\omega)^2]^2}$$

Letting $K_V = \frac{3\sigma_V^2 V}{L_V}$; $\quad b = \frac{V}{L_V}$

results in the following:

$$\Phi_V(\omega) = K_V \frac{(b^2/3+\omega^2)}{(b^2+\omega^2)^2}$$

The autocorrelation is

$$\Psi(\tau) = \frac{K_V}{2\pi} \int_{-\infty}^{\infty} \frac{(b^2/3+\omega^2)}{(b^2+\omega^2)^2} \cos \omega\tau d\omega$$

After considerable manipulation the following results:

$$\Psi(\tau) = K_V \begin{cases} \frac{-e^{-\tau b}}{6b} [b\tau - 2]; & \tau > 0 \\ \frac{-e^{\tau b}}{6b} [b\tau + 2]; & \tau < 0 \end{cases}$$

$$\phi(m) = K_V \begin{cases} \frac{-e^{-mTb}}{6b} [bmT - 2]; & m > 0 \\ \frac{e^{mTb}}{6b} [bmT + 2]; & m < 0 \end{cases}$$

$$\Phi(Z) = \sum_{m=-\infty}^{\infty} \phi(m) Z^{-m}, \quad \text{Let } B = e^{-Tb}$$

$$= K_V \left\{ \sum_{m=-\infty}^{0} Z^{-m} \frac{e^{mTb}}{6b} [bmT+2] + \sum_{m=0}^{\infty} \frac{-e^{-mTb}}{6b} Z^{-m} [bmT-2] - \frac{1}{3b} \right\}$$

$$\Phi(Z) = K_V \left\{ -\frac{T}{6} \sum_{n=0}^{\infty} n(Ze^{-Tb})^n + \frac{1}{3b} \sum_{n=0}^{\infty} (Ze^{-Tb})^n \right.$$

$$\left. -\frac{T}{6} \sum_{m=0}^{\infty} m \left(\frac{e^{-Tb}}{Z}\right)^m + \frac{1}{3b} \sum_{m=0}^{\infty} \left(\frac{e^{-Tb}}{Z}\right)^m - \frac{1}{3b} \right\}$$

$$\Phi(Z) = K_V\left\{-\frac{T}{6}\left[\frac{ZB}{(1-ZB)^2}\right]+\frac{1}{3b}\left[\frac{1}{1-ZB}\right]-\frac{T}{6}\left[\frac{BZ^{-1}}{(1-BZ^{-1})^2}\right]+\frac{1}{3b}\left[\frac{1}{1-BZ^{-1}}\right]-\frac{1}{3b}\right\}$$

$$\Phi(Z) = K_V\left[\frac{1/3b-ZB(T/6+1/3b)}{(1-ZB^2)}+\frac{1/3b-BZ^{-1}(T/6+1/3b)}{(1-BZ^{-1})^2}-\frac{1}{3b}\right]$$

$$\Phi(Z) = \sqrt{K_V}\frac{(a+dZ^{-1})}{(1-BZ^{-1})^2}\cdot\sqrt{K_V}\frac{(a+dZ)}{(1-BZ)^2}$$

where

$A = 1/3b$

$B = e^{-Tb}$

$D = T/6 + 1/3b$

$F = B^2D - AB^2$

$a = \dfrac{-B^3D-BD+2AB^3}{d}$

$d = \sqrt{X}$

$X = \dfrac{(A-AB^4+4F)}{2}\sqrt{\frac{1}{4}(A-AB^4-4F)^2-[2AB^3-B^3D-BD]^2}$

$H(Z) = \sqrt{K_V}\dfrac{a+dZ^{-1}}{(1-BZ^{-1})^2} = \sqrt{K_V}[a+(2aB+d)Z^{-1}+\ldots]$

$h(1) = \sqrt{K_V}(2aB+d)$

$h(0) = a\sqrt{K_V}$

$\phi(0) = \dfrac{K_V}{3b}$

$\phi(1) = \dfrac{BK_V}{6}(\frac{2}{b}-T)$

$R_{00} = \phi(0)-h^2(0) = K_V(\frac{1}{3b}-a^2)$

$R_{10} = \phi(1)-h(1)\,h(0)$

$= K_V[\frac{B}{6}(\frac{2}{b}-T)-a(2aB+d)]$

$R_{11} = \phi(0)-[h(0)]^2-[h(1)]^2$

$R_{11} = K_V[1/3b-a^2-(2aB+b)^2]$

$C_{00} = \sqrt{R_{00}} = \sqrt{K_V(\frac{1}{3b}-a^2)}$

$$C_{10} = \frac{R_{10}}{C_{00}} = \frac{K_V}{\sqrt{K_V(\frac{1}{3b}-a^2)}} \left[\frac{B}{6}(\frac{2}{b}-T)-a(2aB+b)\right]$$

$$C_{11} = \sqrt{R_{11}-C_{10}^2}$$

$$C_{11} = \sqrt{K_V}\sqrt{\left[\frac{1}{3b}-a^2-(2aB+b)^2\right]-\frac{1}{(\frac{1}{3b}-a^2)}\left[\frac{B}{6}(\frac{2}{b}-T)-a(2aB+b)\right]^2}$$

$$y(0) = a\,u(0) + C_{00}\,V(0)$$

$$y(1) = a\,u(1) + (2aB+d)\,u(0) + C_{10}\,V(0) + C_{11}\,V(1)$$

$$y(n) = 2By(n-1) - B^2y(n-2) + a\,u(n) + d\,u(n-1)$$

The component of wind in the "ω" - direction is derived in the same fashion.

5.2.3 Wind Component in the p - q - r Direction

The spectral components in the p, q, r direction are given as follows:

$$\Phi_p(\omega) = \frac{.1\sigma_w^2 \Pi}{bL_w}\left(\frac{\Pi L_w}{4b}\right)^{1/3} \frac{2\left(\frac{\Pi V}{4b}\right)}{\left(\frac{\Pi V}{4b}\right)^2+\omega^2}$$

$$\Phi_q(\omega) = \frac{\Pi^2}{16b^2}\frac{\omega^2}{\left(\frac{V\Pi}{4b}\right)^2+\omega^2}\,\Phi_w(\omega)$$

$$\Phi_r(\omega) = \frac{\Pi^2}{9b^2}\frac{\omega^2}{\left(\frac{V\Pi}{3b}\right)^2+\omega^2}\,\Phi_v(\omega)$$

The p component can be derived in the same fashion as the u-direction wind gust. The derivation for the q component follows:

Let $K_q = \frac{3\sigma_w^2 \Pi b_w}{16b^2}$; $b_w = \frac{V}{L_w}$

$$g = \frac{\Pi V}{4b}$$

Then $$\Phi_q(\omega) = K_w\left[\frac{\omega^2}{g^2+\omega^2}\right]\left[\frac{b_w^2/3+\omega^2}{(b_w^2+\omega^2)^2}\right]$$

From this the autocorrelation function is given by:

$$\Psi(\tau) = \frac{K_w}{2\Pi}\int_{-\infty}^{\infty} \frac{\omega^2}{(g^2+\omega^2)} \left[\frac{b_w^2/3+\omega^2}{(b_w^2+\omega^2)^2}\right] \cos \omega\tau \, d\omega$$

Using contour integration the following results

$$\Psi(\tau) = \begin{cases} [A\tau+B]e^{-b_w\tau}+Ce^{-g\tau} ; & \tau>0 \\ [-A\tau+B]e^{b_w\tau}+Ce^{g\tau} ; & \tau<0 \end{cases}$$

where

$$A = \frac{K_q b_w^2}{6(g^2-b_w^2)}$$

$$B = \frac{-K_q b_w}{3}\left[\frac{2g^2-b_w^2}{(g^2-b_w^2)^2}\right]$$

$$C = -\frac{K_w}{2}\left[g\frac{(b_w^2/3-g^2)}{(g^2-b_w^2)^2}\right]$$

$$= \frac{-K_q g}{2}\left[\frac{\frac{b_w^2}{3}-g^2}{(g^2-b_w^2)^2}\right]$$

In discrete form:

$$\phi(m) = \begin{cases} (ATM+B)e^{-bTM}+ce^{-gTM} & m>0 \\ (-ATM+B)e^{bTM}+ce^{gTM} & m<0 \end{cases}$$

$$\Phi(Z) = \sum_{-\infty}^{\infty} \phi(m)\, Z^{-m}$$

$$\Phi(Z) = \sum_{-\infty}^{0} (B-ATM)e^{bTM}Z^{-m} + \sum_{-\infty}^{0} ce^{gTM}Z^{-m} + \sum_{0}^{\infty}(ATM+B)e^{-bTM}Z^{-m} + \sum_{0}^{\infty} ce^{-gTM}\, Z^{-m} - (B+C)$$

After some manipulation:

$$\Phi(Z) = \frac{B'}{(1-EZ)(1-EZ^{-1})} + \frac{C'}{(1-GZ)(1-GZ^{-1})} + \frac{A'(Z+Z^{-1})-E'}{(1-EZ)^2(1-EZ^{-1})^2}$$

where

$$A' = AT(E+E^3)$$

$$E' = 4E^2AT$$

$$C' = C(1-E^2)$$

$$B' = B(1-E^2)$$

$$E = e^{-bT}$$

$$G = e^{-gT}$$

$$\Phi(Z) = \frac{NUM}{(1-EZ)^2(1-EZ^{-1})^2(1-GZ)(1-GZ^{-1})}$$

$$NUM = K_1 + K_2(Z+Z^{-1}) + K_3(Z+Z^{-1})^2$$

$$K_1 = B'(1+E^2)(1+G^2)+C'(1+2E^2+E^4) - E'(1+G^2)$$

$$K_2 = A'(1+G^2)+E'G-2C'(E+E^3)-B'[(1+G^2)E+(1+E^2)G]$$

$$K_3 = B'EG+E^2C'-A'G$$

The desired form for $\Phi(Z)$ is

$$\Phi(Z) = \frac{(a+bZ+cZ^2)(a+BZ^{-1}+cZ^{-2})}{(1-EZ)^2(1-GZ)(1-EZ^{-1})^2(1-GZ^{-1})}$$

Therefore

$$K_1 = a^2+b^2+c^2-2ac$$

$$K_2 = b(a+c)$$

$$K_3 = ac$$

Solving for a, b, c letting

$$Q = \sqrt{K_1+2K_2+4K_3}$$

$$R = \frac{K_2}{b}$$

$$b = \frac{Q}{2} - \frac{\sqrt{Q^2-4K_2}}{2}\ ;\ a = \frac{R+\sqrt{R^2-4K_3}}{2}$$

$$c = \frac{K_3}{a}$$

Choose H(Z) to be

$$H(Z) = \frac{a+bZ^{-1}+cZ^{-2}}{(1-EZ^{-1})^2(1-GZ^{-1})}$$

$$H(Z) = a+[b-a(2E+G)]Z^{-1}+\left[c-a(E^2+2GE)+(2E+G)[b+a(2E+G)]\right]Z^{-2}$$

$$h(0) = a$$

$$h(1) = b=a(2E+G)$$

$$h(2) = c-a(E^2+2GE)+(2E+G)[b+a(2E+G)]$$

$$\phi(0) = B+C$$

$$\phi(1) = (AT+B)E+CG$$

$$\phi(2) = (2AT+B)E^2+CG^2$$

$$R_{00} = \phi(0) -h^2(0)$$

$$R_{10} = \phi(1) -h(0)h(-1)-h(1)h(0)$$

$$R_{11} = \phi(0) - [h(0)]^2 - [h(1)]^2$$

$$R_{20} = \phi(2) - h(2)h(0)$$

$$R_{21} = \phi(1) - h(1)h(0) - h(2)h(1)$$

$$R_{22} = \phi(0) - [h^2(0) + h^2(1) + h^2(2)]$$

$$C_{00} = \sqrt{R_{00}}\ ;\ C_{10} = \frac{R_{10}}{C_{00}}\ ;\ C_{11} = \sqrt{R_{11} - C_{10}^2}$$

$$C_{20} = \frac{R_{20}}{C_{00}}\ ;\ C_{21} = \frac{R_{21} - C_{10}\,C_{20}}{C_{11}}$$

$$C_{22} = \sqrt{R_{22} - C_{20}^2 - C_{21}^2}$$

$$y(0) = a\,u(0) + C_{00}\,V(0)$$

$$y(1) = h(0)u(1) + h(1)u(0) + C_{10}V(0) + C_{11}V(1)$$

$$y(2) = h(0)u(2) + h(1)u(1) + h(2)u(0) + C_{20}V(0) + C_{21}V(1) + C_{22}V(2)$$

$$y(n) = (G+2E)y(n-1) - (2GE+E^2)y(n-2) + E^2Gy(n-3) + a\,u(n) + b\,u(n-1) + c\,u(n-2)$$

The component of wind in the r direction is found in a similar fashion.

Some typical wind gust profiles are shown in Figures 5.2 and 5.3 for different random number sequences.

Reference

1. Background Information and User Guide for MIL-F-8765B(ASG) "Military Specifications - Flying Qualities of Piloted Airplanes," August 1969, AFFDL-TR-69-72.

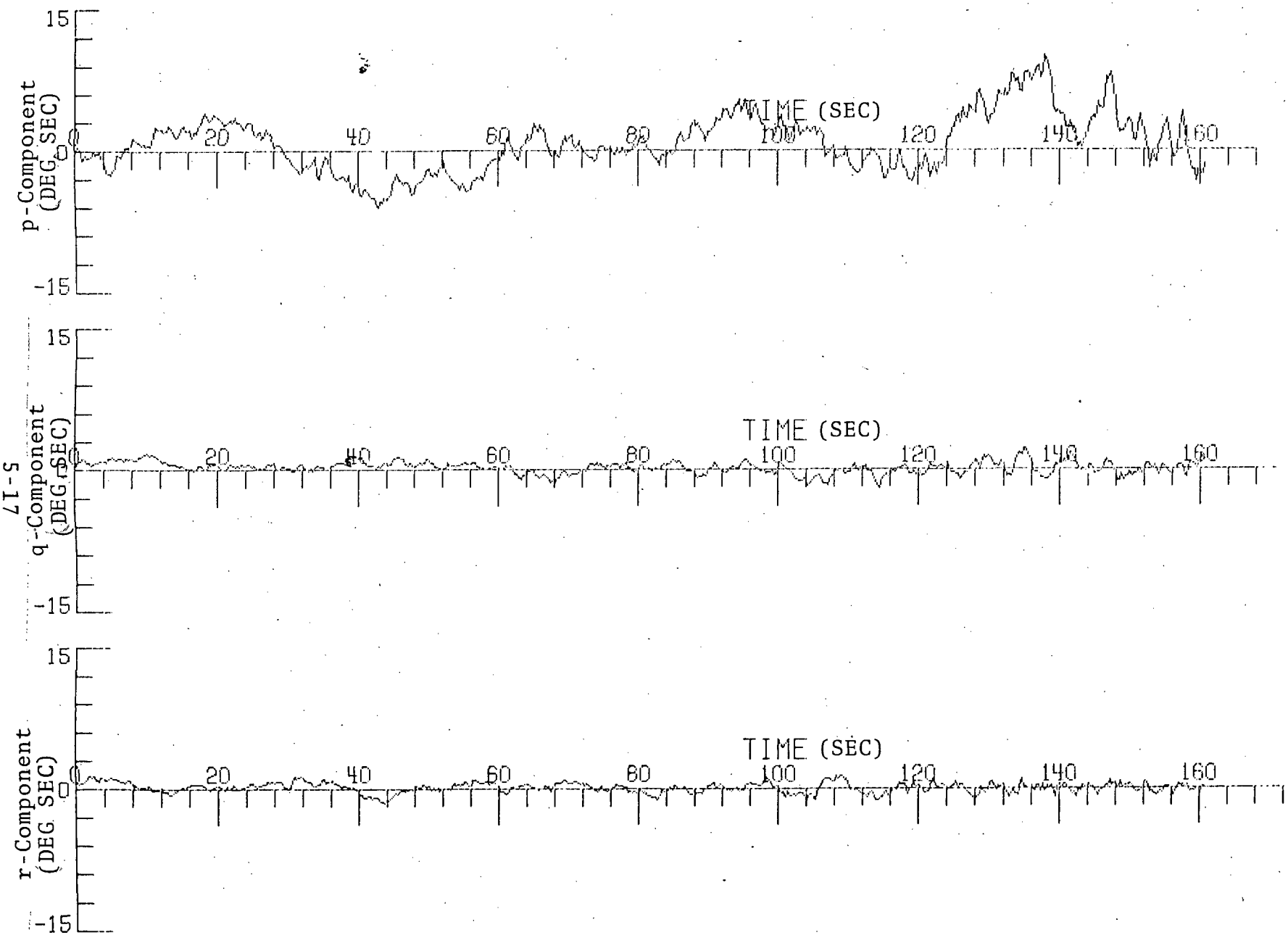

Figure 5-2. Wind Gust Profile (Standard Deviation Equal 1.5 feet/sec.).

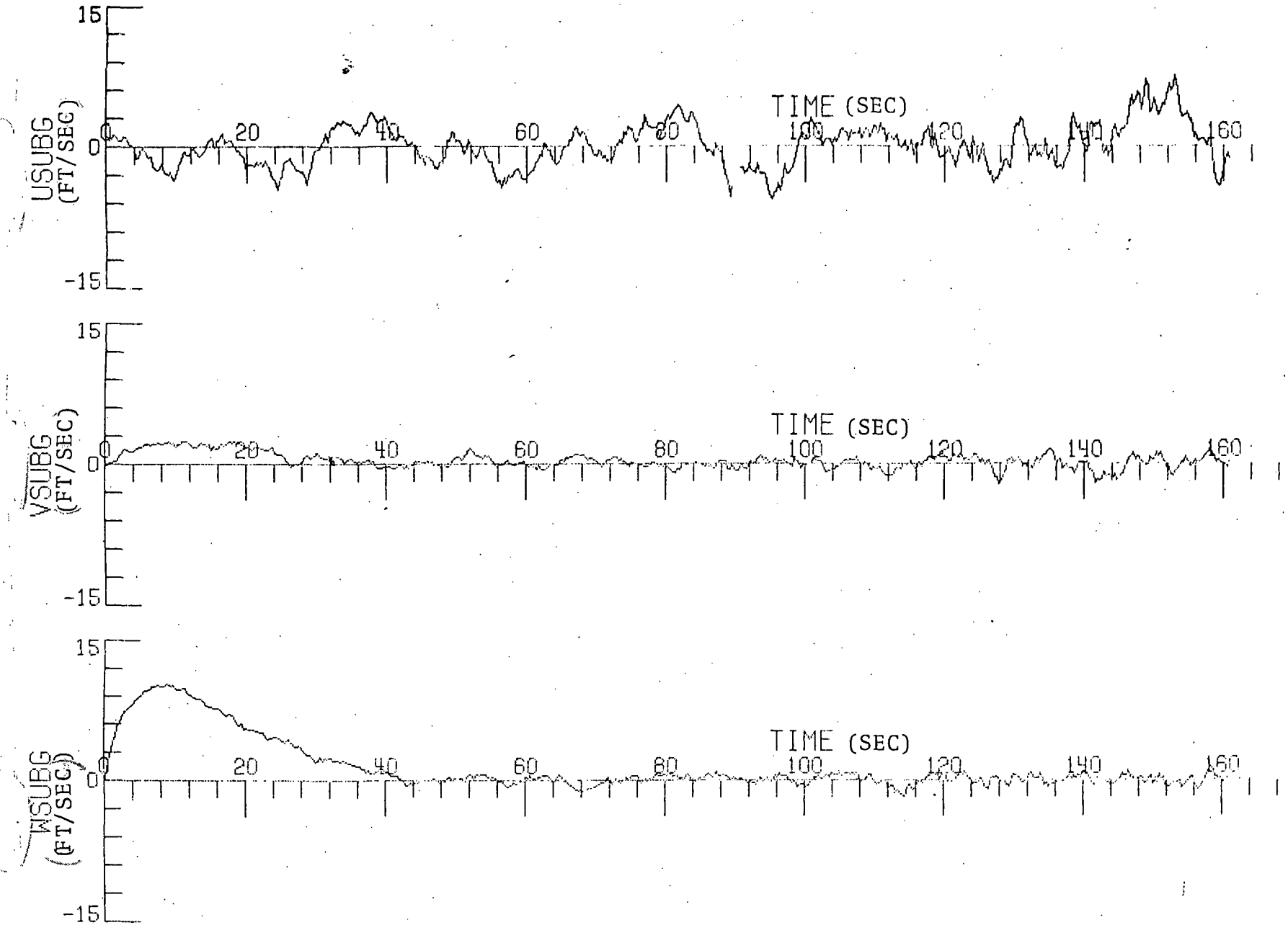

Figure 5-3. Wind Gust Profile (Standard Deviation Equal 1.5 feet/sec.).

6.0 AIRCRAFT CONTROL SYSTEMS

In this section the Boeing 737's control systems are discussed. The "A" and "C" control systems provide inputs to the aircraft ailerons and elevator servos. The spoiler, rudder and autothrottle servo configurations are the same for both the "A" and "C" systems.

6.1 "A" Control System

The "A" control system used in this study is presented in block diagram form in Figure 6-1 and 6-2. One major problem encountered with implementing the "A" system was the fact that it was originally designed for a Boeing 727-100 aircraft. When used with the Boeing 737 the aircraft ability to track a glideslope/localizer was not satisfactory for the purposes of the subject simulation study. Information regarding the modifications that were necessary to convert the control system from a Boeing 727-100 to a Boeing 737 was not available.

In order to provide a control system that would track a glideslope/localizer reasonably well, several constants were changed in the control systems. The modified "A" control system does provide an improved tracking ability as illustrated in Figures 6-3 and 6-4. When, or if, additional information becomes available, it will be relatively easy to modify the control system and rerun the tests to ascertain if there are any changes in the conclusions.

The state variables for the "A" control system are identified on the diagrams. The state equations for the control system are as follows:

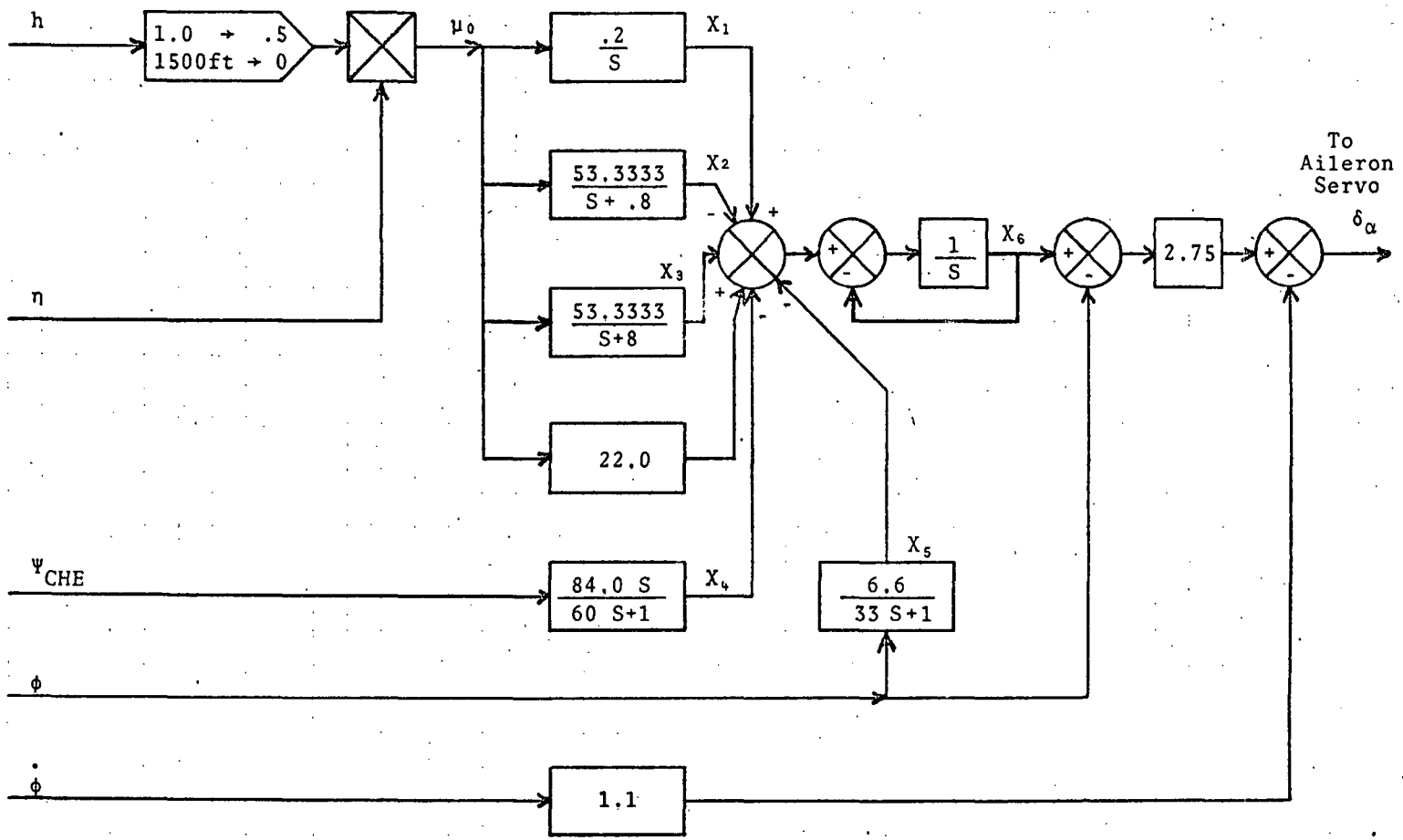

Figure 6-1. System A Lateral Block Diagram.

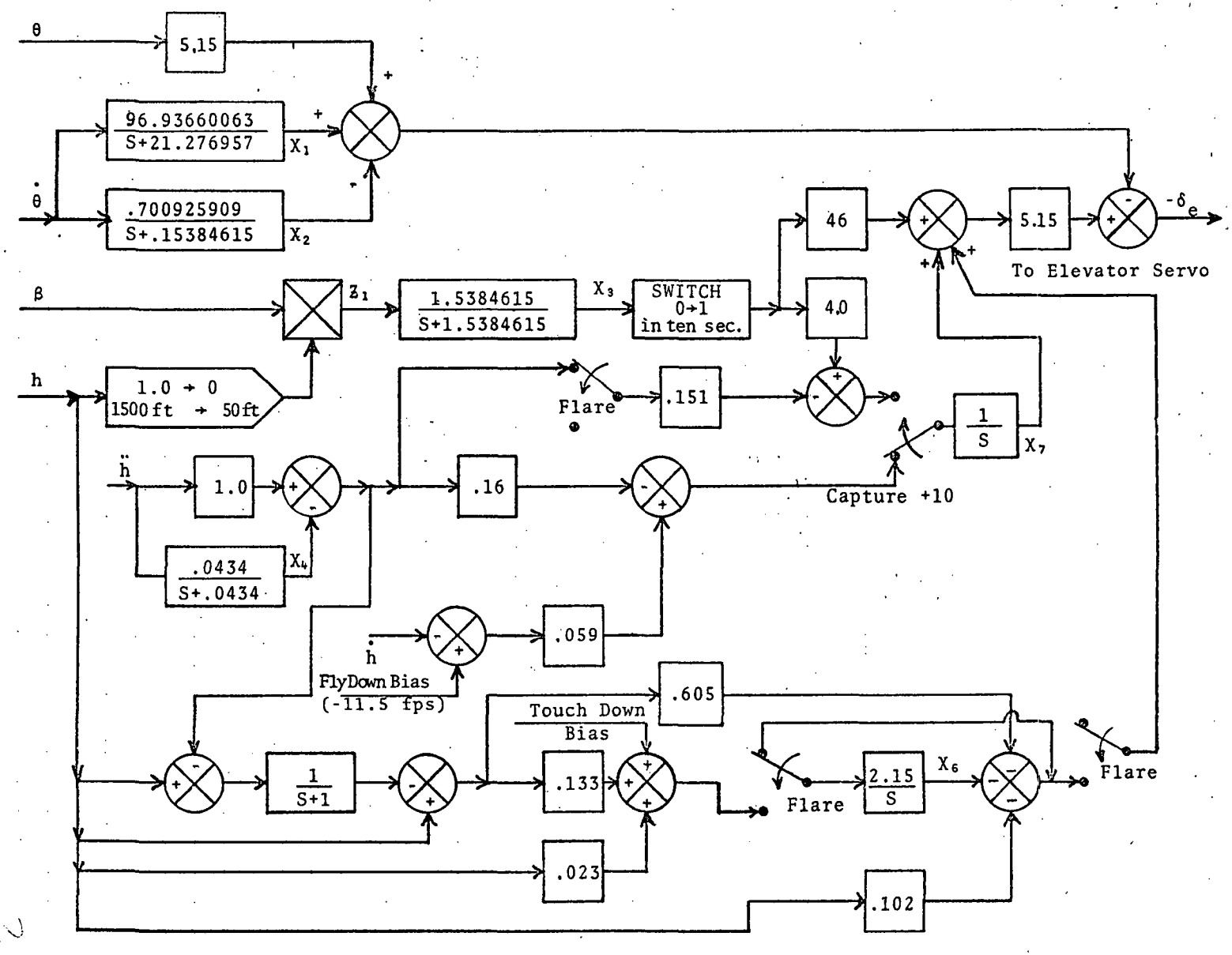

Figure 6-2. System A Longitudinal Block Diagram.

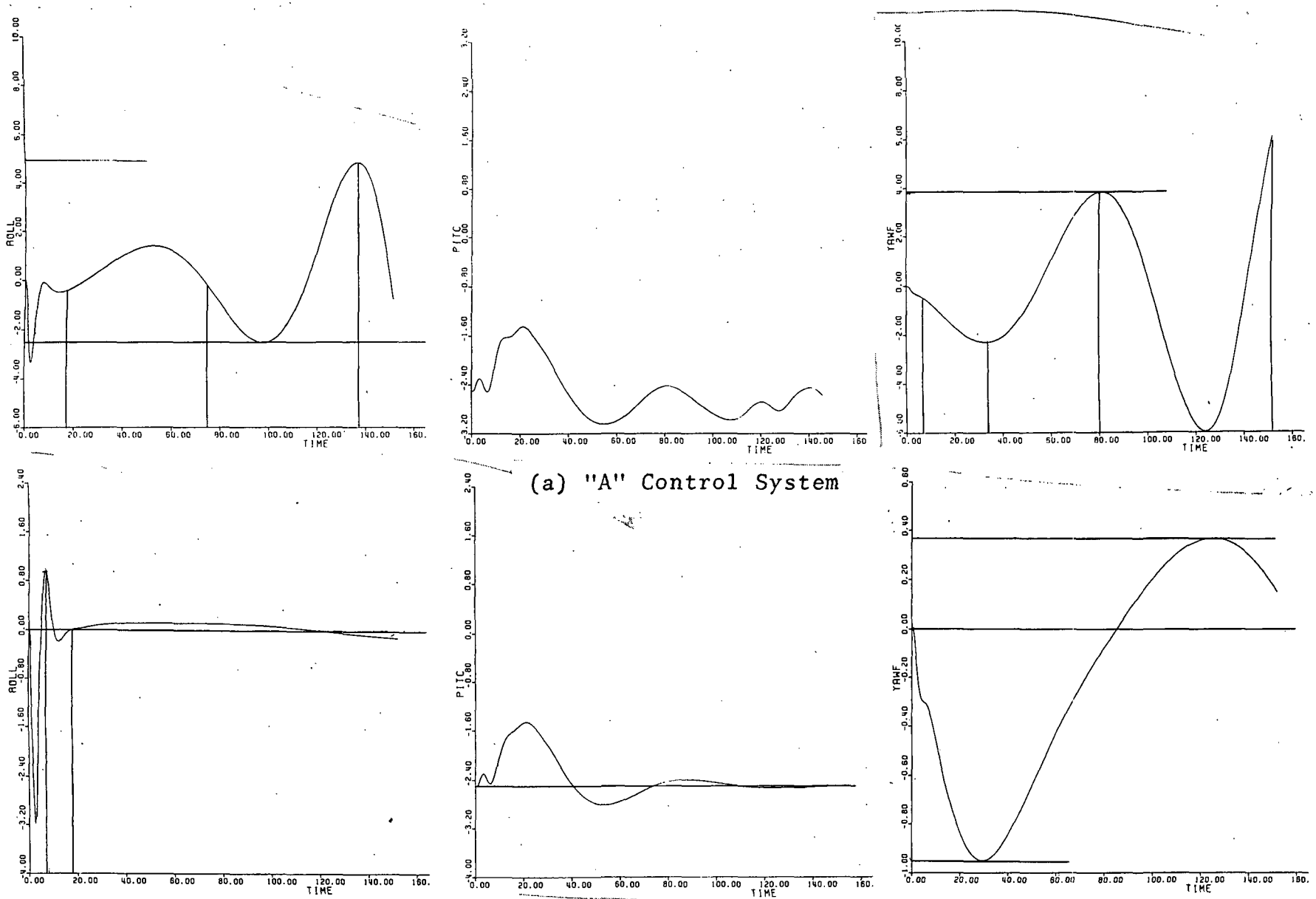

Figure 6-3. "A" Control System Performance.

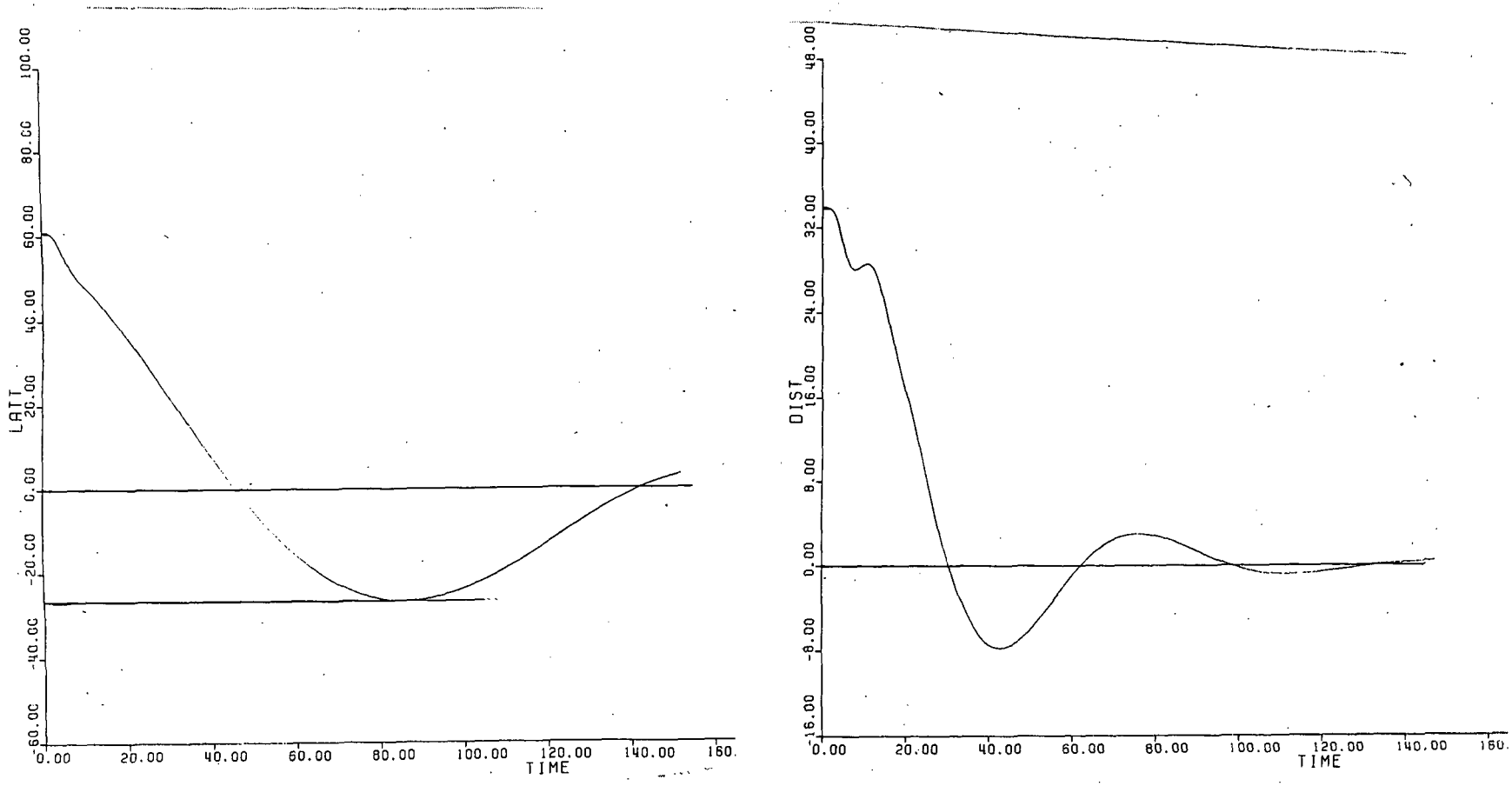

Figure 6-4. Modified "A" Control System Offsets From Localizer and Glide Slope.

LATERAL

$$\dot{X}_1 = .2\ U_o \tag{6-1}$$

$$\dot{X}_2 = -.8X_2 = 53.33333\ U_o \tag{6-2}$$

$$\dot{X}_3 = -8.0X_3 + 533.33333\ U_o \tag{6-3}$$

$$\dot{X}_4 = -.01666666X_4 + 1.4\dot{\lambda} \tag{6-4}$$

$$\dot{X}_5 = .03030303X_5 + .2\phi \tag{6-5}$$

$$\dot{X}_6 = X_1 - X_2 + X_3 - X_4 - X_6 + 22.0\ U_o - X_5 \tag{6-6}$$

$$\delta_{ac} = 2.75(X_6 - \phi) - 1.1\dot{\phi} \tag{6-7}$$

LOGITUDINAL

$$\dot{X}_1 = -P_3X_1 + P_2\dot{\Theta} \tag{6-8}$$

$$\dot{X}_2 = -P_5X_2 + P_4\dot{\Theta} \tag{6-9}$$

$$\dot{X}_3 = -P_6X_3 + P_6Z_1 \tag{6-10}$$

$$\dot{X}_4 = -P_{20}X_4 + P_{20}\ddot{h} \tag{6-11}$$

$$\dot{X}_5 = -X_5 + h - \ddot{h} + X_4 \tag{6-12}$$

$$\dot{X}_6 = P_{15}[P_{19} + P_{18}(h - X_5)] + P_{17}h - PDUM(X_6) \tag{6-13}$$

$$\dot{X}_7 = -P_{11}(\ddot{h} - X_4) + P_8X_3 + P_{13}(-11.5 - \dot{h}) \tag{6-14}$$

$$-\delta_e = -[P_1(\Theta) + X_1 - X_2] + P_{10}[P_9(X_3) + X_{17} \tag{6-15}$$

$$-P_{14}(h - X_5] - P.DUMM(X_6) - P_{16}(h) \tag{6-16}$$

Where if flare is false then:

$$P_1 = 5.15$$

$$P_2 = 96.93660063$$

$$P_3 = 21.276957$$

$$P_4 = .700925902$$

$$P_5 = .15384615$$

$$P_6 = 1.5384615$$

P_8 = 4.0

P_9 = 46.0

P_{10} = 5.15

P_{11} = .151

P_{12} = .16

P_{13} = 0.0

P_{14} = 0.0

P_{15} = 2.15

P_{16} = 0.0

P_{17} = -.102

P_{18} = -.605

P_{19} = 0.0

P_{20} = .043478261

PDUM = 1.0

PDUMM = 0.0

If flare is true the values of the following constants are changed.

P_{19} = .232

P_{18} = .133

P_{17} = .023

P_{14} = .605

P_{16} = .102

PDUMM = 1.0

PDUM = 0.0

If Capture + 10 is not true the values of the following constants are:

$$P_{11} = .16$$

$$P_8 = 0.0$$

$$P_{13} = .059$$

$$P_9 = P_9 * .1 * TIME$$

6.2 "C" Control System

The block diagram for the "C" control system is presented in Figures 6-5 and 6-6. The state variables are identified on the diagram. The following state equations are used in the simulation:

LATERAL

$$\dot{X}_1 = 2.5X_1 + 8.75\Psi_{TA} \quad (6\text{-}17)$$

$$\dot{X}_2 = .85\Psi_{TA} + 4U_o - .05X_2 \quad (6\text{-}18)$$

$$\dot{X}_3 = 9U_o \quad (6\text{-}19)$$

$$\dot{X}_4 = 5.0[X_1 + X_2 + X_3 - X_4] \quad (6\text{-}20)$$

$$\delta_{ac} = 2.75[X_4 - \phi] - 1.1\dot{\phi} \quad (6\text{-}21)$$

LONGITUDINAL

FLARE IS FALSE

$$\dot{X}_1 = -1/3X_1 + .19444\ddot{h} \quad (6\text{-}22)$$

$$\dot{X}_2 = .01X_2 - .002\dot{h} \quad (6\text{-}23)$$

$$\dot{X}_3 = -.05X_3 + .05X_2 + \ddot{h} + .06\dot{h} \quad (6\text{-}24)$$

$$\dot{X}_4 = .067(Z_1 - X_4 - .025X_3 - .00109V_G) \quad (6\text{-}25)$$

$$\dot{X}_5 = 7.8Z_1 \quad (6\text{-}26)$$

$$-\delta_e = .103(X_5 + 42.2X_4)(50) - 2.0085X_3 - 5.5\dot{\theta} \quad (6\text{-}27)$$

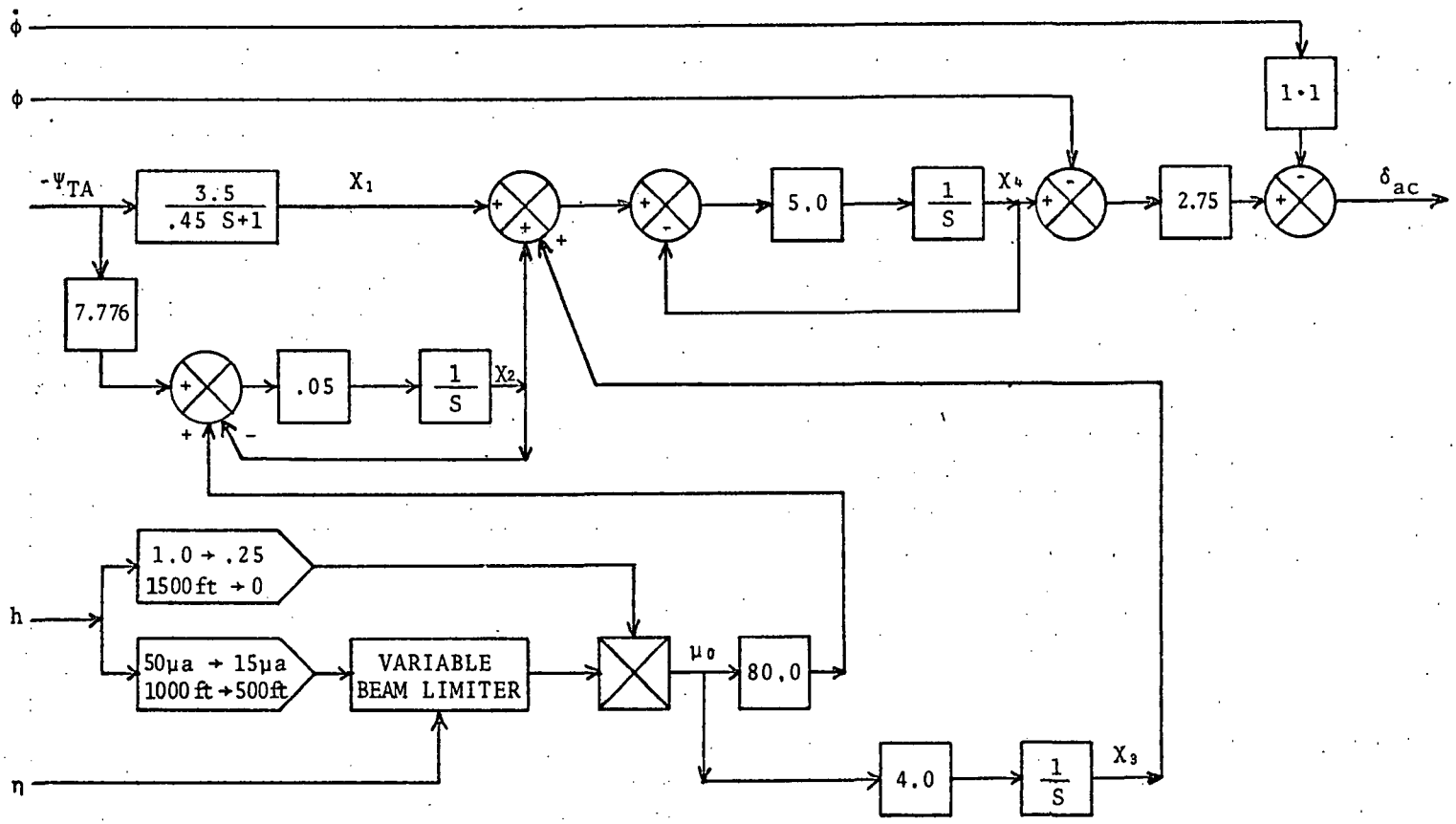

Figure 6-5. System "C" Lateral Block Diagram.

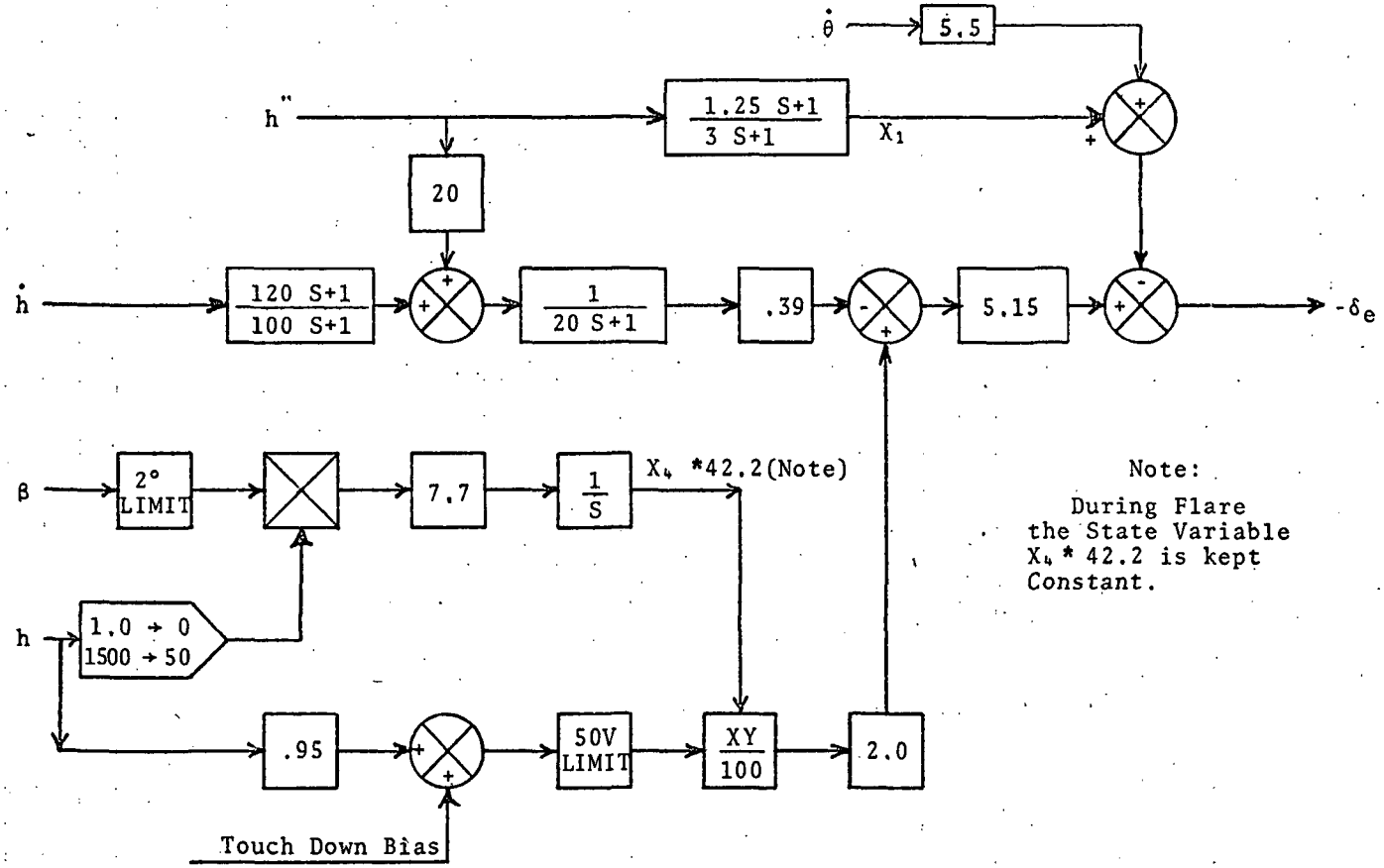

Figure 6-6(a). System "C" Longitudinal Block Diagram When Flare is True.

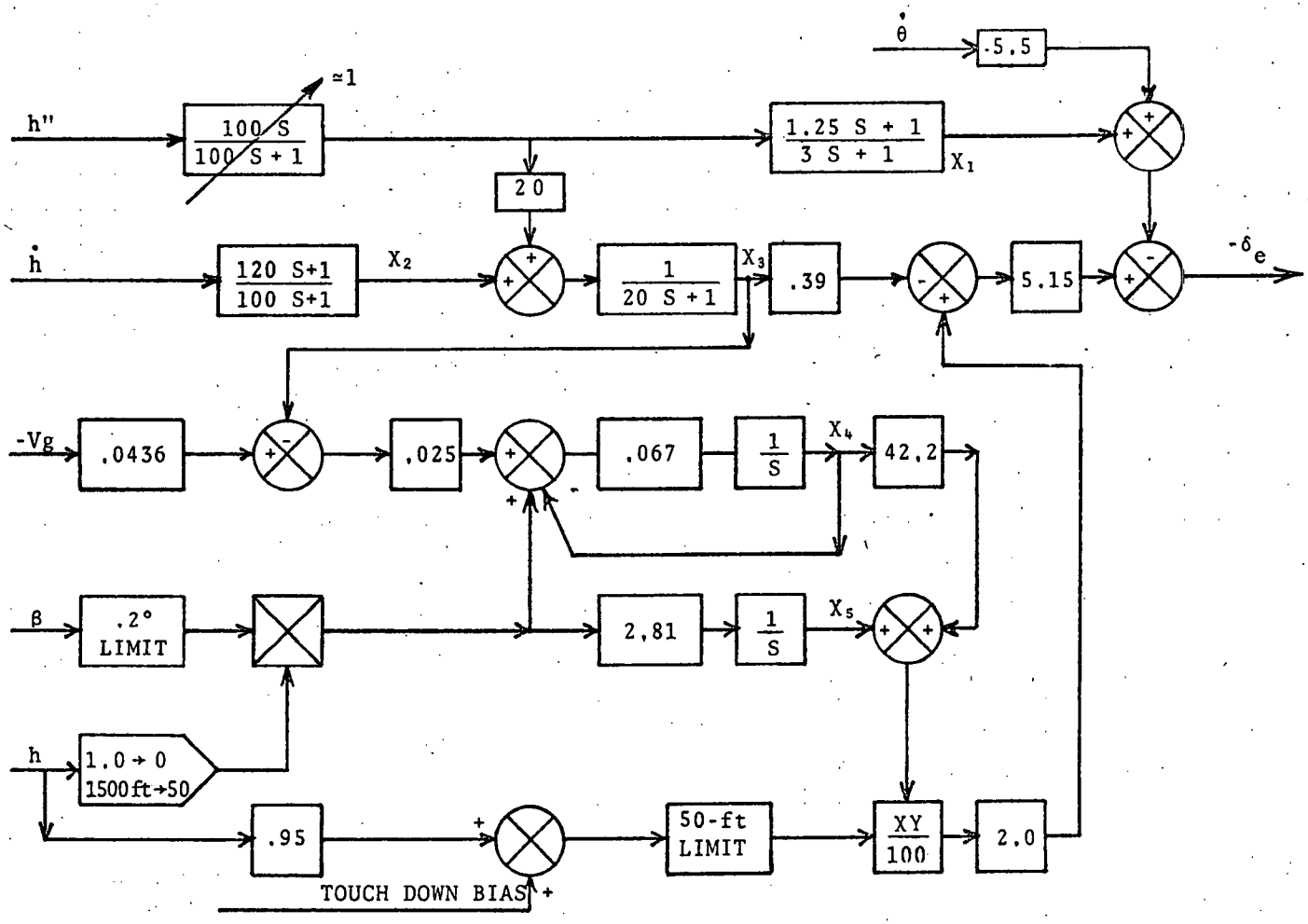

Figure 6-6(b). System "C" Longitudinal Block Diagram When Flare is False.

FLARE IS TRUE

$$\dot{X}_1 = -1/3X_1 + .19444\dot{h} \quad (6\text{-}28)$$

$$\dot{X}_2 = -.01X_2 - .002\dot{h} \quad (6\text{-}29)$$

$$\dot{X}_3 = -.05X_3 + .05X_2 + \dot{h} + .06\dot{h} \quad (6\text{-}30)$$

$$-\delta_e = .103(2.3 + .95h)(X_4 42.2) \quad (6\text{-}31)$$
$$-(X_3 2..0085) - 5.5\Theta - (X_1 + .41667\dot{h})$$

6.3 Autothrottle

The autothrottle control system for the 737 is a ninth-order system which regulates the engine thrust in a nonlinear fashion. For the purposes of simulation, several simplifications were made in the autothrottle control system. This was justified because many of the time constants in the system were of very short duration (i.e. the integration interval used in the simulation was larger by an order of magnitude than many of the time constants). Also, the thrust versus throttle function was approximated as a straight line. This is due to the fact that the aircraft is initially in equilibrium. All changes in thrust are excursions from the equilibrium. The initial equilibrium point is hypothesized to be in an approximately linear portion of the curve; therefore, a small change will be linear.

The block diagram is shown in Figure 6-7. The state equations are:

$$\dot{X}_1 = -G_5X_1+G_1G_2G_4\ U_1-G_2G_3G_4X_1-G_4G_6U_2 \qquad (6\text{-}32)$$

$$\dot{X}_2 = -G_{10}X_2+G_8G_9X_1-G_9G_7U_2 \qquad (6\text{-}33)$$

$$\delta_{THRUST} = G_{12}X_2+G_{11}G_{12}(1-\cos\phi) \qquad (6\text{-}34)$$

The change in force from the equilibrium value is given by:

$$\nabla FORCE(KLBS) = .305556(\delta_{THRUST}) \qquad (6\text{-}35)$$

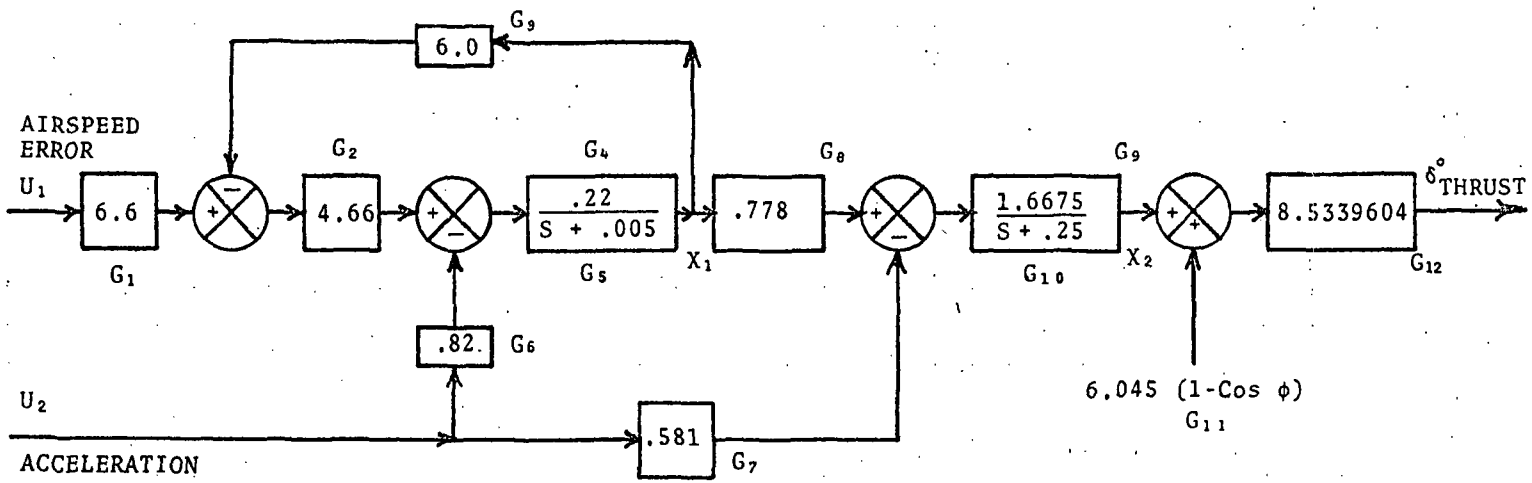

Figure 6-7. Autothrottle Control System.

6.4 Rudder Control System

The rudder control system is comprised of two distinct parts. One part, the yaw rate damper has been specifically designed for the Boeing 737; the second part, the augmented rudder control system, was designed for the Boeing 727. Lack of information has made it impractical to realistically change the gains to correspond to the actual Boeing 737 configuration. Computer simulation studies performed with this control system have shown that it is not optimal. A truly coordinated turn, i.e., the resulting acceleration lies in the plane of symmetry, is not actually obtained. However, it is felt that the amount of error introduced does not invalidate the results.

The block diagram is shown in Figure 6-8. The state equations are as follows:

$$\dot{X}_1 = 1.3X_1 + .0642\dot{\Psi} \qquad (6\text{-}36)$$

$$\dot{X}_3 = -.434789X_3 - .25348498\phi \qquad (6\text{-}37)$$

$$\delta_r = -.8\dot{\phi} - X_2 - .580425\phi + 9.25806902 \qquad (6\text{-}38)$$
$$[.21044776\dot{\Psi} - X_1]$$

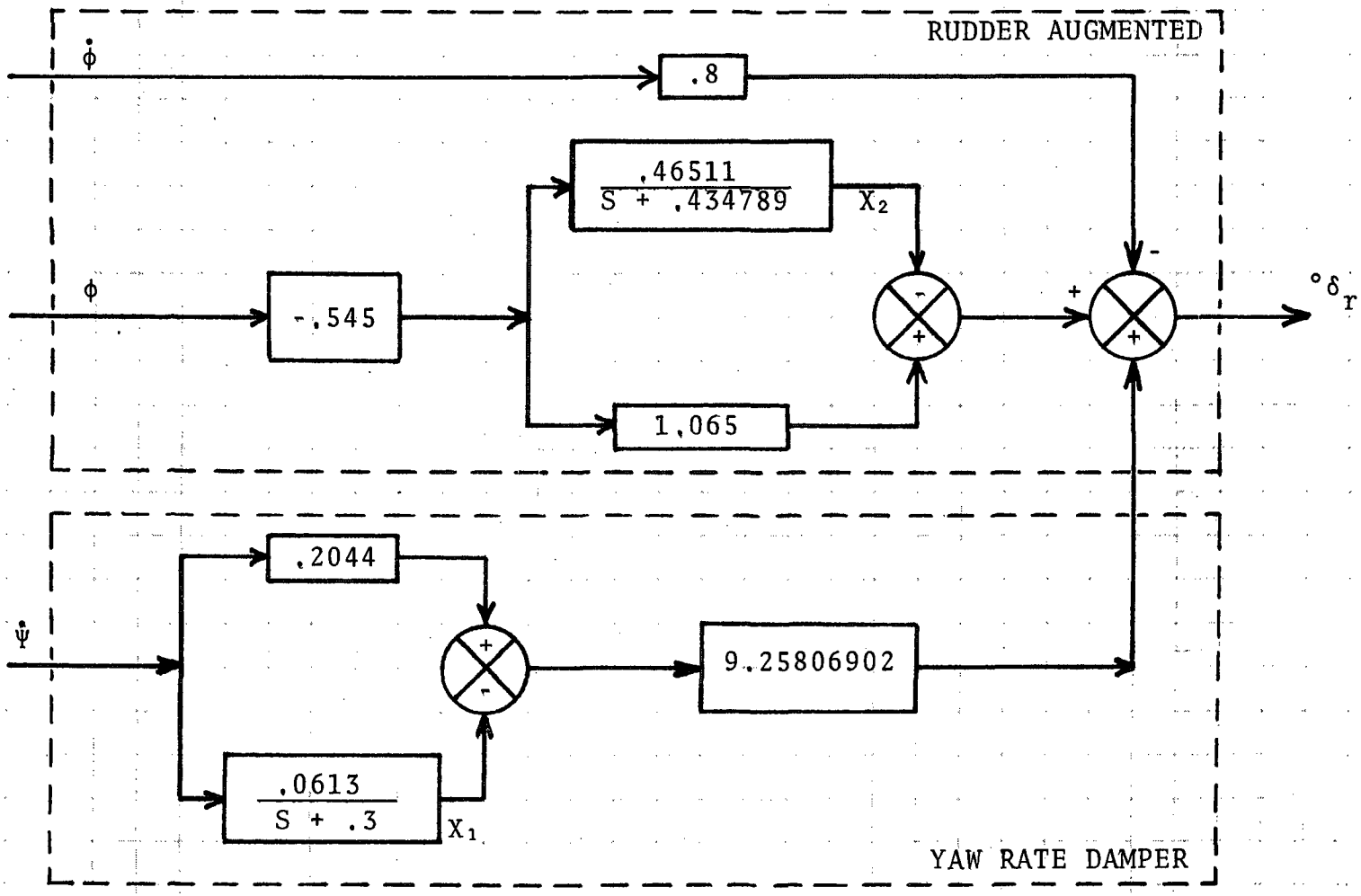

Figure 6-8. Rudder Control System.

6.5 Spoilers

For the Boeing 737, the spoiler deflection is a non-linear function of the pilot wheel angle which is a function of aileron deflection. Figure 6-9 shows the graphical relationship between the spoiler and the pilot wheel angle. The following equation relates the spoiler setting to aileron deflection:

$$\delta_{sp} = .0722\ \delta_a^2 + .1\ \delta_a \qquad (6\text{-}39)$$

Where:

δ_{sp} is the spoiler setting in degrees

δ_a is the ailerons setting in degrees

The variation in δ_a is $\pm$ 15°

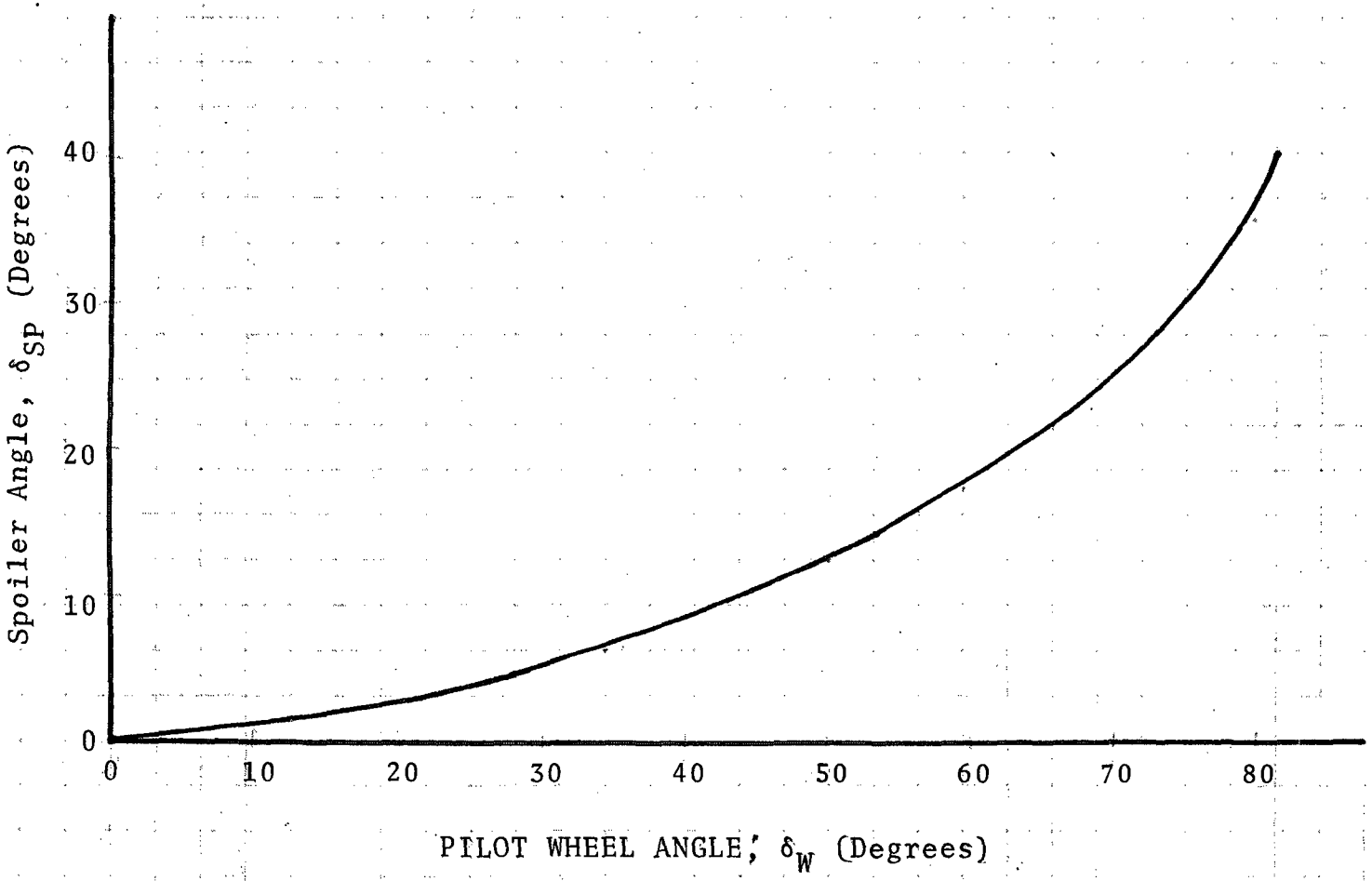

Figure 6-9. Spoiler Angle as a Function of Pilot Wheel Angle.

6.6 Calculation of Control System Input Variables

For the most part all the variables needed by the control system are obtained directly from the aircraft equations of motion. The angular information needed consists of roll, pitch, yaw, rollrate, pitchrate and yawrate. The linear accelerations can be calculated in the following manner:

$$a_X = U_o * \dot{U} \quad \text{acceleration in X direction} \quad (6\text{-}40)$$

$$a_Y = U_o * (\beta + \dot{\Psi}) \quad \text{acceleration in Y direction} \quad (6\text{-}41)$$

$$a_Z = U_o * (\dot{\alpha} - \dot{\Theta}) \quad \text{acceleration in Z direction} \quad (6\text{-}42)$$

None of the above measured quantities are perturbed by errors. When the simulation is performed in this manner, the only errors considered are those associated with the MLS.

Errors were introduced into the lateral beam measurement and into the glideslope difference. For a discussion of the errors see Section 7.

7.0 MICROWAVE LANDING SYSTEM

This section of the report is divided into two parts. Part 7.1 presents a general discussion of the proposed MLS. This discussion is based on the version of the MLS described in the RTCA SC-117 report.

In part 7.2, models for both the Doppler and Scanning Beam versions are described. This model takes into account the type of signal processing that would take place with either the Conventional Scanning Beam or Doppler System. In both cases error terms are developed along with their appropriate probability density functions.

To make the simulation as realistic as possible a model is developed for the scattering of an electromagnetic wave from a discrete reflector. This model not only accounts for specular reflections but reflections about the specular point as well. The results presented in Section 3 are based upon the models described in Section 7.2. These results are preliminary in the sense that considerable testing can now be performed with the present models. In addition, multiple reflections can also be considered with some modification to the program.

7.1 Discussion of Proposed Microwave Landing System

The MLS is viewed as a replacement to the present landing systems used at most commercial and military airports. Several options of system requirements are considered which depend upon the type of facility: military, general aviation or commercial; and the classification of the facility: Category I, II or III. System concepts have been developed to meet these requirements and the basic techniques for providing angular information are variations of either the scanning-beam principle or detection of Doppler frequency from a moving RF source. Separate systems are used for azimuth and elevation guidance functions. Most of the information presented in this section is taken from the RCTA report and the reader is advised to review that document as well as the contractor reports on MLS design if more detailed information on the proposed MLS is desired.

7.1.1 MLS Requirements

Basically, the MLS is to provide azimuthal and elevation angle position accuracy exceeding that provided by the present localizer and glide slope systems. Requirements fall into two general categories – during the normal approach phase, the aircraft derives information from the basic guidance systems; while at the point in the approach corresponding to the flare maneuver, a short-range precision guidance system is employed. Each system has its own set of accuracy requirements with Figure 7-1 presenting the coverage and accuracy requirements in pictorial form Figure 7-2 presents coverage and accuracy requirements for various system configurations. These configurations correspond to different guidance functions provided and facility performance categories. Configuration K is the complete system providing azimuth information of -60° to +60° and elevation information of 0-20°. The requirements for the K system are designed to provide sufficient information for curved approaches and to effect landings at zero visibility. In addition to angular coverage and accuracy, the system incorporates a DME function and data transmission from ground to air which includes the particular guidance function being performed at that particular time as well as associated data – runway number, airport characteristics, wind information, etc. The proposed location of facilities to implement the MLS is illustrated in Figure 7-3.

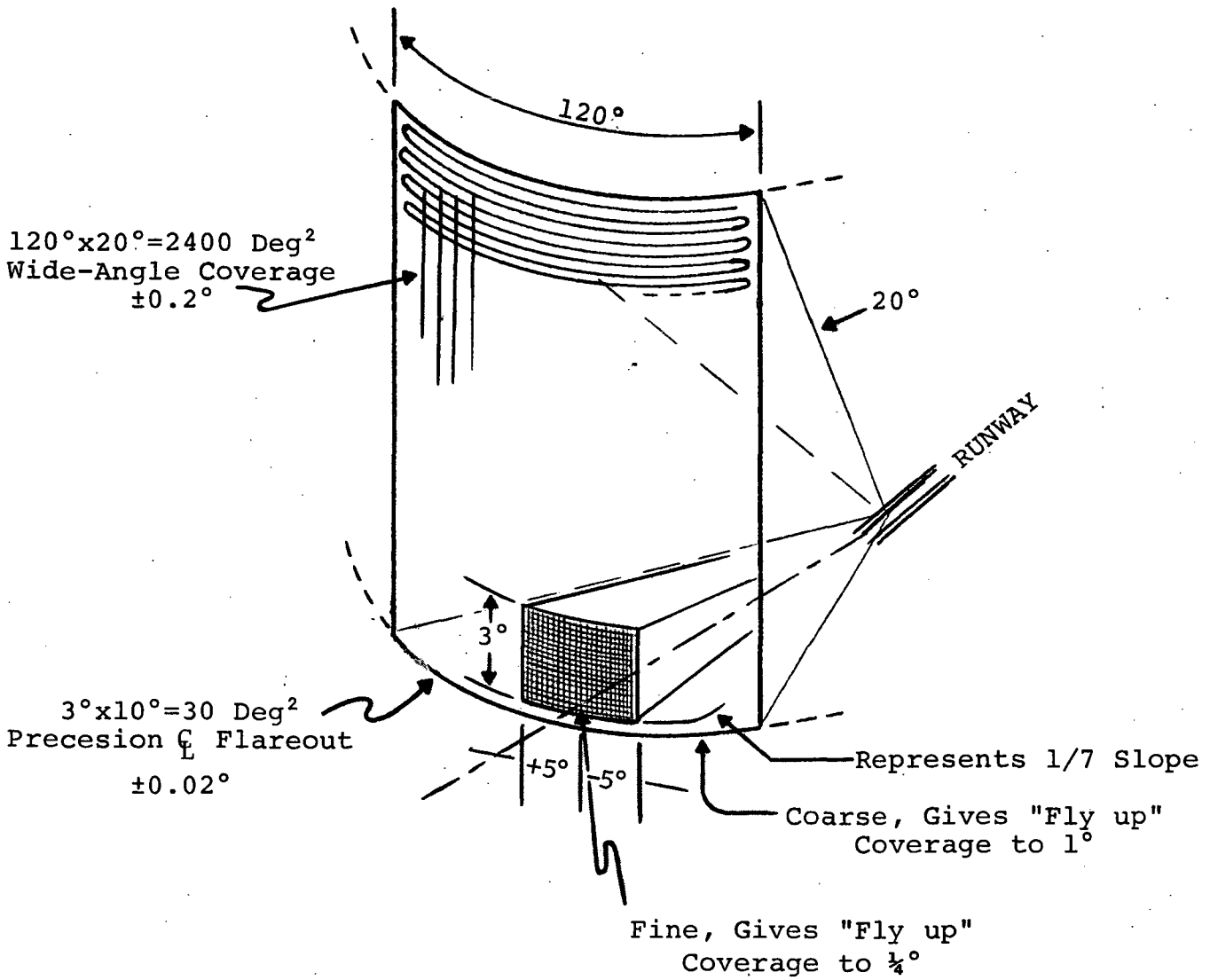

$$\text{Accuracy Ratio} = \frac{10}{1}$$

Proportional Coverage = 100 to 1

Figure 7-1. COVERAGE VOLUME AND GENERAL ACCURACY REQUIREMENTS

CONFIGURATION	B	D	E	F	G	I	K
	Straight Az Basic DME	Straight Az Straight El Basic DME	Straight Az Select El Basic DME	Straight Az Straight El Basic DME	Straight Az Select El Precise DME	Curved Az Curved El Precise DME Missed Appr.	Curved Az Curved El Precise DME Missed Appr.
FACILITY PERFORMANCE	CAT. I	CAT. I	CAT. I	CAT. II	CAT. II	CAT. III	CAT. III
MINIMUM GUIDANCE ALT	150 FT	150 FT	150 FT	50 FT	50 FT	TD	TD
COVERAGE							
ELEVATION	NA	8°	20°	8°	20°	20°	20°
AZIMUTH	$\pm 20^{\circ}$	$\pm 20^{\circ}$	$\pm 20^{\circ}$	$\pm 20^{\circ}$	$\pm 20^{\circ}$	$\pm 40^{\circ}$	$\pm 60^{\circ}$
MISSED APPROACH	---	---	---	---	---	$\pm 40^{\circ}$	$\pm 40^{\circ}$
ACCURACY* (noise)							
ELEVATION (2σ)	NA	7 FT	7 FT	1.4 FT	1.4 FT	1.4 FT	1.4 FT
AZIMUTH (2σ)	26 FT	26 FT	26 FT	11 FT	11 FT	9 FT	9 FT
RANGE (σ)	300 FT	300 FT	100 FT	100 FT	20 FT	20 FT	20 FT
DATA RATE (Max)	2.5 Hz	5 Hz	5 Hz	5 Hz	5 Hz	10 Hz	10 Hz
RUNWAY LENGTH	7000 FT			12,000 FT		14,000 FT	

*Accuracy refers to the decision height for CAT. I and II Configurations and to the runway threshold for Configurations I and K.

Figure 7-2. SYSTEM CONFIGURATIONS AND REQUIREMENTS

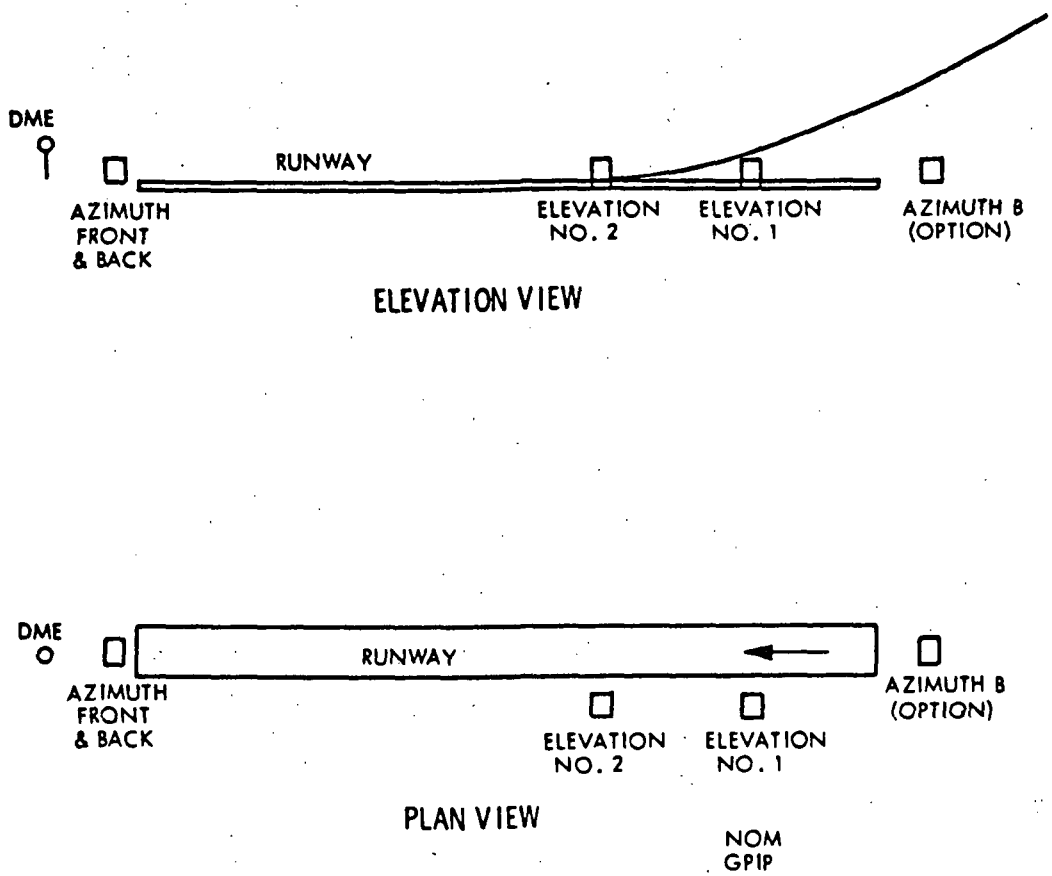

Figure 7-3. GENERAL SITING PLAN CONFIGURATION
SYSTEMS I AND K

7.1.2 Signal Format

A proposed frequency allocation plan for the MLS is presented in Figure 7-4. Two hundred 0.6-MHz bands at C-band are suggested for the transmission of angle data. Precision angle data are transmitted at Ku-band. Twenty DME channels are provided with each channel using ten pulse codes, giving a total of 200 frequency/code channels.

For the scanning-beam system, the transmission of angular information follows the law

$$F = F_m + A\,\theta$$

where

F_m = the mean modulation frequency = 110 kHz

A = angle scale factor = 500 Hz per degree for all functions

θ = beam angle = typically -60° to +60° in azimuth.

Basically, the modulating frequency is selected as a function of angular position and Figure 7-5 shows the spectrum of the transmitted signal. As the beam scans in angle, the aircraft receiver detects a portion of the signal, when illuminated by the ground antenna, and angle data are determined by measuring the modulating frequency of the received signal. A possible scan sequence is shown in Figure 7-6. Supplementary data are transmitted from 0 to 80 kHz between the referencing carrier and the first modulation sidebands.

The Doppler system is based on the principle that the amount of Doppler shift detected from a moving RF source is dependent upon the aspect of the detector relative to the line of motion of the source. The Doppler is proportional to the cosine of the angle between the line-of-motion and the direction to the detector, or to the sine of the angle between the normal of the line-of-motion and the direction to the detector. The travelling RF source is implemented by a linear

array of antennas which are systematically energized and deenergized to effect a moving RF source. In order to provide guidance information using this technique, two arrays are used – sine array and cosine array. The sine array, or main array, is normal to the glidepath and the cosine, or subsidiary array, is colinear with the glidepath. The two arrays are necessary since angular information from one source would give a conical coordinate and it is necessary for this application to have planar coordinates. The subsidiary array provides the additional information necessary to convert to planar information.

The Doppler system provides a frequency difference between the reference carrier and the angle sideband that is a function of the rate of movement of the phase center of the sideband radiator and the relative direction of the receiving point. The extent of the Doppler spread and the off-set of the sidebands from the carrier are given in Figure 7-7.

After combination of the sine and cosine components, the angle scale factors are, typically:

Azimuth:	333 Hz per degree
Elevation 1:	1 kHz per degree
Elevation 2:	2 kHz per degree.

The different angle data functions time-share the same frequency range.

Figure 7-7 presents frequency data of interest for the Doppler system and is based on the above mentioned scale factors. As indicated the Doppler signal is commutated above and below the reference signal. This is performed since the signal travels in both directions on the array and commutation is necessary to make the absolute value of Doppler shift from the reference the same for both directions of travel on the array. It is interesting to note that the ground reflected component of the elevation signal will be at a different frequency than the direct signal. This can be used to advantage to produce a nonfluctuating, uncontaminated signal.

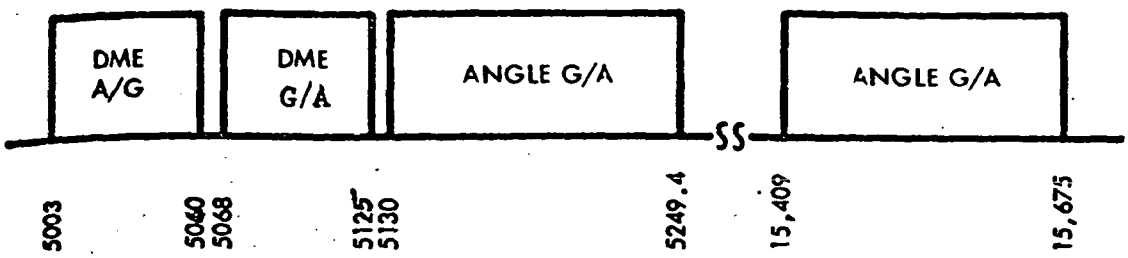

CHANNEL	DME A/G	DME G/A	ANGLE C-BAND	ANGLE Ku-BAND
1	5003	5068	5130.0	15,409.0
2	5003	5068	5130.6	15,409.9
5	5003	5068	5132.4	15,412.6
6	5003	5068	5190.0	15,413.5
7	5003	5068	5190.6	15,414.4
10	5003	5068	5192.4	15,417.1
11	5006	5071	5133.0	15,418.0
15	5006	5071	5135.4	15,421.6
16	5006	5071	5193.0	15,422.5
181	5057	5122	5184.0	15,571.0
191	5060	5125	5187.0	15,580.0
195	5060	5125	5189.4	15,583.6
196	5060	5125	5247.0	15,584.5
200	5060	5125	5249.4	15,588.1

Figure 7-4. LGS FREQUENCY ALLOCATION PLAN

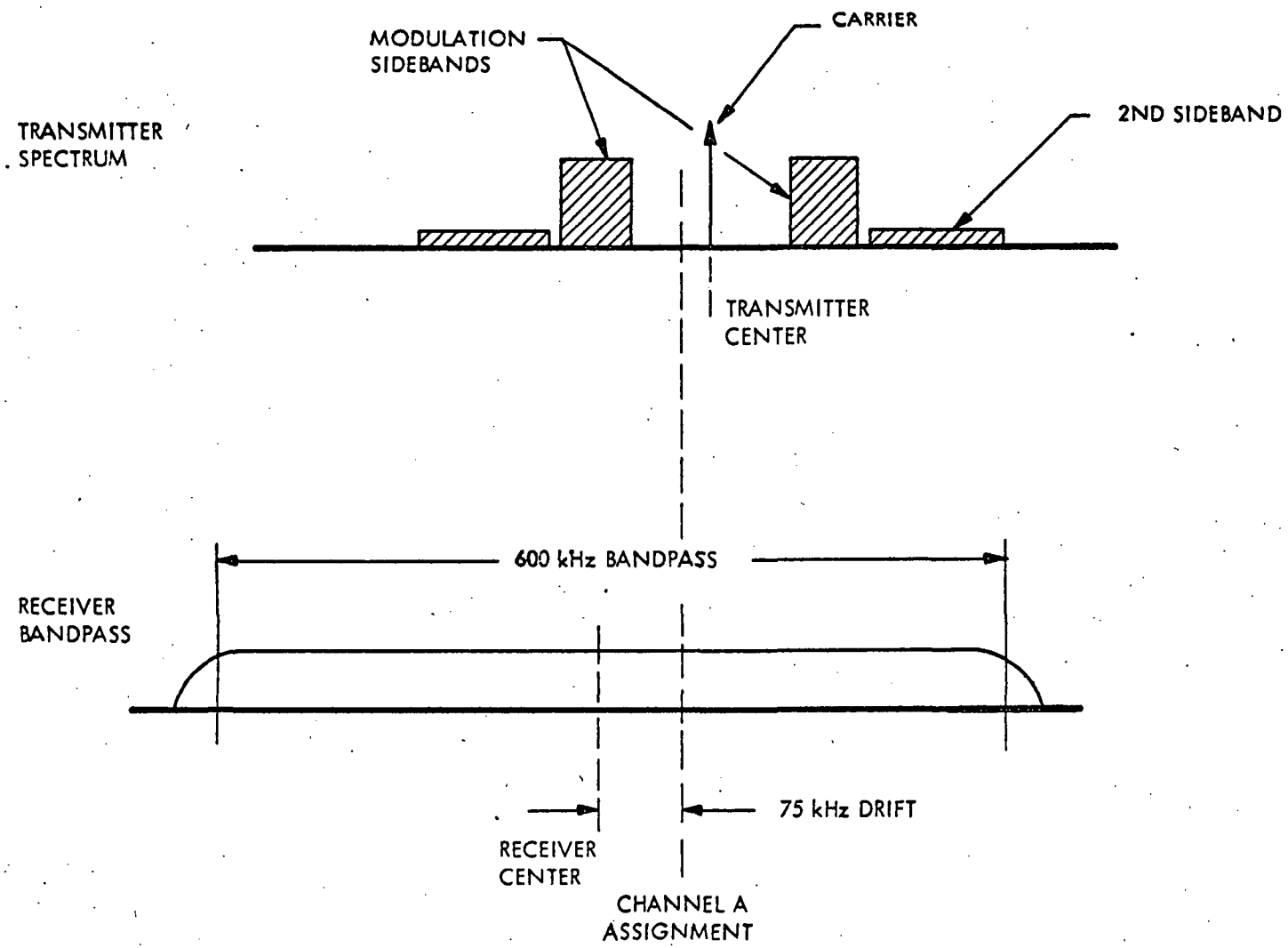

Figure 7-5. FREQUENCY SPECTRUM AND RECEIVER BANDPASS

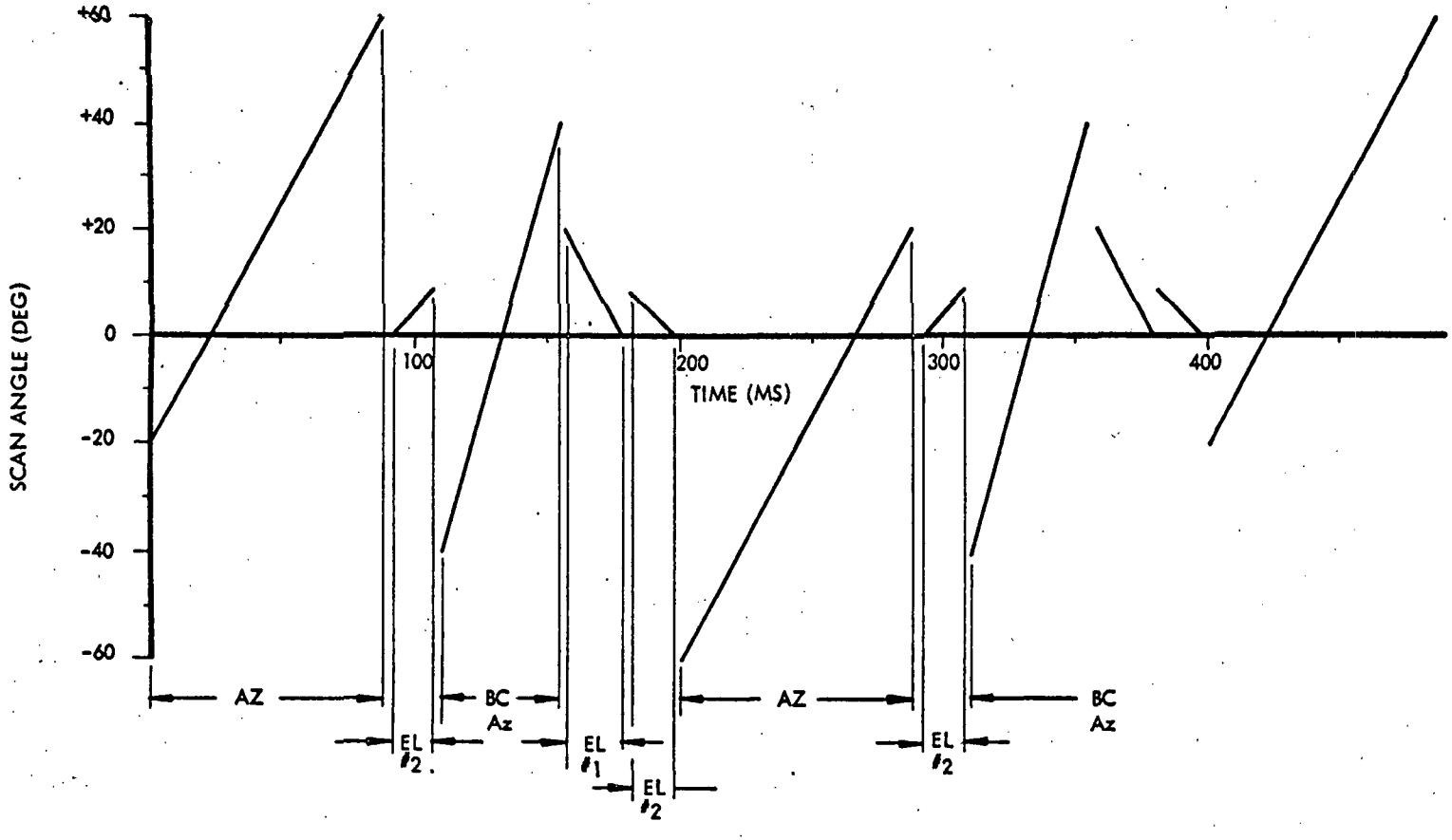

Figure 7-6. TYPICAL SCAN CYCLE FOR MECHANICALLY SCANNED ANTENNAS

The reference signal is radiated from a fixed antenna and is necessary to cancel the effects of the Doppler created by aircraft motion. Figure 7-8 presents the location and orientation of the antennas for the Doppler system and Figure 7-9 presents possible time sequencing of the various functions.

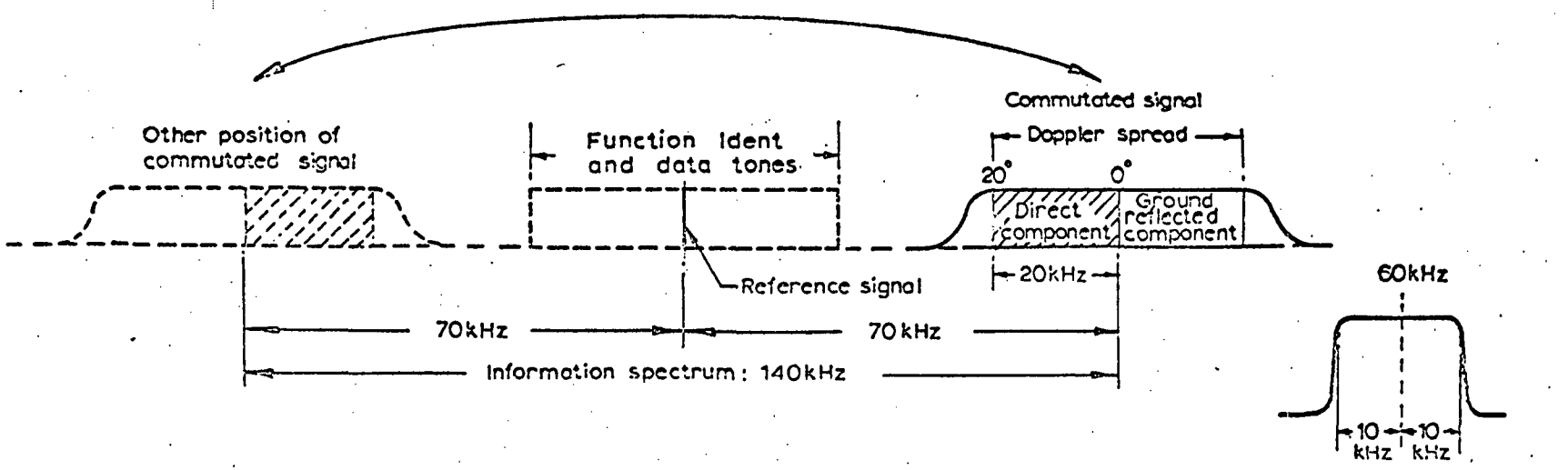

Figure 7-7a. ELEVATION SIGNAL

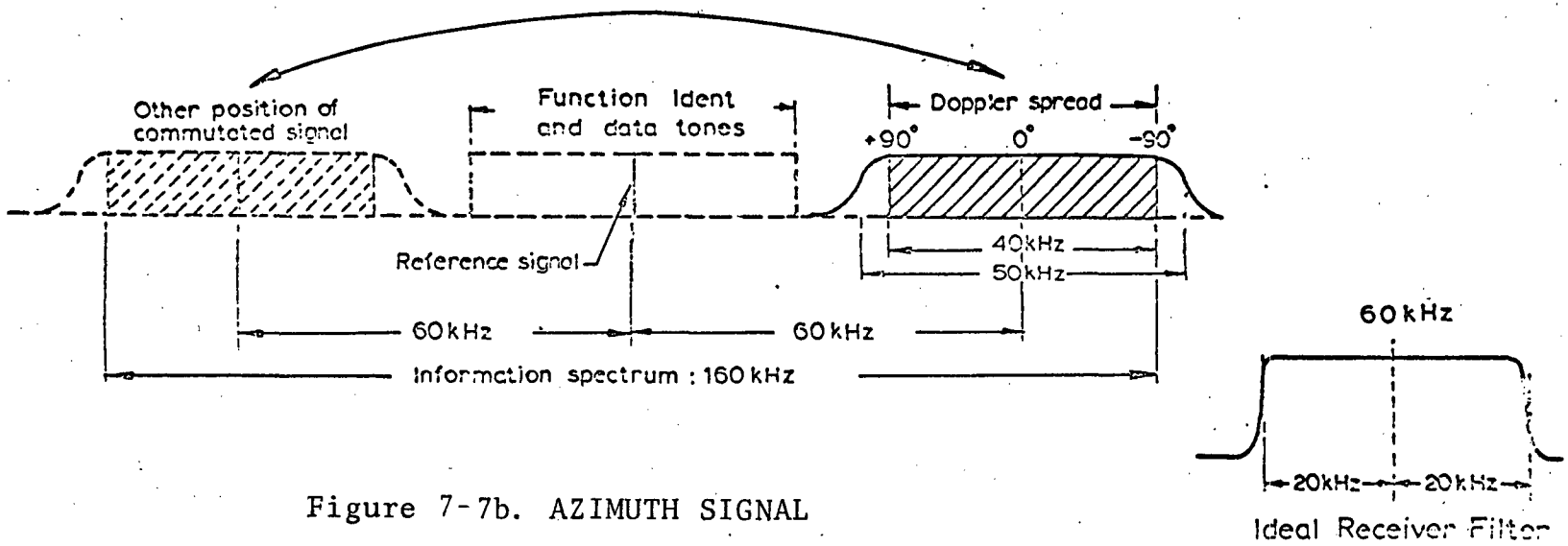

Figure 7-7b. AZIMUTH SIGNAL

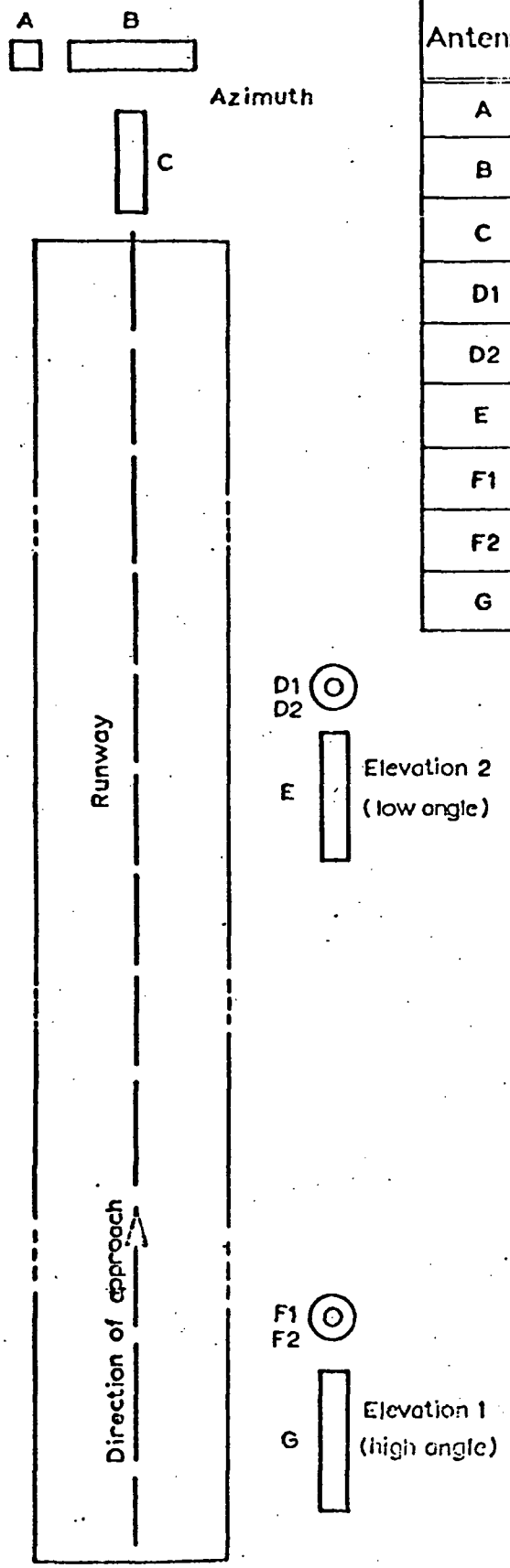

Antenna	Service	Number of radiators in array	Length of array
A	Azimuth reference	—	—
B	Main Azimuth Array (sine) front and back	150	60λ
C	Subsidiary Azimuth Array (cosine)	90	36λ
D1	Main Elevation 2 Array (sine)	30	60λ
D2	Elevation 2 Reference	—	—
E	Subsidiary Elevation 2 Array (cosine)	30	10λ
F1	Main Elevation 1 Array (sine)	60	60λ
F2	Elevation 1 Reference	—	—
G	Subsidiary Elevation 1 Array (cosine)	30	10λ

Figure 7-8. ANTENNA POSITIONS

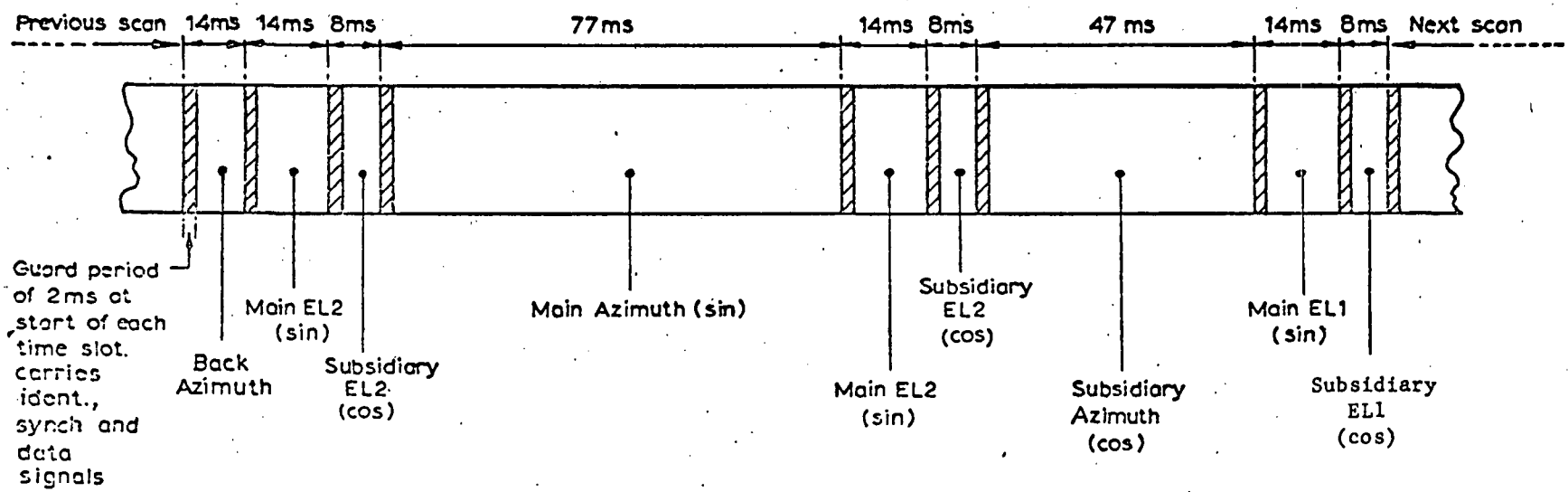

Figure 7-9. TIME SEQUENCE OF SIGNALS

7.1.3 Design Concepts

As mentioned previously, the azimuth and elevation channels are of primary importance in the operation of the MLS. Data signaling should be quite accurate due to the low data rates involved; and as a result, are not of primary importance to the simulation model and are not discussed here. The inherent errors in the MLS system are closely tied to the characteristics of the propagation channel (presented in Section 7.3), the signaling format (previously discussed in this section) and the design of the Az/El detector and processor.

7.1.3.1 Conventional Scan MLS

Several receiver concepts might be defined satisfying the requirements of the Az/El sensor. A design considered typical is shown in block diagram form in Figures 7-10 and 7-11.

Referring to Figure 7-10, the signals from the "C"-band and "Ku"-band antenna system are fed through low-loss broadband preselectors. An IF frequency of 490 MHz, as in this concept, will yield a noise figure of 2 dB and have 10 dB of gain per stage. This IF frequency is high enough to provide sufficient spurious rejection without an extremely complicated preselector. Broadband preselectors were chosen because of their simplicity and small size and weight. The "C"-band preselector considered in the concept uses stripline resonators. The "Ku"-band preselector uses waveguide resonators.

In the conventional-scan MLS, the angle of azimuth and elevation is determined by measuring the average value of modulation frequency during beam transit. This is accomplished in the processor by selecting a well defined central portion of the beam having the highest signal level for processing and, thereby, reducing the effects of noise, sidelobes and spurious signals which are below a predetermined threshold level.

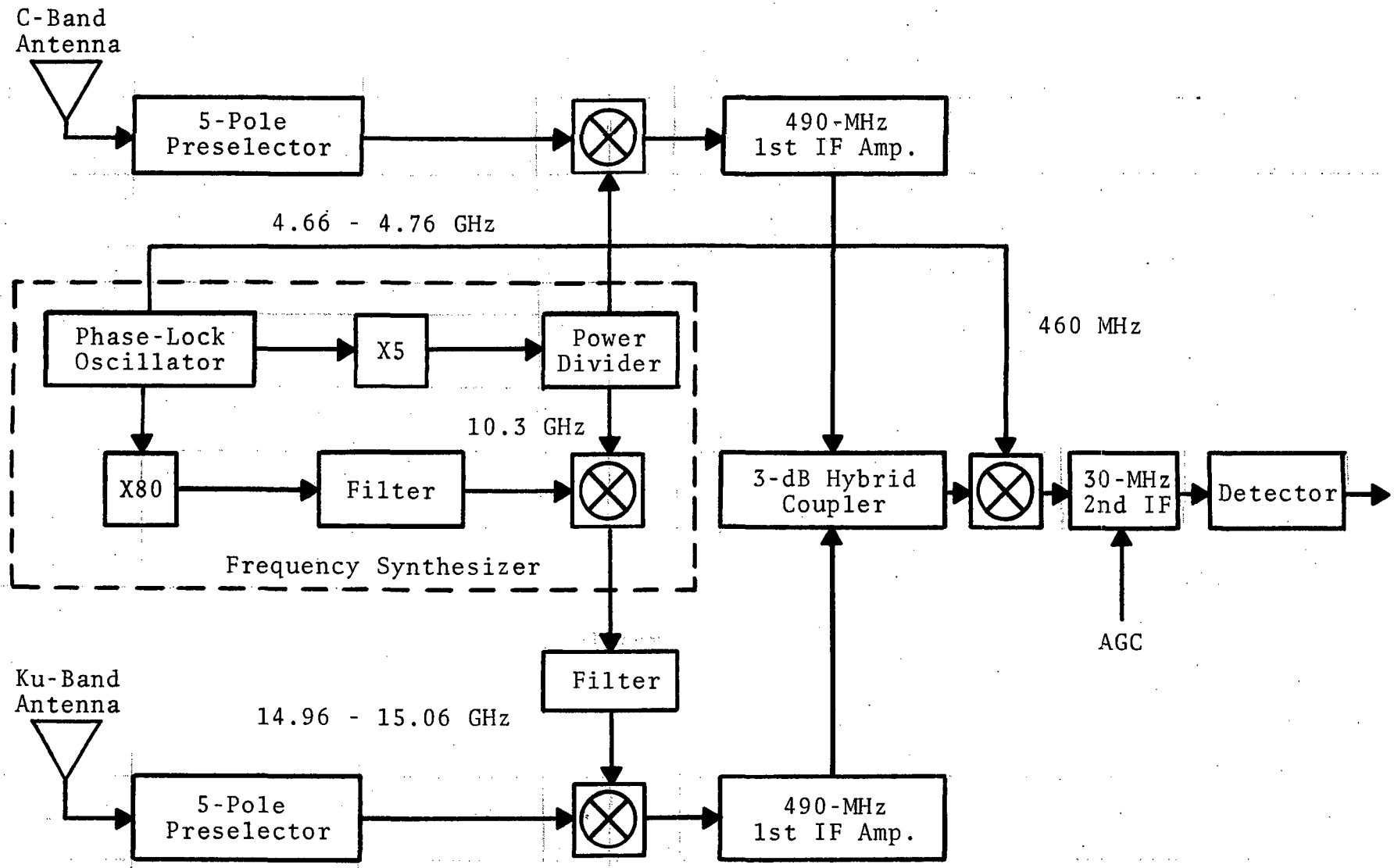

Figure 7-10. LGS Receiver Block Diagram.

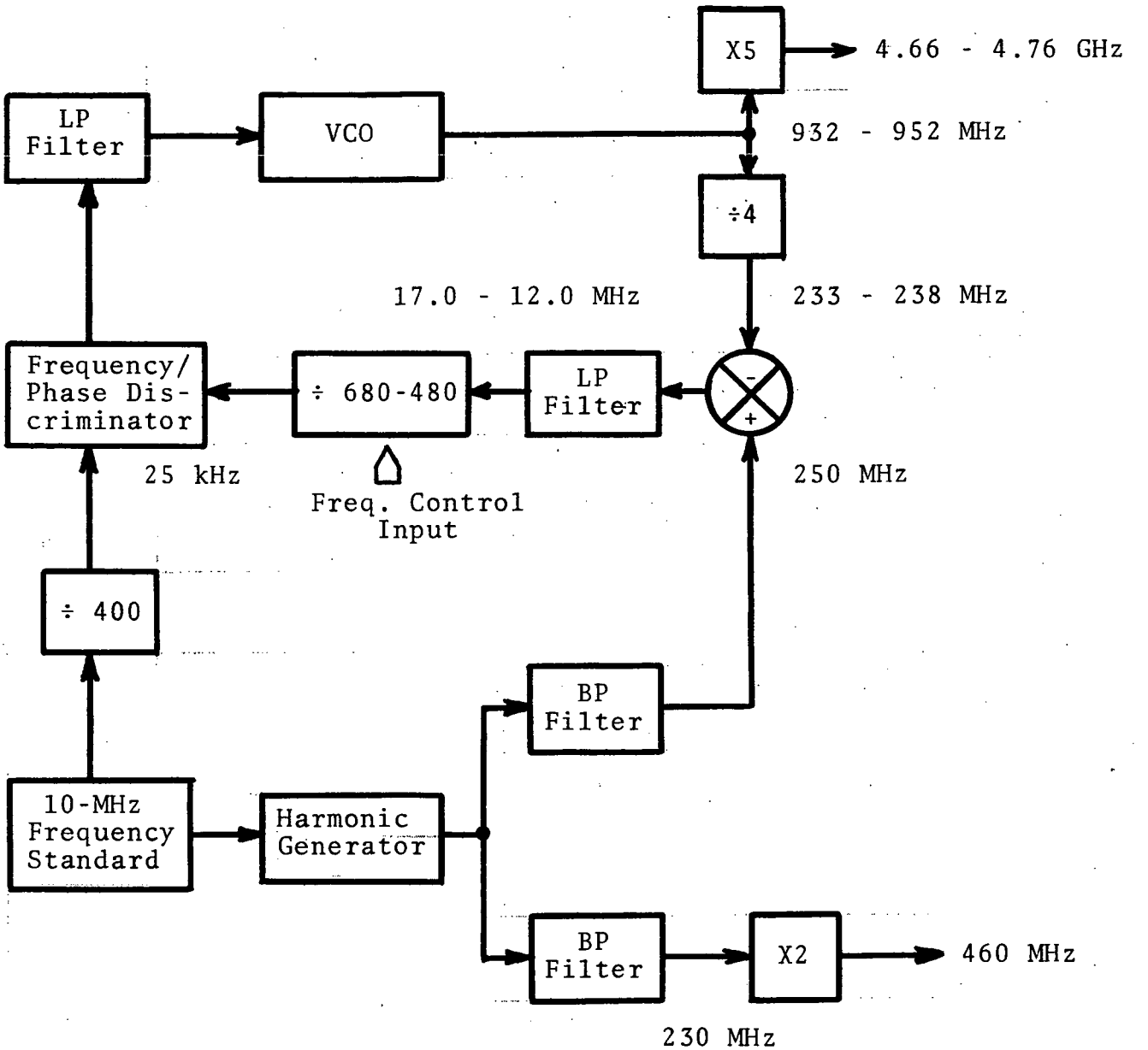

Figure 7-11. FREQUENCY SYNTHESIZER

This threshold level is typically adjusted to be 3 dB to 10 dB below the peak signal level on the nose of the beam. The time of transit of the beam during which it exceeds the threshold level is known as "dwell time".

The extent of the baseband spectrum is determined by the dwell time – the longer the dwell time, the less spectrum spread and the less "cross-talk" between data sidebands. For example, increasing the dwell time by 2:1 would allow reduction of the tone filter bandwidth by a factor of 2 with attendant S/N enhancement.

Assuming that beamwidth and beam scan rate are fixed, the dwell time may be maximized in the processor by reducing the threshold level as low as possible, consistent with providing adequate protection against sidelobes and multipath. Theoretical studies and actual narrowband antenna patterns indicate a reasonably constant pattern slope in the range from -3 dB to -15 dB with some steepening of the slope around -10 dB. Sidelobes are typically down greater than 20 dB.

The processor concept shown in Figure 7-12 is essentially an analog-to-digital converter which processes the frequency analog of angle sampled during the beam dwell time and converts it to a digital representation of the angle for use by instrumentation and AFCS systems. For the purpose of simplicity, processing of only azimuth and Elevation 1 scan functions are considered.

In this concept, a frequency discriminator is used in conjunction with voltage controlled oscillators in phase lock loops to provide a system of "centroid" tracking of the beam angle modulation. A common discriminator, gated by signals derived from the function identification tone codes, is time shared between two tracking oscillators; one for azimuth and one for elevation. The tracking oscillators must be capable of tracking beam angle modulation frequencies from 70 kHz to 140 kHz, corresponding to the modulation frequency range of azimuth and elevation angles served by the MLS.

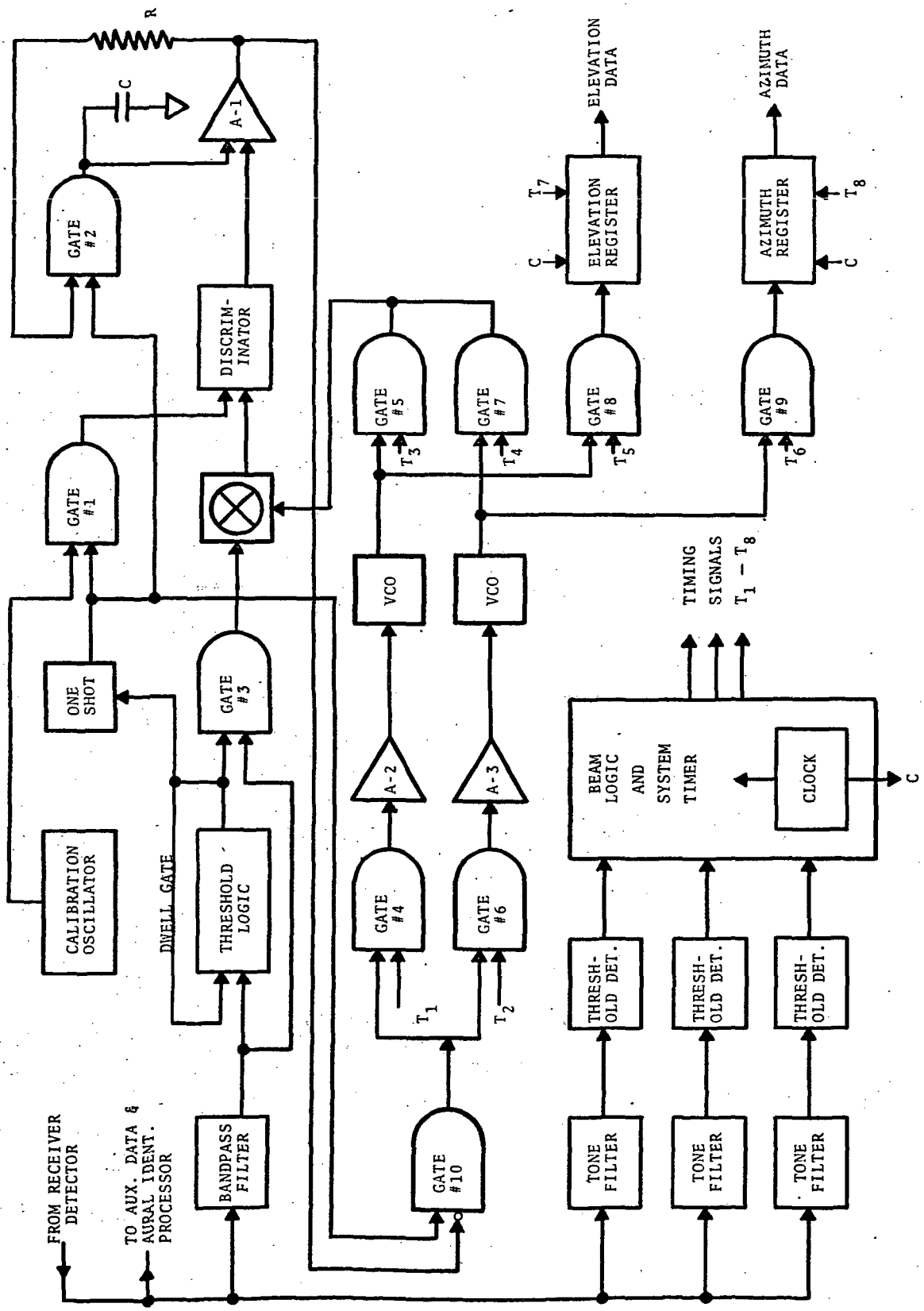

Figure 7-12. Conventional Scan-Angle Data Processor.

The discriminator is centered at 500 kHz and has a bandpass of ±50 kHz. VCO frequencies from 360 to 430 kHz are mixed with the angle modulation frequencies of 70 to 140 kHz to produce the 500-kHz center frequency of the discriminator. Deviation in the sum frequencies from 500 kHz will result in a polarized error voltage at the output of the discriminator which is used to servo the azimuth and elevation angle frequencies.

The discriminator must be broadband because of spectrum spreading resulting from the relatively short dwell time provided by the conventional scan LGS. The inherent stability of broadband discriminators is not sufficient to meet the accuracy requirements of the tracking system so self-calibrate loops are required. The discriminator self-calibrate circuit operates automatically after each beam passage and modulation frequency measurement. The trailing edge of the dwell gate is differentiated to trigger a "one-shot" which opens Gate 1, applying a precision 500-kHz calibration signal to the input of the discriminator. The "one-shot" also closes Gate 10, keeping the discriminator output off the VCO's and opens Gate 2, completing the feedback path around operational amplifier A1.

The airborne receiver processes ground-to-air DME pulse replies in the 5068-to 5125-MHz region of C-band, angle tone signals in the 5130-to 5249.4-MHz region, and Elevation 2 angle signals at Ku-band. The 20-channel frequency synthesizer/multiplier provides low-side local oscillator injection for the angle receiver, and DME receiver in addition to transmitter excitation. In the DME receiver, the local oscillator injection is always 65.0 MHz lower than the reception frequency; hence, the IF is 65.0 MHz. The angle, or Az-El, receiver utilizes a dual-frequency first IF at 128 and 188 MHz, each with a 3-MHz bandwidth. This arrangement provides for each group of 10 angle channels corresponding to the associated DME frequency. The second local oscillator

produces 10 crystal-controlled frequencies (spaced by 0.6 MHz) in two groups of 5 to provide a fixed second IF amplifier with a 410-kHz bandwidth. The Ku-band signals are down-converted to the 400-to 417.1-MHz IF band by the tripled C-band LO frequencies (5003-5060 MHz). The second LO produces 10 crystal-controlled frequencies (spaced by 0.90 MHz) in order to provide a fixed second IF which is common with the Az-El receiver. Figure 7-13 indicates the various frequencies for the 3 receiver and transmitter functions in a typical case.

The airborne decoder/processor performs the following functions:

a. angle function identification and switching
b. angle decoding
c. planar conversion
d. auxiliary data decoding
e. auxiliary data processing and output
f. range decoding and processing.

Processing of DME range measurements and certain other above functions are well known and will not be discussed at this point. Other items are more unique and will be considered.

7.1.3.2 Doppler System Angle Data Processor

Figure 7-14 shows a simplified block diagram of a typical angle, or Az-El, processor.

A set of frequency filters and associated differential detectors are used for angle and auxiliary data decoding. A relatively fast response AGC amplifier responds to signal level changes from the various angle transmitters in 1 to 2 milliseconds. A data processor stores and parity checks the auxiliary data words. It also computes differential path angles and aircraft altitude for the flare computer.

All angle data Doppler frequencies are in the same frequency band from 40 - 80 kHz (the elevation uses a lesser range of 50 - 70 kHz); consequently, a common digital counting type angle decoder is utilized to provide the appropriate

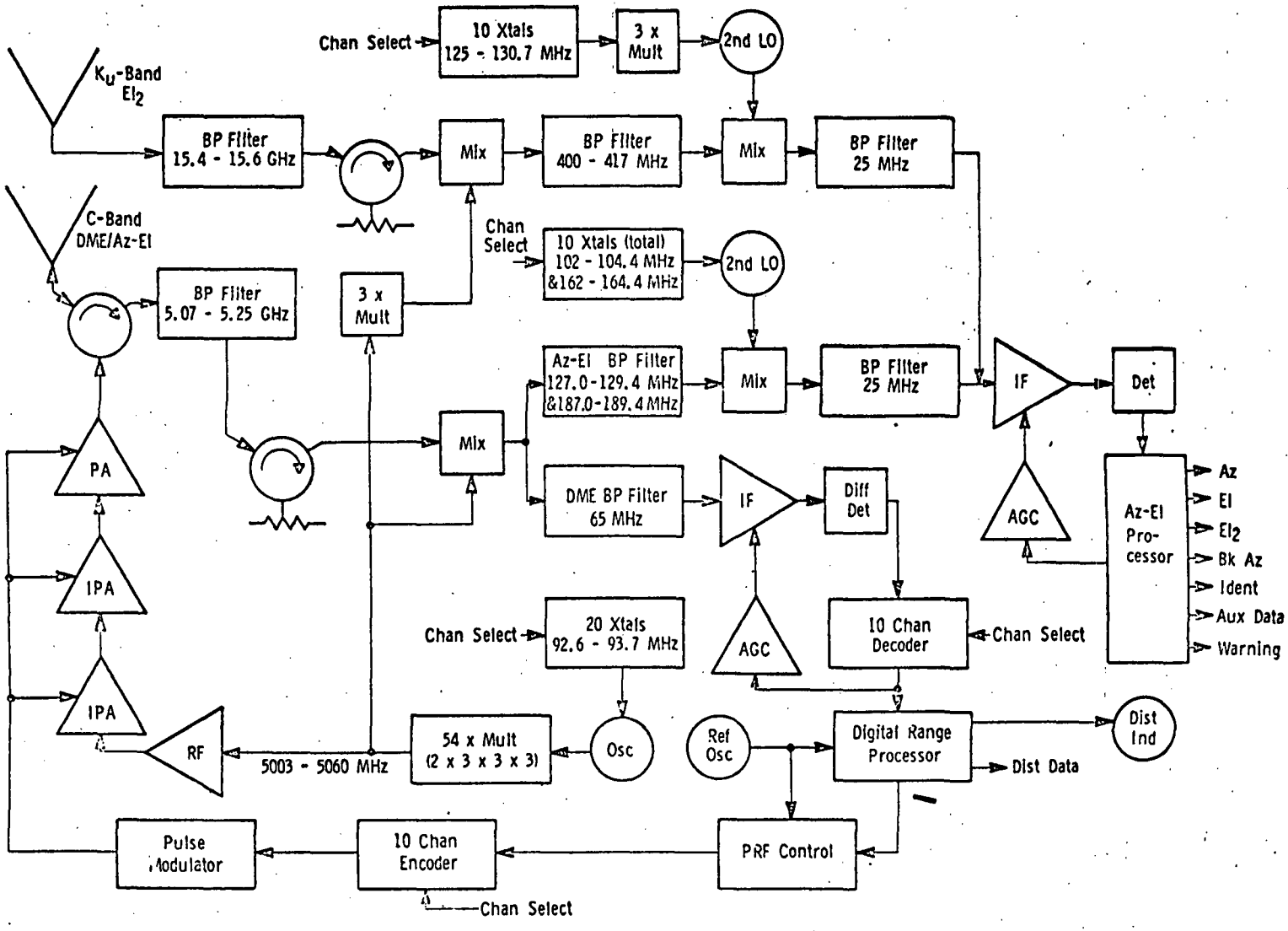

Figure 7-13. AIRBORNE LGS BLOCK DIAGRAM

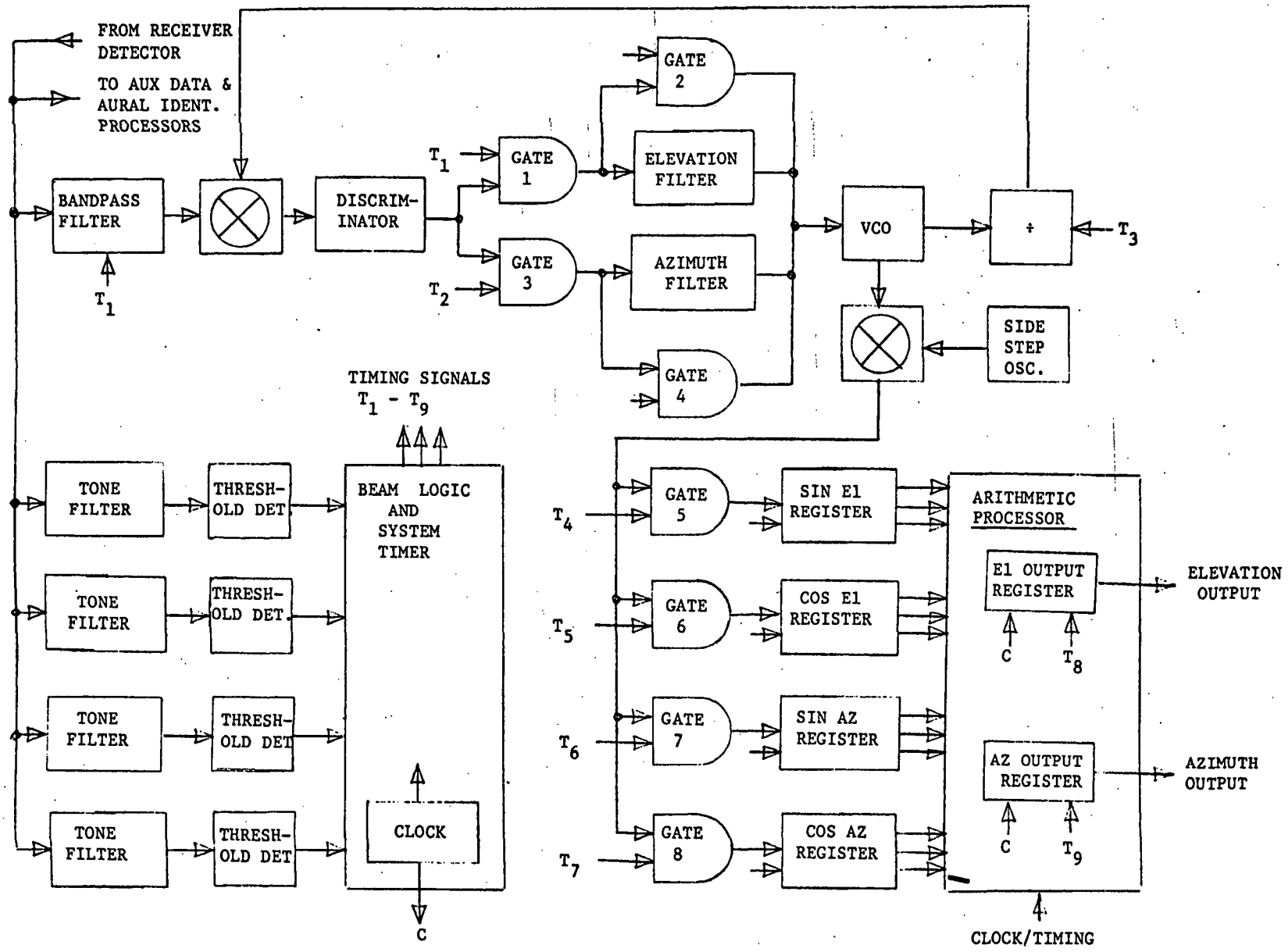

Figure 7-14. DOPPLER SCAN ANGLE DATA PROCESSOR

aircraft azimuth and elevation bearing angles. Counting over essentially the whole time slot for each angle function is done as previously described in order to minimize granularity.

In one Doppler scan processor concept a "centroid" tracking filter, using a phase lock loop similar to that described for the conventional scan processor, is used. The discriminator in the tracking loop will require self-calibration when used in configuration K (ICAO CAT III) systems; however, because of the longer dwell time of the Doppler scan system and allowable narrower discriminator bandwidth, self-calibrate will probably not be required for configuration F (ICAO CAT II) systems.

A count-down technique utilizing a digital divider is used in the phase lock loop to scale the tracking oscillator to a frequency high enough to provide the required angle function resolution. The scale factor, in cycles per degree, is different for each angle function in the Doppler scan system; therefore, the scale factor of the digital divider must be changed for each angle function.

A local oscillator signal, derived from the frequency synthesizer, is used to side-step the tracking oscillator frequency so that when the side-stepped frequency is gated into the sin/cos registers, the count is such that sin = 0 and cos = 1 at 0°.

The counter gate and sin/cos registers for the azimuth and elevation angle functions are sequenced by the timing unit to derive the sin/cos function data. The sin/cos function data, as accumulated in the registers, are further processed by the arithmetic unit to provide a digital output of azimuth and elevation angle to the resolution required by the system configuration.

7.2 Microwave Landing System Models

This section describes the models which are used in the simulator to generate errors which are characteristic of Doppler and Scanning Beam Microwave Landing Systems. These models account for the signal processing, and propagation effects including reflections and scattering from discrete reflectors.

In the transmission of signals by electromagnetic waves, multipath interference is a source of distortion. The susceptibility of different modulation systems to multipath distortion as well as methods of combating it have received wide attention [References 1-6]. Many of the previous studies are concerned with multipath resulting from reflections from the ground plane. This type of multipath is somewhat predictable and most MLS designs adequately minimize its effects. The case of discrete multipath reflections such as buildings and aircraft is not as well understood and therefore presents a more severe problem for potential MLS systems. The purpose of this section is to gain a better understanding of the discrete multipath process and to develop a mathematical model which can be used with the aircraft simulation to study the effects on the aircraft due to this type of distortion. A block diagram of the communication channel is presented in Figure 15 and a geometrical sketch is given in Figure 7-20. As can be seen in Figure 7-20, discrete multipath results from the vectoral addition of a direct and reflected wave. The reflected wave has a time delay, phase shift and amplitude attenuation with respect to the direct wave caused by the reflecting properties of the building.

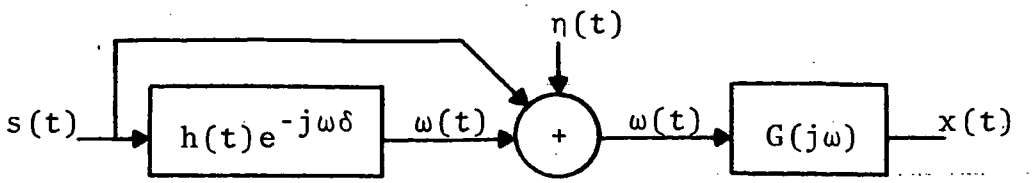

where

$s(t)$	=	transmitted signal either AM or FM
$h(t)e^{-j\omega\delta}$	=	multipath channel characterized by time varying impulse response
$\eta(t)$	=	addative Gaussian noise, not necessarily white
$G(j\omega)$	=	receiver transfer function.

Figure 7-15. Representation of Communication Channel

The carrier frequency is assumed to be sufficiently larger than the video signal bandwidth, so that the transmitted wave is a narrow band signal with the carrier frequency as the central frequency. For both the Doppler scanning beam and conventional scanning beam systems this is a very good assumption.

The multipath condition is represented by $h(t)e^{-j\omega\delta}$, consisting of a number of alternate paths. The final signal at the receiver antenna is the algebraic sum of the signals travelling along the different paths. The receiver or demodulator consists of a linear detector in the AM case and a limiter-discriminator in the FM case, both idealized so that the communication system is perfect except for multipath.

In order to proceed the characteristics of the multipath model must be considered. There is, unfortunately, very little emperical data which bears closely upon the problem. From the data that has been collected [7-10] it is possible to make some reasonable conjectures. First of all the discrete multipath can be adequately described in terms of a finite number of spurious paths characterized by corresponding relative amplitudes and differential time delays in relation to the direct signal.

If $\mathrm{Re}[s(t)e^{j\omega_o t}]$, $t\varepsilon\ (-\infty,\infty)$ is transmitted, where $S(\cdot)$ is a complex-valued low-pass waveform and ω_o is the carrier frequency, then $[\rho(t)e^{j\omega_o t}]$, $t\varepsilon\ (-\infty,\infty)$ is received where $\rho(t) = \Sigma a_k[S(t-t_k)e^{j\Theta_k}] + \eta(t)$. The propagation medium is described by the set of path variables $[a_k, t_k, \Theta_k]_0^\infty$. The time delay of the reflected wave is given by t_k; the phase shift by Θ_k, and the amplitude attenuation by a_k. We will assume that the noise is Gaussian but not necessarily white, and is of no special interest in this development.

The time delays that we are concerned with are of the order of a few hundredth's of a microsecond and the carrier frequency is in the gigahertz range. Thus an error in the order of one nanosecond in the time delay will cause a change of π radians in the carrier phase. Such changes will constantly take place in the case of a fixed transmitter and an aircraft approaching a runway. Therefore it was assumed that the carrier phase, ϕ, of the various paths are mutually independent random variables which are uniformly distributed between $(0, 2\pi)$ [10]. The assumption will also be made that the sequences of path delays $[\delta]$ and strengths [a] are well approximated by their deterministic values. This assumption is more difficult to justify but is appears reasonable when one considers the frequencies [50 kH] and the high signal to noise ratio that we are concerned with [11 pp 134].

7.2.1 Doppler System (DS)

Let $s(t) = V(t)\cos\omega_c t$ and

$V(t) = A\cos\omega_\Delta t$

Also let $[a_i]$, $[\tau_i]$ i=0, 1--- , characterize the multipath amplitude coefficients and differential time delays, and to simplify the notation we shall take $a_o = A$, $\tau_o = 0$, denoting the direct signal or the signal with no multipath. Then the signal received when multipath is present can be written

$$\omega(t) = \sum_{i=0}^{n} a_i[V(t-t_i)\cos(\omega_c t-\phi_i)]$$

Assuming a linear detector the received video signal x(t) is the envelope of $\omega(t)$ or

$$x(t) = [(\Sigma a_i V(t-t_i)\cos\phi_i)^2+(\Sigma a_i V(t-t_i)\sin\phi_i)^2]^{1/2}$$

For simplicity we shall consider only the two path case (i.e., a direct and reflected signal) i=),1 then

$$x(t) = [(a_o V(t)+a_1 V(t-\delta)\cos\phi)^2+(a_1\sin\phi V(t-\delta))^2]^{1/2}$$

After some algebra and ignoring the DC component the following results

$$x(t) = (K^2+C^2)^{1/2}\cos(2\omega_\Delta t + \text{arc tan } C/K)$$

$$A = a_o^2+2a_o a_1\cos\phi\cos\theta+a_1^2\cos^2\theta$$

$$B = a_1^2\sin^2\theta$$

$$C = a_o a_1\cos\phi\sin\theta+\frac{a_1^2}{2}\sin^2\theta$$

$$K = (A-B)/2$$

The error term $y = \text{arc tan } \frac{C}{K}$ can be approximated by $y = \frac{C}{K}$

where

$$y = \frac{A+B\cos\phi}{D+E\cos\phi}$$

The variables have been redefined so as to express the error as a function of the ratio (R) of the interference to direct signal component

$$R = \frac{a_1}{a_2} = \frac{\text{reflected}}{\text{direct}}$$

$$A = \left(\frac{a_1}{a_o}\right)^2 \frac{\sin(2\theta)}{2}$$

$$B = \frac{a_1}{a_o} \sin\theta$$

$$D = 1 + \frac{a_1}{a_o}^2 \frac{\sin(2\theta)}{2} + \left(\frac{a_1}{a_o}\right)^2 \cos^2(2\theta)$$

$$E = \frac{a_1}{a_o} \sin\theta + 2\left(\frac{a_1}{a_o}\right)^2 \cos\theta$$

In summary, the assumptions have been made that a_o, a_1, and θ are well approximated in the measurement interval by their deterministic values whereas ϕ is a uniformly distributed random variable in the interval.

In order to determine the statistics of the error, y, the following standard procedure is employed[11]. If the density of X is $f_x(X)$ and if $y = g(X)$ then to solve for $f_y(y)$ we solve the equation $y = g(X)$ in terms of y. If $X_1, X_2 \cdots X_\eta$ are all its real roots $y = g(X_1) = g(X_2)$

then

$$f_y(y) = \frac{f_X(X_1)}{|g'(X_1)|} + \cdots \frac{f_X(X_n)}{|g'(X_n)|}$$

where

$$g'(X) = \frac{dg(X)}{dX}$$

For the case at hand

$$g'(\phi) = \frac{[AE-BD]\sin\phi}{[D+E\cos\phi]^2}$$

The equation in ϕ, $g(\phi)=y$, has two roots in the interval $[0, 2\Pi]$

$$\phi_1(y) = \cos^{-1}\frac{A-yD}{yE-B}, \qquad 0 \leq \phi_1 \leq \Pi$$

$$\phi_2 = 2\Pi - \phi_1, \qquad \Pi < \phi_2 \leq 2\Pi$$

and algebraically the following results are obtained;

$$g'[\phi_1(y)] = \frac{[B-Ey]\sqrt{(B-Ey)^2-(A-yD)^2}}{[BD-AE]}, \qquad g'[\phi_2(y)] = -g'[\phi_1(y)]$$

$$\left[f_y(y)\right]_{DS} = \begin{cases} \dfrac{BD-AE}{\pi(B-Ey)\sqrt{(B-Ey)^2-(A-yD)^2}} & \dfrac{B-A}{E-D} < y < \dfrac{A+B}{E+D} \\ 0 & \text{otherwise} \end{cases}$$

In Figure 7-16 the probability density function $f_y(y)$ is plotted for various values of R. As y approaches the asymptotes $f_y(y)$ tends to infinity, but the area under the PDf curve always remains equal to unity. In the limit as R approaches zero the PDF degenerates into a Durac delta function at the origin. This is expected since R equal to zero implies the absence of any multipath interfernece. For all values of R, y has a zero mean value.

It can also be seen that discrete multipath results in a non-stationary random process. As the aircrafts orientation changes the probabilistic law governing the error statistics changes drastically. From this the need for a dynamic simulation can clearly be seen. The aircraft signal processor will be confronted by non-stationary random error which will be a function of its descent trajectory. In order to adequately test any signal processor or aircraft control system an accurate dynamic model of the environment must be used. This is especially true in our case because the PDF changes drastically for small changes in R.

7.2.2 Conventional Scanning Beam System (CSB)

The received signal in the CSB case can be represented in the absence of multipath as

$$f(t) = \cos(\omega_c t + \psi(t))$$

where

$$\frac{d}{dt}[\psi(t)] = V(t) = A\cos\omega_m t$$

"A" being the maximum deviation, V(t) is the video signal normalized to have a maximum of unity and ω_c the carrier frequency.

When multipath is present the received signal is

$$X(t) = \Sigma a_i \cos[\omega_c t - \phi_i - \psi(t-\tau_i)]$$

Making the assumption of strong limiting and an ideal discriminator, the received video signal y(t) with multipath is given by, except for a constant factor.

$$y(t) = \frac{\Sigma A_i V(t-\tau_i)}{\Sigma A_i}$$

where

$$A_i = a_i \sum_j a_i \cos[\phi_i - \phi_j + \Psi(t-\tau_i) - \Psi(t-\tau_j)]$$

In the two path case

$$A_o = A(A+a\cos\psi)$$

$$A_1 = a[A\cos\psi+a]$$

$$y(t) = \frac{A[A+a\cos\psi]V(t)+a[a+A\cos\psi]V(t-\tau)}{a^2+A^2+2aA\cos\psi}$$

where

$$\psi = \phi+\Psi(t-\tau)-\Psi(t)$$

In order to proceed it will be necessary to consider the $\cos\psi$ term

$$\cos\psi = \cos[\psi(t-\tau)-\psi(t)+\phi]$$

where

$$\psi(t) = \cos\omega_\Delta t$$
$$\psi(t-\delta) = \cos(\omega_\Delta t-\theta)$$

$$\cos\psi = \cos[\cos(\omega_\Delta t-\theta)-\cos\omega_\Delta t+\phi]$$
$$\cos\psi = \cos[B\cos\omega_\Delta t+E\sin\omega_\Delta t+\phi]$$

Letting

$$B = \cos\theta-1$$
$$E = \sin\theta$$

$$\cos\psi = [\cos[B\cos\omega_\Delta t]\cos[E\sin\omega_\Delta t] -$$

$$\sin[B\cos\omega_\Delta t]\sin[E\sin\omega_\Delta t]\cos\phi$$

$$-\sin\phi[\sin[B\cos\omega_\Delta t]\cos[E\sin\omega_\Delta t]$$

$$+\cos[B\cos\omega_\Delta t]\sin[E\sin\omega_\Delta t]$$

To a good order of approximation for the case at hand

$$\cos\psi = J_o(E)\ J_o(B)\ \cos\phi$$

where

$J_o(\cdot)$ = the modified Bessel function.

Letting $K = J_o(E)\cdot J_o(B)$ and $a_1 = \frac{a}{A}$

the detected signal is then

$$y(t) = \frac{(1+a_1\cos\psi)\cos\omega_\Delta t+[a_1^2+a_1\cos\psi]\cos(\omega_\Delta t-\theta)}{1+a_1^2+2a_1\cos\psi}$$

$$y(t) = \frac{(1+a_1K\cos\phi)\cos\omega_\Delta t+[a_1^2+a_1K\cos\phi]\cos(\omega_\Delta t-\theta]}{1+a_1^2+2a_1K\cos\psi}$$

$$y(t) = \frac{[1+2a_1K\cos\phi+a_1^2]\cos\omega_\Delta t+[a_1^2+a_1K\cos\phi]\sin\omega_\Delta t}{1+a_1^2+2a_1K\cos\phi}$$

$$y(t) = \cos\omega_\Delta t+\frac{(a_1^2+a_1K\cos\phi)\sin\theta}{1+a_1^2+2a_1K\cos\phi}\sin\omega_\Delta t$$

$$y(t) = \rho\cos(\omega_\Delta t+\Gamma)$$

$$\Gamma = \arctan\frac{[a_1^2+a_1K\cos\phi)\sin\theta}{1+a_1^2+2a_1K\cos\phi}$$

ρ = magnitude of phasor

$$\Gamma \cong \frac{a_1^2 \sin\theta + a_1 K \sin\theta\cos\phi}{1+a_1^2+2a_1 K\cos\phi}$$

$$\Gamma = \frac{A+F\cos\phi}{D+G\cos\phi}$$

where

$$A = a_1^2 \sin\phi$$

$$F = a_1 J_o(E) J_o(B) \sin\theta$$

$$D = 1+a_1^2\cos\theta$$

$$G = a_1 J_o(E) J_o(B)[2+E]$$

$$E = \cos\theta - 1$$

$$B = \sin\theta$$

Several observations can be made at this time. First of all the error equations for the Doppler and Conventional Scanning beam are similar. This is to be expected since both systems are quite similar [12]. The major differences revolve around implementation and equipment; two matters which don't concern us here.

Secondly, the approximation made in obtaining Γ should be quite reasonable in light of the fact that a_1 will be small. The Bessel function will also be a valid approximation owing to the fact that δ will be in the order of .02 to .1 microseconds which will make θ small and hence "B" and "E" small making it possible to ignore all Bessel functions of higher order than zero.

By analogy with the Doppler system the probability density function for the conventional scanning beam system is given by

$$\left[f_y(y)\right]_{CSB} = \begin{cases} \dfrac{FD-AG}{\pi(F-Gy)\sqrt{(F-GY)^2-(A-yD)^2}} & \dfrac{F-A}{G-D} < y < \dfrac{F+A}{G+D} \\ 0 & \text{otherwise} \end{cases}$$

In Figure 7-17 the probability density function fy(y) is plotted for various values of R. In comparing Figure 7-16 and 7-17 it is seen that the PDF for the DS and CSB are very similar.

7.2.3 Digital Simulation of Probability Density Function

Given a sequence of random numbers, how can one generate a sequence of random observations from a given probability distribution? The first step is to construct the cumulative distribution function, $F(X) = P[x \leq X]$, where x is the random variable involved. This can be done by writing the equation for this function, or by graphically plotting the function, or by developing a table giving the value of x for uniformly spaced values of F(x) from 0 to 1.

The second step is to generate a random decimal number between 0 and 1. This is done by obtaining a random integer number having the desired number of digits (including any leading zeros) and then placing decimal points in front of it. The final step is to set $P[x \leq X]$ equal to the random decimal number and solve for x. This value of x is the desired random observation from the probability distribution. This procedure is illustrated in Figure 7-18 for the case where the cumulative distribution function is plotted graphically and the random decimal number happens to be .5269.

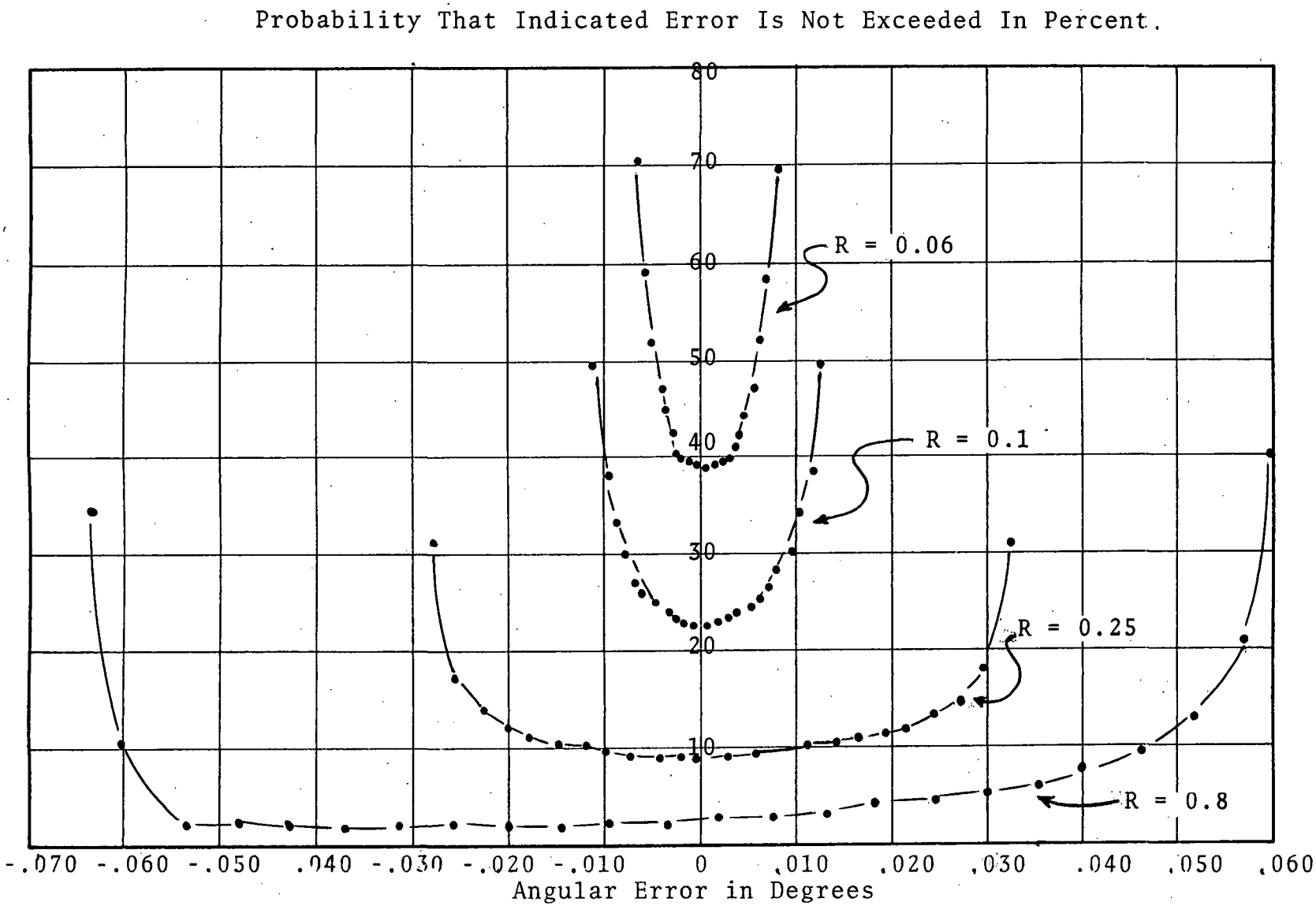

Figure 7-16. Probability Density Function for Doppler System.

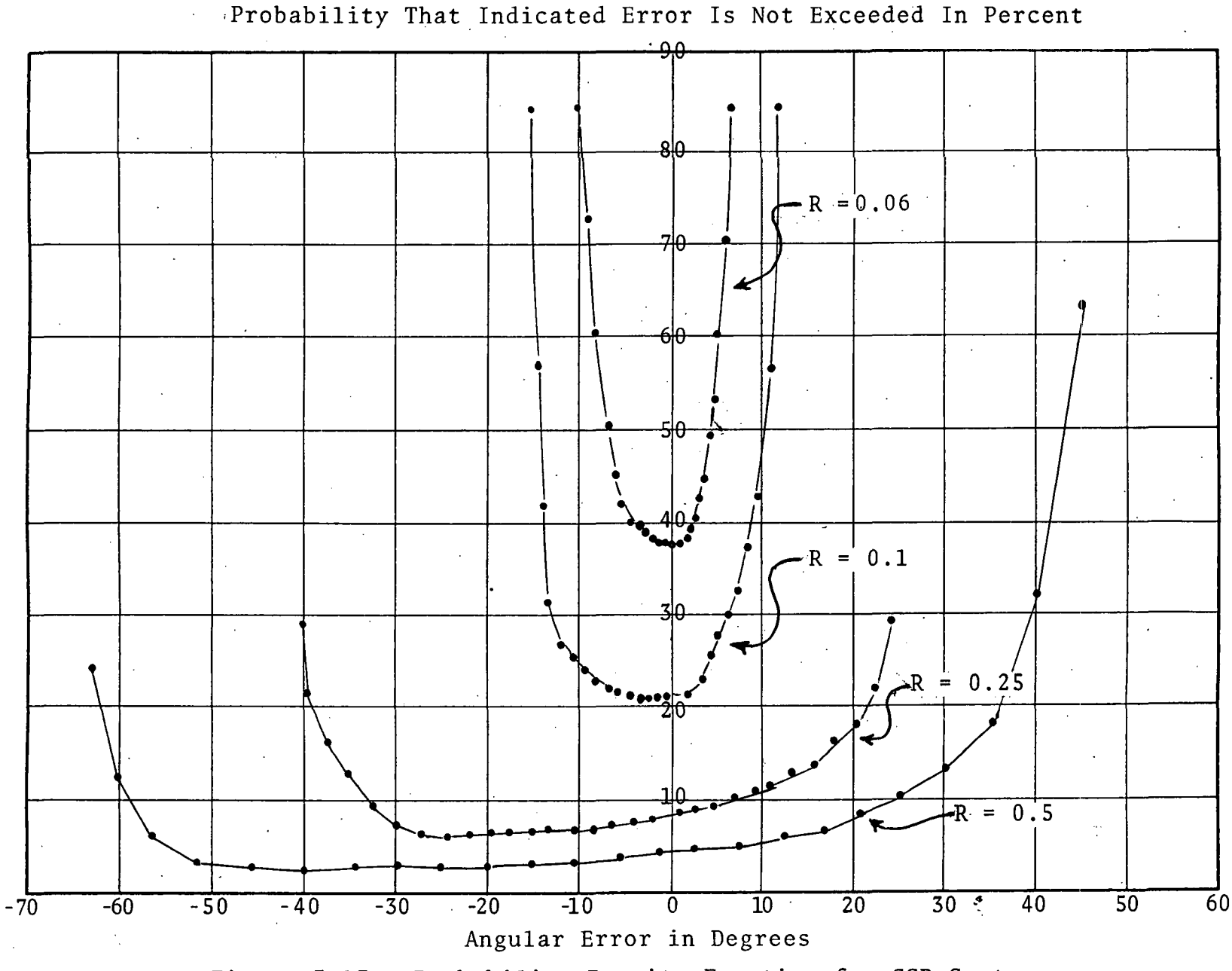

Figure 7-17. Probability Density Function for CSB System.

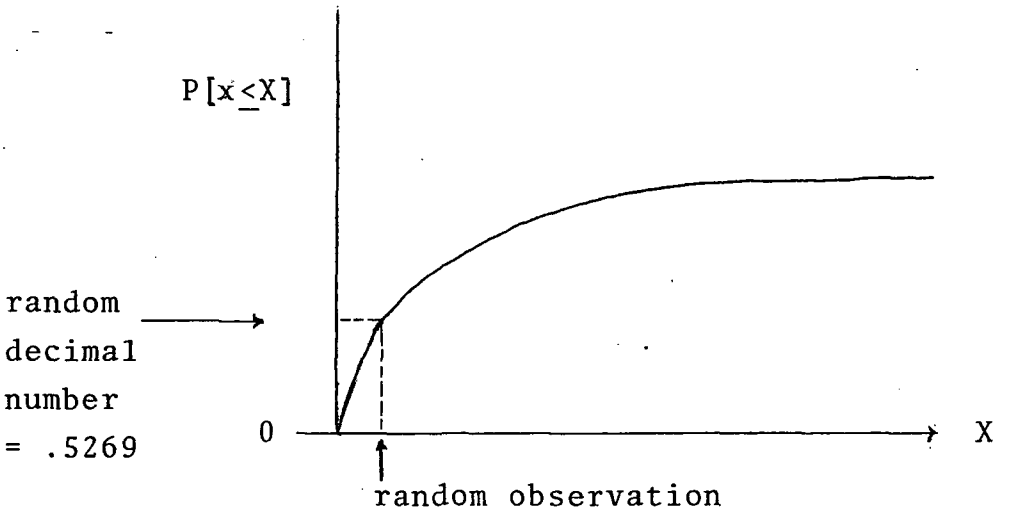

Figure 7-18. Probability Distribution Function

When the given probability distribution is continuous, the procedure outlined above actually approximates this continuous distribution by a discrete distribution whose irregularly spaced points have equal probabilities. However, this is not particularly serious since the approximation can be made as accurate as desired by using a sufficiently large number of digits for the random number. Perhaps the greatest danger is that the approximation will be adequate everywhere except in the extreme tails of the distribution. One refinement that would rectify this is to generate a second random number whenever the first one is (for the case of three-digit random numbers) 000 or 999 in order to select a value of $P[x \leq X]$ within the range from 0.000000 to 0.000999 or from 0.999000 to 0.999999.

For the case at hand it will be necessary to integrate $f_y(y)$ in order to find the cumulative probability density function

$$P[x \leq X]_{Doppler} = \frac{BD-AE}{\pi(B-E_y)\sqrt{(B-E_y)^2-(A-Dy)^2}}$$

defining the following terms

$$K = AE-DB$$
$$C = E^2-D^2$$
$$b = 2KD$$
$$a = -K^2$$

$$P = \frac{(BD-AE)}{\pi\sqrt{-a}} \quad \text{arc sin} \quad \frac{by+2a}{y\sqrt{b^2-4aC}}$$

$$\sin[\pi P] = \frac{by+2a}{y\sqrt{b^2-4aC}}$$

$$y = \frac{2a}{2KE\sin[\pi P]-b}$$

A random number generator that can be used on the CDC 6400 computer is given below in Fortran:

```
IY   =   IX(65549)
IY   =   IY+576460752303423487+1
YFL  =   YFL*.3552713678 x 10^-14
```

The procedure is then the following. A random number is obtained and designated as P in the above equation. From it a value of y is calculated which will then have the specified probability density function. The same procedure is used for both Doppler and Conventional Scanning systems. The formulas are quite similar involving changing the definitions of the variables used.

7.2.4 Calculation of Path Constants

In all the equations developed for the error function the variables have been expressed as functions of the multipath channel, i.e., (a_1/a_o) the ratio of the indirect field strength to the field strength of the direct signal, and θ which is the product of ω_Δ and the difference in time delay between the direct and reflected wave. In order to accurately describe the error it is important to accurately calculate the path constants. Simple ray theory was not considered percise enough to capture all the variations of the discrete multipath reflector. For this reason a more involved model was used. For a complete description reference [9] should be consulted. What follows is a summary discussion which will acquaint the reader with the formulas that were used.

The basic problem can be formulated in the following manner. An electromagnetic wave E_i and H_i is incident on a surface A with boundary contour L as shown in Figure 7-19. It is desired to determine the resultant E-field at an arbitrary point P.

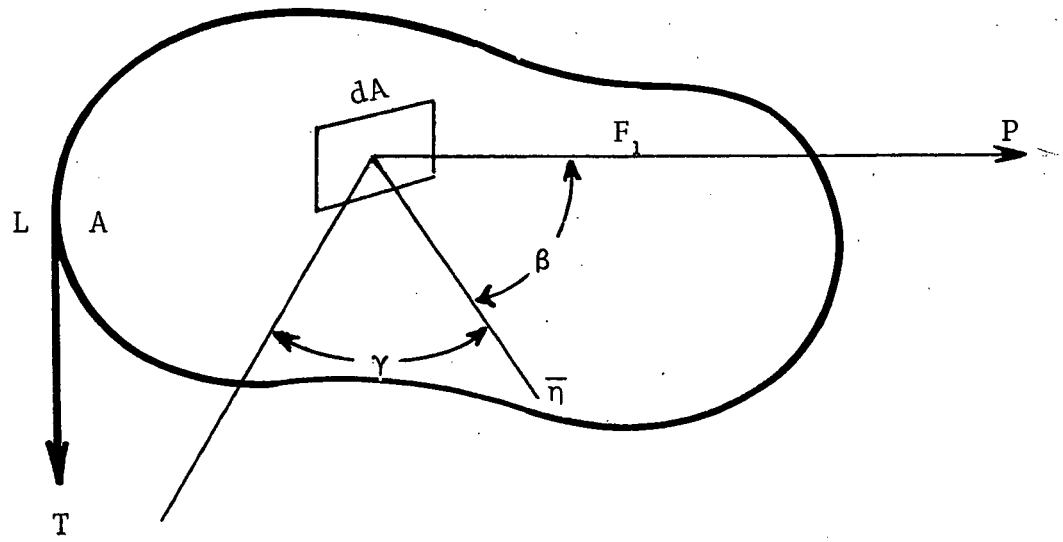

Figure 7-19. Scattering of an Electromagnetic Wave

The resultant field $\bar{E}$ at P is the sum of the incident field and the scattered field

$$\bar{E}(P) = \bar{E}_i(P)+\bar{E}_S(P)$$

The method used to solve this problem is called Greens Theorem. Denote by $\bar{E}$, $\bar{H}$ the field on Σ, then assuming as usual harmonic time dependence, it can be shown that the E-field at P

is given by

$$\bar{E}(P) = \frac{1}{4\pi}\int_{\Sigma} [-j\omega\mu\ (\bar{\eta}x\bar{H})G+(\bar{\eta}X\bar{E})x\ \bar{\nabla}G + (\bar{\eta}\cdot\bar{E})\bar{\nabla}G]dS - \frac{1}{4\pi j\omega\tilde{\epsilon}}\int(\bar{T}\cdot\bar{H})\bar{\nabla}GdS$$

where

$G = \frac{e^{-jkr}}{r}$

$\bar{\eta}$ = unit normal to Σ

T = unit tangent to Γ

ω = angular frequency

μ = permeability

K = propagation constant = $\sqrt{\mu G}$

ϵ = dielectric constant

j = $\sqrt{-1}$

r = distance from P to a point Q on Σ

Making use of the assumptions that in MLS cases the points P of interest are in the far field (Fraunhofer) zone of $\bar{E}_S$, so that τ is large. Also only the E field will be considered because E/H is the intrensic impedance and is constant. We assume that W/λ, where W is the width of the building under consideration, is generally greater than 100. Making these assumptions

then

$$E_S(P) = \frac{j}{2\lambda}\int_A (\cos\beta+\cos\gamma)G\bar{E}_{r_t}dA$$

The geometry of the situation is shown in Figure 7-20. The field at the receiver directly from the antenna and ignoring ground reflections is

$$E_D = \frac{2jF(\phi_R)}{D_R}e^{-jRD_R}$$

where $F(\phi_R)$ is the antenna gain pattern which will be modelled as $\cos^2(\cdot)$. E_D does not account for the ground image because it is believed that the lobing will be reduced to a minimum in MLS applications.

For a vertical wall

$$E_S(P) = \frac{j}{2\lambda} \int_A E_R M_G G dA$$

$$M_G = (\cos\beta - \cos\gamma)\cos(\beta - \gamma)$$

M_G is called the reflection modulus for the Green's theorem method. The projection of the center of the base of the wall onto the ground plane was chosen as the reference point so that a simple form could be obtained. D_B and R_B are the slant distances from this reference point to the antenna and the receiver respectively.

$$E_R = -j \frac{R_B}{\lambda} F(\phi_P) M_G^* \frac{H_B W_\omega}{D_B R_B} *$$

$$[S_i[(A_A - A_R)H_B] - S_i[(A_A + A_R)H_B] *$$

$$[S_i[K(\sin\gamma - \sin\beta)W_{\omega/2}]e^{-jk(l_B + R_B)}$$

where

H_B = height of wall

W_ω = width of wall

$A_A = KH_A/D_B$

$K = 2\pi/\lambda$

$A_R = KZ_R/R_B$

$S_i(X) = \sin X/X$

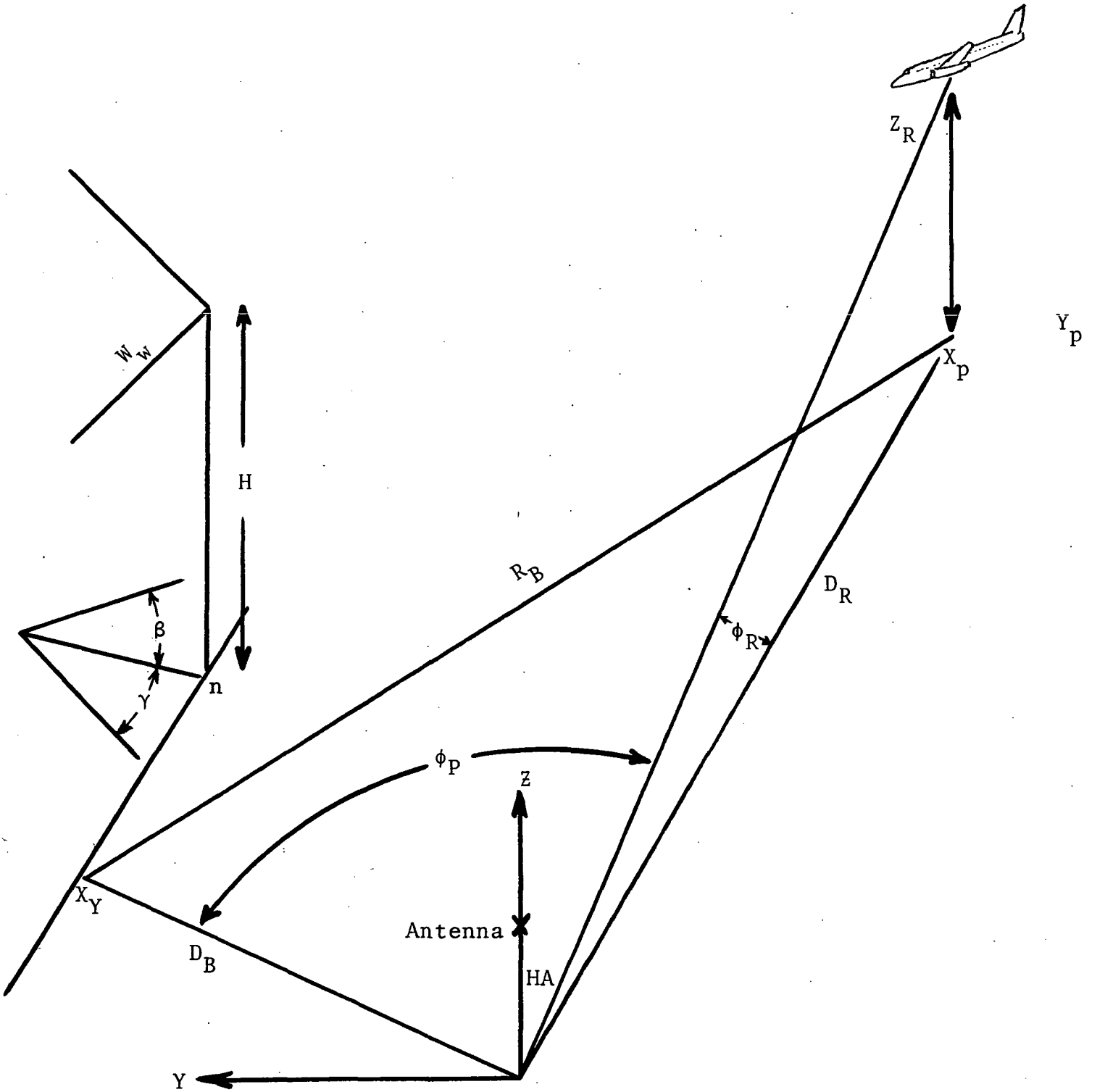

Figure 7-20. Multipath Geometry.

The direct and reflected fields are calculated at each point along the aircraft trajectory. These values are then used in the equation for the error term. It should be noted that the ratio of the reflected field to the direct field is required so that any scalling factors which may have been necessary are thereby excluded. The assumptions made in deriving E_D and E_R appear to be reasonable for MLS applications. Since E_D and E_R are calculated for points in space the basic models can be used for general curved approaches. All that is necessary will be some slight changes or modifications in the existing computer program.

7.2.5 Simulation of Gaussian Noise Term

The Gaussian noise term which is present in both the localizer and glideslope channels is not necessarily uncorrelated. Very little information exists as to its true statistical properties. In light of this fact it was felt that it would be better to model the noise term as correlated. The procedure used to do this is similar to the method presented in the section on the wind model. However, it was felt that the autocorrelation could be reasonably approximated as

$$R(\tau) = \sigma^2 e^{-\alpha|\tau|}$$

where σ is the standard deviation of the random noise term. A brief derivation of the recursive filter follows. If more detail is desired the interested reader is referred to the section on Gust Wind. Given

$$\text{Given} \qquad R(\tau) = \sigma^2 e^{-\alpha|\tau|}$$

$$\text{Then} \qquad \phi(m) = \sigma^2 e^{-\alpha T|m|}$$

The Z-transform of $\phi(m)$ is obtained by taking the sum of the individual Z-transforms of the parts for $m \geq 0$ and $m < 0$. Letting $A = e^{-\alpha T}$ we have

$$\Phi(Z) = \left[\frac{\sigma\sqrt{1-A^2}}{1-AZ^{-1}}\right] \left[\frac{\sigma\sqrt{1-A^2}}{1-AZ}\right]$$

Hence

$$H(Z) = \frac{\sigma\sqrt{1-A^2}}{1-AZ^{-1}}$$

$$= \sigma\sqrt{1-A^2} \quad [1+AZ^{-1} + A^2Z^{-2} + \ldots.]$$

Then

$$L(o) = \sqrt{1-A^2}$$

$$C_{oo} = \sqrt{\phi(o)-h^2(o)}$$

$$y(o) = \sigma\sqrt{1-A^2} \quad u(o) + \sigma Av(o)$$

Since u(o) and v(o) are independent and their values do not enter the expression for y(n) for $n \geq 1$, y(o) can be generated more simply from a single random variable having the appropriate variance. Finally for $n \geq 1$

$$y(n) = \sigma\sqrt{1-A^2} \quad u(n) + Ay(n-1)$$

The values of sigma are taken from the RTCA specification. The values are presented below.

Configuration / Coordinate		D CAT.I	F CAT.II	K CAT.III
AZ	BIAS	2.18×10^{-3} rad	1.57×10^{-3}	$.628\times10^{-3}$
	RANDOM	1.15×10^{-3}	$.575\times10^{-3}$	$.41\times10^{-3}$
	TOTAL	2.46×10^{-3}	1.67×10^{-3}	$.741\times10^{-3}$
EL	BIAS	$.872\times10^{-3}$ rad	$.872\times10^{-3}$	$.872\times10^{-3}$
	RANDOM	1.02×10^{-3}	$.61\times10^{-3}$	$.61\times10^{-3}$
	TOTAL	1.35×10^{-3}	1.06×10^{-3}	1.06×10^{-3}

Since the correlation time is not known a priori it is a variable that can be changed in the program. The effects of different correlation times upon the aircraft is presented in the Results section of this report.

REFERENCES

[1] J. H. Painter, S. C. Gupta, L. R. Wilson "Multipath Modeling for Aeronautical Communications," IEEE Transactions on Communications, May 1973, pp 658.

[2] O. P. Hakonsen "Improved Antenna Systems for ILS Localizers," IEEE transactions on Aerospace and Electronic Systems, May 1972, pp 273.

[3] I. S. Reed, H. Blasbaly "Multipath Tolerant Ranging and Data Transfer Techniques for Air-to-Ground and Ground-to-Air Links," IEEE Transaction on Communications, April 1970, pp 423.

[4] J. L. Wong, I.S. Reed, Z. A. Kaprielian "A Model for the Radar Echo from a Random Collection of Rotating Dipole Scatters," IEEE Transactions on Aerospace and Electronic Systems, March 1967, pp 171.

[5] P. A. Bello, C. J. Boardman "Effect of Multipath on Ranging Error for an Airplane-Satellite Link," IEEE Transactions on Communications, May 1973, pp 564.

[6] S. Ramakuskna, M. Sachidananda "Calculating the Effect of Uneven Terrain on Glide Path Signals," IEEE Transactions on Aerospace and Electronic Systems, May 1974, pp 379.

[7] G. L. Turin et al "A Statistical Model of Urban Multipath Propagation," IEEE Transactions on Vehicular Technology, February 1972, pp 1.

[8] Capt. P. S. Demko "Polarization/Multipath Study," U. S. Army Electronics Command, Fort Monmouth, N.J., June 1972.

[9] "Multipath and Diffraction Effects of Structures on Localizer Systems," Report No. FAA-RD-70-20, August 1970.

[10] R. Rosien, L. Sanders "The Performance of the Doppler Microwave Landing System in a Multipath Environment," presented at the 14th Guidance and Control Panel Symposium, Nato/AGARD, June 1972.

[11] A. Papoulis "Probability, Random Variables, and Stochastic Processes," McGraw Hill, 1965.

[12] C. W. Earp, F. G. Overburg, P. Sotheott "Doppler Scanning Guidance System," Elec. Communications, Volume 46, No. 4, 1971.